The Effect of Aerodynamic Drag Forces on the Formation Flying of Satellites

Thesis · December 2009

DOI: 10.13140/RG.2.1.2889.7445

1 author:

Tyler Reid
Xona Space Systems
51 PUBLICATIONS **955** CITATIONS

SEE PROFILE

The Effect of Aerodynamic Drag Forces on the Formation Flying of Satellites

by

Tyler Reid

Project Supervisor

Professor Arun K. Misra

Department of Mechanical Engineering

McGill University

Montréal, Quebec, Canada

December 2009

A thesis submitted to McGill University in partial fulfillment of the requirements of the Undergraduate Honours Program

Acknowledgements

First and foremost, I would like to thank my supervisor Professor Arun K. Misra. He was an extraordinary mentor and teacher throughout my brief time working with him. He gave me several opportunities to attend conferences and to give presentations at meetings which continued to fuel my interest in space in addition to gaining experience as a researcher. As an undergraduate student, his technical guidance and career path advice were truly invaluable and have allowed me to focus the direction of my future studies.

I would also like to thank my family, who has always supported me. My special thanks go to my mother, grandmother, brother, and father who have always been there and have made my studies and this thesis possible. I would also like to thank my friends who I have had the honour of working with throughout my time at McGill. And of course to Sara, who has supported me the whole way.

Finally, I would like to acknowledge the financial support for this project which was provided by the Canadian Space Agency, The National Science and Engineering Research Council of Canada, as well as McGill University.

Abstract

In this thesis, the effect of aerodynamic forces on the formation flight of satellites is examined. In order to study spacecraft relative motion in low Earth orbits, the predominant perturbation forces in this altitude range must be included in the analysis. Thus, a simplified linear dynamic model which includes effects due to the non-spherical nature of the Earth (J_2 effects) as well as those due to atmospheric drag must be developed for use in stability analysis and in the design of control laws. A set of linearized differential equations of motion which includes J_2 effects has been developed for circular reference orbits by authors Schweighart and Sedwick (2002). Based on these equations, a set of linearized equations of relative motion were developed which also includes the effects due to atmospheric drag. These ideas were then extended to reference orbits of small eccentricity. This resulted in a set of linear differential equations of motion which take into account J_2 and drag perturbations as well as the true eccentric nature of the reference orbit. Numerical simulation results are presented which characterize the effects of drag both projected circular and in-track formations. Further results are shown which demonstrate the accuracy of the linear dynamic model for certain cases.

Résumé

Dans cette thèse, l'effet des forces aérodynamiques sur le vol en formation des satellites est examiné. Afin d'étudier le mouvement relatif en orbite terrestre basse, les forces de perturbation prépondérante dans cette gamme d'altitude doivent être incluses dans l'analyse. Ainsi, un modèle linéaire simplifié dynamique qui inclut les effets dus à la nature non-sphérique de la Terre (les effets J_2) ainsi que celles dues à la traînée atmosphérique doit être développé pour être utilisé dans l'analyse de la stabilité et à la conception du système de contrôle. Un ensemble d'équations différentielles linéarisées du mouvement, qui inclut les effets J_2 a été développé pour les orbites circulaires par les auteurs et Schweighart Sedwick (2002). Avec ces équations, un ensemble d'équations linéarisées du mouvement relatif ont été développé qui inclut les effets dus à la traînée atmosphérique. Ces idées ont ensuite été étendues à des orbites de référence de modeste excentricité. Cela a abouti à un ensemble d'équations différentielles linéaires du mouvement qui prennent en compte les perturbations de J_2 et traînée atmosphérique ainsi que l'excentricité de l'orbite. Résultats de simulations numériques sont présentés qui caractérisent les effets de la traînée atmosphérique sur les formations du type ‘ projected circular’ et ‘in-track .’ D'autres résultats sont présentés, lesquels démontrent la fiabilité du modèle dynamique linéaire pour certains cas.

Nomenclature

Roman Symbols

$\mathbf{a}_{Drag}$	Drag perturbative acceleration vector acting on the reference orbit, expressed in the Hill frame
$\Delta\mathbf{a}_{Drag}$	Relative drag perturbative acceleration vector expressed in the Hill frame
$\mathbf{a}_{J_2}$	J_2 perturbative acceleration vector acting on the reference orbit, expressed in the Hill frame
$\Delta\mathbf{a}_{J_2}$	Relative J_2 perturbative acceleration vector expressed in the Hill frame
A	Spacecraft's cross-sectional area
a	Semi-major axis of the reference orbit
$\mathbf{C}$	Damping matrix for the circular reference orbit linearized dynamic system formulation
$\mathbf{C}_e$	Damping matrix for the eccentric reference orbit linearized dynamic system formulation
C_D	Spacecraft's coefficient of drag
c	Constant used in Schweighart-Sedwick (2002) formulation, see Appendix B
d	Characteristic length associated with the formation geometry
E	Eccentric Anomaly of the reference orbit
e	Eccentricity of the reference orbit
$\mathbf{f}_{Drag}$	Absolute drag perturbative acceleration acting on a spacecraft
$\hat{\mathbf{f}}_{Drag}$	Non-dimensionalized $\mathbf{f}_{Drag}$
$\Delta\mathbf{f}_{Drag}$	Relative drag perturbative acceleration of the Deputy spacecraft with respect to the Chief
$\Delta\hat{\mathbf{f}}_{Drag}$	Non-dimensionalized $\Delta\mathbf{f}_{Drag}$
f	True anomaly of the reference orbit

$\dot{f}$	The rate of change of true anomaly of the reference orbit
$\mathbf{G}$	Control gain matrix
$\mathbf{G'}$	Dimensionless control gain matrix
h	Magnitude of specific angular momentum vector of the reference orbit
i	Inclination of the reference orbit
i_{ref}	Initial inclination of the reference orbit (used in Schweighart-Sedwick (2002) formulation, see Appendix B)
J_2	Second spherical harmonic of the Earth's gravitational potential
$\nabla\mathbf{J}_2$	J_2 potential field gradient matrix
$\mathbf{K}$	Stiffness matrix for the circular reference orbit linearized dynamic system formulation
$\mathbf{K}_e$	Stiffness matrix for the elliptical reference orbit linearized dynamic system formulation
k	Constant used in the Schweighart-Sedwick formulation (see Appendix B)
$\hat{k}$	Constant k used in the Schweighart-Sedwick formulation normalized with respect to the mean orbital rate of the initial reference orbit
l	Constant used in the Schweighart-Sedwick formulation (see Appendix B)
$\mathbf{M}$	Generalized inertia matrix for the circular reference orbit linearized dynamic system formulation
$\mathbf{M}_e$	Generalized inertia matrix for the eccentric reference orbit linearized dynamic system formulation
M	Mean anomaly of the reference orbit
m	Spacecraft's mass
n	Mean orbital rate of the reference orbit
n_0	Initial mean orbital rate of the reference orbit
$\hat{n}$	Mean orbital rate of the reference orbit normalized with respect to the initial orbital rate of the initial reference orbit

p	Semi-latus rectum of the reference orbit
q	Constant used in the Schweighart-Sedwick formulation, see Appendix B
$\hat{q}$	Constant q used in the Schweighart-Sedwick formulation normalized with respect to the mean orbital rate of the initial reference orbit
R_e	Mean equatorial radius of the Earth
$\mathbf{r}_{ref}$	Position vector of the reference orbit (or spacecraft), also the position vector of the Hill frame with respect to the center of the Earth
r_{ref}	Radial distance of the reference orbit from the center of the Earth, also the distance of the Hill frame from the center of the Earth
$\dot{r}_{ref}$	The radial velocity component of the reference orbit
$\mathbf{r}_{rel}$	Relative position of the spacecraft with respect to the Hill frame, expressed in the Hill frame
s	Parameter used in Schweighart-Sedwick (2002) formulation, see Appendix B
$\tilde{s}$	Parameter used in Chapter 5 to characterize relative J_2 effects which couple in-plane to out of plane motion (Similar to s)
t	Time
$(\mathbf{v}_{rel})_{xyz}$	Relative velocity of a spacecraft with respect to the Hill frame, expressed in the Hill frame
$\mathbf{v}_{spacecraft_{rel}}$	The absolute velocity of a spacecraft relative to the rotating atmosphere
$\hat{\mathbf{v}}_{spacecraft_{rel}}$	Non-dimensionalized $\mathbf{v}_{spacecraft_{rel}}$
$\mathbf{x}\,,\dot{\mathbf{x}}\,,\ddot{\mathbf{x}}$	Relative position, velocity, and acceleration vectors of a spacecraft with respect to the Hill frame, expressed in the Hill frame
$\hat{\mathbf{x}}\,,\hat{\mathbf{x}}'\,,\hat{\mathbf{x}}''$	Relative non-dimensionalized position, velocity, and acceleration vectors of a spacecraft with respect to the Hill frame, expressed in the Hill frame
$x\,,\dot{x}\,,\ddot{x}$	Radial component of the relative position, velocity, and acceleration of a spacecraft expressed in Hill coordinates
$y\,,\dot{y}\,,\ddot{y}$	In-track component of the relative position, velocity, and acceleration of a spacecraft expressed in Hill coordinates

$z\,,\dot{z}\,,\ddot{z}$	Cross-track component of the relative position, velocity, and acceleration of a spacecraft expressed in Hill coordinates
$\hat{x}\,,\hat{x}'\,,\hat{x}''$	Non-dimensionalized $x\,,\dot{x}\,,\ddot{x}$
$\hat{y}\,,\hat{y}'\,,\hat{y}''$	Non-dimensionalized $y\,,\dot{y}\,,\ddot{y}$
$\hat{z}\,,\hat{z}'\,,\hat{z}''$	Non-dimensionalized $z\,,\dot{z}\,,\ddot{z}$

Greek Symbols

β	Dimensionless spacecraft ballistic coefficient
β_C	Dimensionless ballistic coefficient of the Chief spacecraft
β_D	Dimensionless ballistic coefficient of the Deputy spacecraft
$\dot{\boldsymbol{\theta}}$	Orbital rate vector of the reference orbit
θ	Argument of latitude of the reference orbit
$\dot{\theta}$	Orbital rate of the reference orbit, not necessarily the time derivative of argument of latitude θ
$\ddot{\theta}$	Time derivative of $\dot{\theta}$
μ	Earth's gravitational parameter
ρ	Local atmospheric density
σ	Parameter defined in Chapter 2, equation 2.69, which gives the rotation rate of the reference orbit minus the component of the rotating atmosphere at this given inclination
$\hat{\sigma}$	Non-dimensionalized σ
$\widetilde{\sigma}_1\,,\widetilde{\sigma}_2$	Parameters used in Chapter 4 which are similar in meaning and in definition to σ used in Chapter 2
ς	Parameter defined in Chapter 2, equation 2.70, which in part characterizes the magnitude of the periodic drag effects
$\hat{\varsigma}$	Non-dimensionalized ς
τ	Dimensionless time parameter (time normalized by the mean orbital rate)

φ	Initial phasing angle for cross-track motion, used in Schweighart-Sedwick (2002) formulation
Ω	Right ascension of the ascending node of the reference orbit
ω	Argument of perigee of the reference orbit
$\boldsymbol{\omega}_e$	The angular velocity vector of the Earth
ω_e	The angular velocity of the Earth
$\hat{\omega}_e$	The angular velocity of the Earth normalized with respect the mean orbital rate of the reference orbit

Please note, that in all of the above an over dot indicates differentiation with respect to time and an over hat indicates a quantity which has been non-dimensionalized.

Table of Contents

List of Figures

List of Tables

Chapter 1 - Introduction

There is a recent tendency in the space industry to replace large monolithic satellites with a group of small satellites to perform certain operations. A satellite formation, or distributed space system, is a collection of small satellites which work together to accomplish the objective of a much larger satellite. Satellite formations offer several operational and practical advantages over traditional single satellite missions. Smaller satellites offer faster build times and are usually less expensive. Multiple satellites allow for greater redundancy and more versatility in missions. Cost and launch constraints limit the size of a single spacecraft and thus limit the resolution of onboard antenna arrays and radar dishes. Satellites in formation can be configured into much larger virtual dishes and give rise to unprecedented resolution. Satellite formations can consequently be used as distributed sensors, sparse antenna arrays, and variable baseline interferometers (Scharf et al., 2004). Thus, satellite formations have widespread applications in such fields as astronomy, communications, meteorology, and environmental observations.

When such a group of satellites is used, the satellites must uphold certain formation geometry and relative positions must be maintained. These relative positions can drift due to various perturbation forces such as those due to the non-spherical nature of the Earth (also known as J_2 effects), solar radiation pressure, atmospheric drag, and a variety of other effects. At low altitudes, atmospheric drag forces can be quite significant and can result in a large and undesired drift in the relative motion. In the past, traditional chemical thrusters have been used in orbit station keeping and maneuvering. However, this requires fuel expenditures which not only increases the cost of the spacecraft but can also limit its life due to fuel

constraints. Impulsive thrusters can also contaminate sensitive sensor arrays and optical equipment. Although these types of aerodynamic forces are usually thought of as being a negative effect, it may be possible to use drag for relative station keeping by active actuation of aerodynamic panels. Formation maintenance using methods which do not rely on fuel but rather use other means which are naturally available, such as solar radiation pressure and even electromagnetics, are currently under development. In fact, a technology demonstration formation flying mission that plans to use differential drag forces as the primary means of control is currently under development. Known as JC2Sat, this joint collaboration between the Canadian Space Agency (CSA) and the Japan Aerospace Exploration Agency (JAXA) is slated to be launched in 2010 (see Figures 1-1 and 1-2).

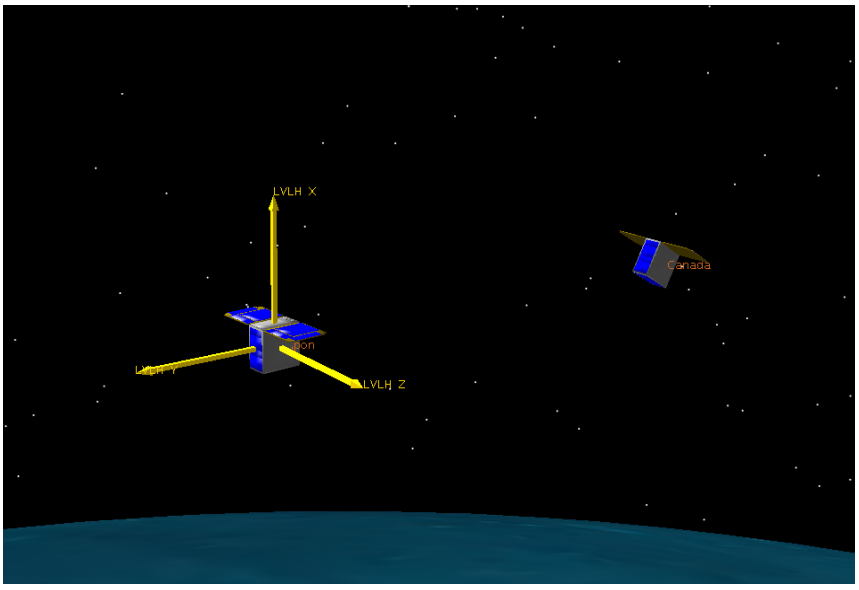

Figure 1-1: An artist's rendering of JC2Sat in flight (Courtesy of the Canadian Space Agency)

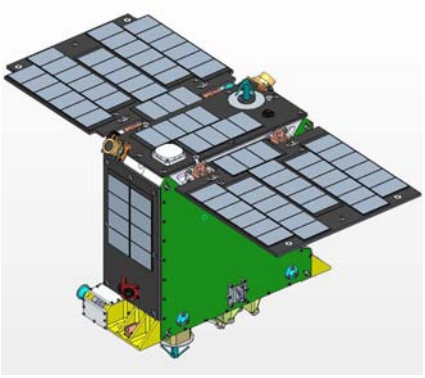

Figure 1-2: JC2Sat Spacecraft (Courtesy of the Canadian Space Agency (CSA))

The goal of this thesis is to examine both the effect of drag on formations and to assess the capability of drag as a means of formation maintenance and control. Simplified linearized dynamic models will be developed which will allow for a better understanding of these aerodynamic forces as well as the formulation of some stability analysis and numerical simulations.

1.1 Literature Review

In this section, a literature review of the dynamics associated with relative motion of spacecraft will be presented. The focus here will be specifically on relative motion which involves some analysis in using atmospheric drag as a means of formation maintenance and control as well as relative motion equations which model the effect of drag on formations. Although some articles are not directly related to atmospheric drag, their contribution in this area should be noted since some of the ideas of this thesis are built upon them. These works are presented chronologically starting with the classic equations of motion traditionally used in this field.

The equations of motion which have been used extensively in this field are known either as the Clohessy-Wiltshire equations (Clohessy & Wiltshire, 1960) or also often as the Hill equations (Hill, 1878). For simplicity, these equations will be referred to as the Clohessy-Wiltshire equations as they are commonly referred to in the context of spacecraft relative motion. These equations describe relative motion with respect to a given reference orbit expressed in the local vertical local horizontal (LVLH) or Hill coordinate frame (refer to Chapter 2, Figure 2-1). Hill (1878) originally developed these relative motion equations in order to study lunar motion. He derived equations governing orbital perturbations with respect to an unperturbed reference orbit and obtained an analytical solution to these equations. Clohessy and Wiltshire (1960) used similar equations to describe the relative motion between spacecraft in the context of spacecraft rendezvous. The Clohessy-Wiltshire equations are constant coefficient linear ordinary differential equations which describe the motion of a Deputy spacecraft with respect to a Chief spacecraft where the Chief spacecraft is assumed to be moving in a circular reference orbit. These equations do not take into account any perturbation forces and thus errors can grow large over time. In the context of spacecraft rendezvous, these equations can be used rather effectively as the time frames under consideration are short and thus errors are small. However, in the context of spacecraft formation flying, where the time frames are of the order of weeks and even years, the errors can grow unboundedly with time and thus these equations are of limited use for long term study.

Leonard et al. (1986, 1989) first examined the feasibility of using differential drag between two spacecraft as the means for controlling their relative positions. In their analysis, the Clohessy-Wiltshire equations were modified to include the effect

of atmospheric drag. The atmospheric drag effect was modeled as a constant force acting opposite to the in-track direction. Both the Chief and Deputy spacecraft were assumed to have drag panels which could be rotated to have an angle of attack of either 0 or 90 degrees. Therefore, the force acting in the in-track direction could be a positive constant, a negative constant, or zero depending on the configuration of the two spacecraft. A coordinate transformation reduced the problem to the simultaneous solution of the double integrator and harmonic oscillator. Based on this, a feedback control law was developed which simultaneously solves these two problems. Their results show that the control law is capable of both formation maneuvering and position maintenance.

Kechichian (1998) derived the full set of second-order nonlinear differential equations which describe the exact motion of a spacecraft subject to drag and J_2 perturbations in a general elliptic orbit, relative to a rotating reference frame which drags and precesses exactly as a given spacecraft attached to its center would.

Melton (2000) derived a time explicit state transition matrix for relative motion with respect to an elliptical reference orbit. Melton approximates terms in the nonlinear equations of motion as expansions up to second order eccentricity. Simulation results show that these equations are valid for eccentricities ranging form 0 to 0.3. These equations are valid for both coplanar and non-coplanar elliptical orbits.

Authors Carter and Humi modified the Clohessy-Wiltshire equations to include the effects of atmospheric drag in two separate papers. In their first work (Humi & Carter, 2002), the relative motion equations developed included a drag force that was proportional to linear velocity. In this work, atmospheric density and spacecraft velocity were both assumed to be inversely proportional to altitude.

Both spacecraft were also assumed to have the same value of ballistic coefficient. Based on these simplifying assumptions, a set of linear differential equations were obtained which can be solved in terms of integrals. This enables the representation of the solution of the problem in terms of a state-transition matrix. The results were then placed in the context of various control methods that had been previously developed by other authors. In their second work (Carter & Humi, 2002), the relative motion equations developed included the effects of a more realistic drag model, one where drag is proportional to the square of velocity. As in their first paper, both velocity and atmospheric density were assumed to be inversely proportional to altitude. When both spacecraft are assumed to have the same ballistic coefficient (or drag constant as it is used in their paper) their equations generalize the Tschauner-Hempel equations (Tschauner & Hempel, 1965) which describe the motion of a chaser spacecraft with respect to a target spacecraft in a general elliptical orbit. When the initial target orbit is circular, the equations simplify to a modified version of the Clohessy-Wiltshire equations and a closed-form analytical solution is derived by Carter and Humi (2002). Based on this analytical solution, a state-transition matrix was constructed.

Schweighart and Sedwick (2002) developed a set of linearized constant coefficient ordinary differential equations of relative motion which include the perturbations due to Earth oblateness (J_2) effects. The newly developed equations are valid for motion with respect to circular reference orbits and are similar both in form and in simplicity to the Clohessy-Wiltshire equations. These equations can be solved analytically and the solution is provided by the authors. Schweighart and Sedwick validated their newly developed equations via comparison with a high precision orbit propagator which included the effects of J_2. Simulation results

showed that these newly developed equations have a maximum modeling error of 0.4% for all cases of orbits and formation geometries.

Franconeri (2003) examined how differential drag can be used as a satellite constellation station keeping strategy. His paper explains how differential drag can be achieved from an operational standpoint, i.e. changing the effective drag area of the spacecraft by means of rotating solar panels or adjusting spacecraft attitude. He also presents how such differential drag calculations could be performed by means of a hypothetical constellation mission example. The example chosen in this study examines an in-plane type constellation where spacecraft are separated by very large distances and thus relative motion equations such as the Clohessy-Wiltshire equations are neither valid nor needed in this analysis. It is discussed qualitatively as to how one would go about designing a mission which would use such a strategy and how it could be implemented. However, explicit detailed calculations are not given. It is written from more of a mission analysis and operations standpoint.

Fourcade (2004) examined using differential drag to perform station keeping maneuvers for an interferometric wheel type of formation flying mission. The interferometric wheel is a concept developed by the Centre National d'Etudes Spaciales (CNES). This type of formation consists of three microsatellites which follow a main radar satellite. The three microsatellites fly in a circular or wheel formation about the larger radar satellite which may or may not be at the center of the formation. In this paper, Fourcade uses differential drag to partially maintain the relative motion. Chemical type impulsive thrusters are used to control the distance between the wheel and the radar satellite and differential drag is used to control the distances between the microsatellites in the wheel. Differential drag is

obtained by changing the attitude of the microsatellites. Based on this concept, analytical expressions for closed-loop control gains are developed. Numerical results show that the method is effective with reasonable accuracy.

Mishne (2004) developed a method to compensate for the secular combined effects of Earth oblateness (J_2) and atmospheric drag perturbations on spacecraft relative motion. The corrections are performed by impulsive velocity maneuvers. The analysis is based on the equations of the variations of the mean orbital elements and is thus not restricted to small eccentricities. Numerical simulation results are presented which demonstrate the effectiveness of the algorithm. The effects of measurement noise and drag uncertainty are also discussed.

Palmerini et al. (2005) examined using atmospheric drag as a means of controlling the relative position between two satellites flying in a formation. The recently developed Carter-Humi equations (Carter & Humi, 2002) are used in their analysis. The focus of the paper is on evaluating optimal control strategies which minimize spacecraft orbit decay. A semi-analytical solution of the Carter-Humi equations (which is needed when ballistic coefficients of the two spacecraft are not equal) is provided as an input to an optimizer based on genetic algorithms. Numerical simulation results show the effectiveness of the genetic algorithm optimization scheme.

Jigang and Yulin (2006) examined the application of the phase plane method to develop control methods using differential drag for co-planar formations. The control law developed was based on the assumption that the rate of change of the difference between the semi-major axes of the two spacecraft was constant. When this assumption is made, the phase trajectory becomes a group of parabolas as was the case in the paper presented by Leonard et al. (1986, 1989). Simulation results

show that the control method is capable of reducing the drift and keeping it bounded.

Sabatini and Palmerini (2006) developed a linear quadratic regulator (LQR) for low altitude formation flying. The control law presented is based on the recently developed Carter-Humi equations (Carter & Humi, 2002) which includes the effect of atmospheric drag. The controller is built on the assumption that correctional thrusts can be made on a continuous basis. Numerical simulations were performed which take into account the effects of both atmospheric drag and J_2 perturbations in order to evaluate the effectiveness of the controller. The results show that the LQR based on the Carter-Humi equations (Carter & Humi, 2002) is more efficient than one which is based on the simpler Clohessy-Wiltshire equations and thus results in a significant savings in fuel at low altitudes.

Kumar et al. (2007) investigated the feasibility of using differential drag as a means of nano-satellite formation control. Analytic Graphics Inc's (AGI) Satellite Tool Kit (STK) software is used to initially assess the magnitude of the drifts caused by differential drag at different altitudes. Using STK's High Precision Orbit Propagator the effective range of altitudes for which formation maintenance with differential drag is feasible is determined. Different atmospheric density models and factors that affect atmospheric density such as solar flux and geomagnetic activity are considered. The information obtained is then used to show that it is feasible to use differential drag for spacecraft formation control. A simple PID controller is then implemented that adjusts the cross sectional areas of the satellites such that the energies of the orbits remain equal. Numerical results are presented which demonstrate that the control law can maintain the formation with reasonable accuracy.

Théron et al. (2007) presented a solution based on periodic feedback control laws to the problem of station keeping for a small spacecraft near an eccentric reference orbit. Linearized equations of relative motion for a satellite near an eccentric reference orbit are derived in the presence of the second zonal gravitational harmonic (J_2) and atmospheric drag perturbations. The obtained linear continuous time model is then descretized and a state feedback control law with performance requirements defined by the generalized H_2 operator norm may be computed by a linear inequality-based algorithm. Extended LMI conditions allow the design of a single H_2 LTI controller for linear N-periodic discrete-time systems. Non-linear numerical simulations are presented which demonstrate the efficiency of the approach.

Kumar and Ng (2008) evaluated the performance of the control law proposed by Leonard et al. (1986, 1989) in a real perturbative environment. In their paper, they elaborate on the same method and consider factors such as time varying natural perturbations, erroneous measurements, attitude errors, and large separation distances. Some modifications are also proposed to the original control law to make it more efficient in terms of control usage. This study was done in order to validate the use of Leonard et al.'s controller for formation maneuvering and formation keeping for the upcoming JC2Sat (Japan Canada Joint Collaboration Satellite) mission. This is a technology demonstration mission which is slated to be the first mission to demonstrate formation assembly, formation maneuvering, and formation keeping using only differential drag. Numerical simulations using a high precision in-house orbit propagator demonstrate that the controller performs satisfactorily in general.

Bevilacqua and Romano (2008) developed a method which exploits atmospheric drag to perform rendezvous maneuvers with multiple spacecraft in low Earth orbits. In their analysis the recently developed Schweighart and Sedwick equations (Schweighart & Sedwick, 2002) are used to describe the relative motion. Although these equations are limited to nominally circular orbits, they include the effects of linearized J_2 perturbations. The control methods developed in this work are based on the approach taken by Leonard et al. (1986, 1989). The relative natural dynamics of the chaser with respect to the target are decoupled into a secular motion and a periodic oscillation. The control scheme first controls the secular motion using differential drag and then implements an oscillation reduction scheme. Their control scheme presents several improvements to the method developed by Leonard et al (1986, 1989). The new technique eliminates the problem of having a residual distance at the end of the maneuver as well as the need for a numerical optimization routine as the maneuvers are based on an analytical expression. Numerical simulations are presented which validate the proposed control scheme.

Silva (2008) derived a set of linearized differential equations of relative motion which include the in-plane effects of dynamic atmospheric drag, i.e. drag with respect to a moving atmosphere. In his analysis, the atmosphere was assumed to be rotating at a mean rate which is equal to the rotation rate of the Earth. The analysis is limited to circular reference orbits and the final result is similar in simplicity and form to the Clohessy-Wiltshire equations. This system of differential equations strictly does not have constant coefficients. However, if local atmospheric density is assumed to remain constant, at least over certain altitude ranges, these equations can be assumed to have constant coefficients over limited time intervals.

Numerical simulation results are given which compare the fidelity of the model in comparison to the full non-linear equations. The results demonstrate a significant increase in precision when compared to the predictions made by the Clohessy-Wiltshire equations.

1.2 Objectives of Thesis

As shown by the preceding literature review, extensive work has been done in developing the dynamics of spacecraft relative motion as well modeling the various perturbation forces which these types of missions can encounter. However, the precision of each of these models is somewhat limited. In low Earth orbits, both J_2 and atmospheric drag perturbations are significant and models which encompass either one effect or the other are incomplete for studying or planning missions in this altitude range. A simplified linear dynamic model which includes both effects is currently unavailable.

The assumption of a circular reference orbit is also limiting. Although many missions are designed to be nearly circular, achieving and maintaining a perfectly circular orbit is very difficult in practice. The small eccentricities of these orbits can give rise to a drift in the formation geometry over time which will not be predicted by a dynamic model which assumes a circular reference orbit. More complex non-linear dynamic models do exist; however, these are of limited value in analysis or in the design of control laws. Hence, the development a simplified linear dynamic model which accounts for Earth oblateness (J_2), atmospheric drag, as well as the true eccentric nature of the reference orbit is the ultimate objective of this thesis.

First, a formulation will be developed in which both J_2 and atmospheric drag perturbations will be included which will be valid for circular reference orbits. These equations will then be extended to reference orbits of small eccentricity. A more detailed outline of the thesis is given in the next section.

1.3 Outline of Thesis

Chapter 2 will begin by introducing the coordinate frames used in the relative motion analysis as well as the other coordinate frames used in this thesis. Following this, the primary goal of this chapter is to develop a set of linearized equations of motion which include the effects due to J_2 and aerodynamic drag perturbations. A set of linearized differential equations of motion which includes the effects of the non-spherical nature of the Earth (J_2) has been previously developed for circular orbits by Schweighart and Sedwick (2002). These relative motion equations represent a set of constant coefficient linear ordinary differential equations which can be solved analytically. The thesis builds on these equations by including the effects of atmospheric drag while maintaining their linearity and relative simplicity. These equations, which are valid for circular reference orbits, will be used to perform some preliminary stability analysis as well as numerical simulations to assess both the effect of drag and the capabilities of drag as a means of formation maintenance and control. These numerical simulation results will be presented separately in Chapter 3.

The final goal of this thesis is to develop a formulation which includes the previously mentioned perturbations forces but which is valid for elliptical orbits. Thus, the subject of Chapter 4 is on extending the equations developed in Chapter

2 to elliptical orbits of small eccentricity. This small eccentricity assumption will be utilized to reduce the complexity of these equations to a form which is similar in simplicity to those developed in Chapter 2. Chapter 5 will present numerical simulation results based of the equations developed in Chapter 4. These simulations will first be used to evaluate the validity of the equations by comparing the results with those obtained in Chapter 3. Then, some preliminary results for motion in elliptic orbits will be presented. Chapter 6 will close with an overview of the findings of this thesis and will give an outline for future work in this area.

Chapter 2 - Relative Motion Equations for Circular Orbits

The effect of aerodynamic forces on the formation flying of satellites with respect to circular reference orbits is the subject of this chapter. More precisely, linearized equations of motion which account for the perturbations due to aerodynamic drag and J_2 potential will be developed. First, the coordinate frames used in the analysis will be defined. Then, the equations of motion will be developed. The starting point for the analysis will be the linearized equations of motion presented by Schweighart and Sedwick (2002). This highly accurate, yet simplified dynamic model already takes into account effects due to J_2 potential. The goal of this chapter will be to modify these equations so that they take into account the effects due to linearized drag. This dynamic model will then be used to carry out a preliminary stability analysis. Finally, numerical simulations will be shown which demonstrate the effects of J_2 perturbations and aerodynamic drag on spacecraft formations of certain geometry. These simulation results will be used for assessing the feasibility of using differential drag as a means of formation maintenance and control.

2.1 Coordinate Frames

In this section, a description of the coordinate frames used in the relative motion equations formulation and in this text will be given.

Shown in Figure 2-1 are the two reference frames used in this chapter, the Earth-Centered Inertial (X-Y-Z) and the Hill (x-y-z) frames. The Earth-Centered

Inertial (ECI) frame has its origin at the center of the Earth and the Earth's equator defines the fundamental X-Y plane. The X-axis points in the direction of the vernal equinox, the Z-axis is aligned with the Earth's rotation vector, and the Y-axis completes the right hand orthogonal coordinate system.

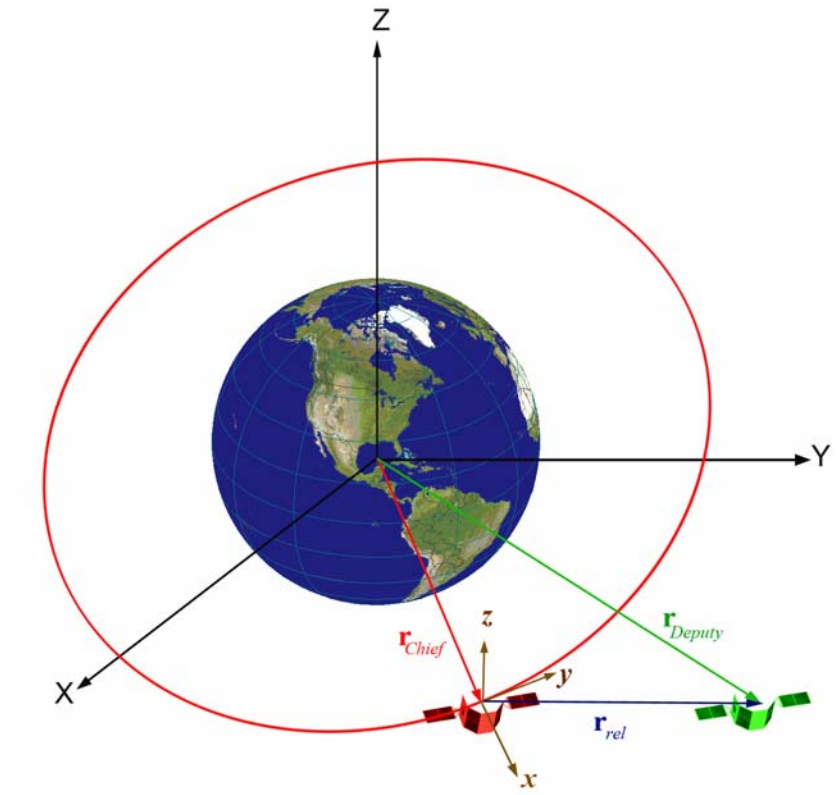

Figure 2-1: *x-y-z* Hill coordinate frame and the X-Y-Z Earth Centered Inertial (ECI) Frame

The coordinate frame which is used in the relative motion analysis is known as the Hill frame and it is designated by the *x-y-z* axes in Figure 2-1. In this thesis, the Hill frame is used to describe the motion of a particular spacecraft known as the Deputy with respect to a fictitious spacecraft known as the Chief which travels in a defined reference orbit. The origin of the Hill frame lies at the center of mass of this imaginary Chief spacecraft and thus moves with it along the pre-defined reference orbit trajectory. As a result, the Hill frame rotates at the same rate as the

imaginary spacecraft's orbital rate $\dot{\theta}$. Furthermore, the x-y-z axes of the Hill frame are defined as follows: the x-axis points along the radial direction of the imaginary spacecraft, the z-axis is perpendicular to the reference orbital plane, and the y-axis completes the right handed orthogonal coordinate system. Commonly, the x direction is known as the radial direction, the y direction is known as the in-track or along-track direction, and the z direction is known as the cross-track or out-of-plane direction as per their physical meanings.

Another method of orbit description (used in Chapter 4) is that which uses the classical orbital elements. We need six quantities to specify the state of a spacecraft in space. There are several equivalent forms that these six quantities may take. For example, in the ECI frame, the state $\mathbf{X}$ is described as follows:

$$\mathbf{X} = \begin{bmatrix} X & Y & Z & \dot{X} & \dot{Y} & \dot{Z} \end{bmatrix}^T \tag{2.1}$$

In terms of the classical orbital elements, the state can be equivalently described as:

$$\mathbf{X} = \begin{bmatrix} a & e & i & \Omega & \omega & f \end{bmatrix}^T \tag{2.2}$$

where, in the context of closed elliptical orbits, a is the semi-major axis of the elliptical trajectory, e is the eccentricity of the ellipse, i is the inclination of the orbital plane with respect to the equatorial reference plane, Ω is the right ascension of the ascending node, ω is the argument of perigee, and f is the true anomaly (refer to Figure 2-2). The semi-major axis a and the eccentricity e define the geometry of the closed elliptical trajectory of the spacecraft. The inclination i and the right ascension of the ascending node Ω are angles that define the orientation of the orbital plane with respect to the ECI coordinate frame. More specifically, the right ascension of the ascending node is defined as the angle in the equatorial plane measured positively from the $\hat{\mathbf{i}}_x$ unit vector (shown in Figure 2-2) in the ECI frame to the point on the equatorial plane where the satellite crosses the equator moving

from south to north. The argument of perigee ω is an angle which is measured in the orbital plane from the ascending node and it locates the closest point of the orbit to the center of the Earth (or equivalently the surface of the Earth). This parameter is used to describe the orientation of the ellipse within the orbital plane. The final element, the true anomaly f, determines the current position of the spacecraft within the orbital plane. This angular parameter is measured in the orbital plane with respect to the argument of perigee. Another angular quantity which is worth noting is the argument of latitude θ. This angular quantity is defined as the sum of the argument of perigee ω and the true anomaly f (shown in Figure 2-2):

$$\theta = f + \omega \tag{2.3}$$

This quantity arises in several instances in this thesis and it is defined as the angle measured between the ascending node and the satellite's position vector. It is an especially useful parameter in the case of inclined circular orbits where argument of perigee is undefined.

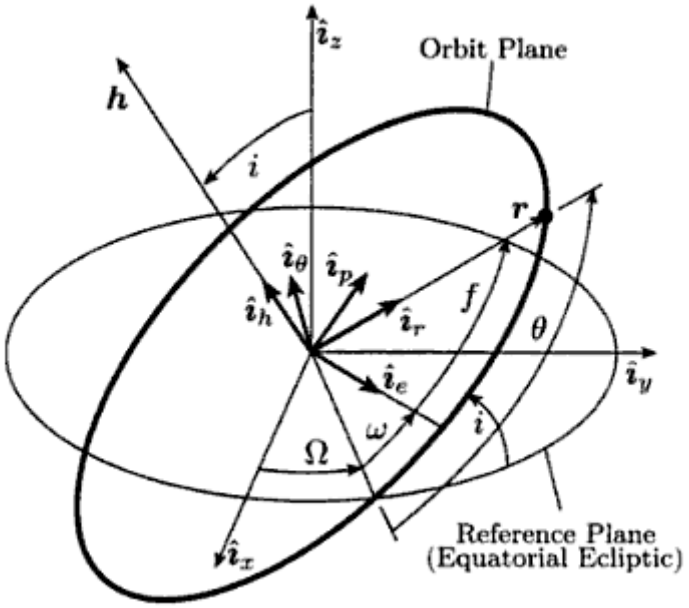

Figure 2-2: Classical Orbital Elements (Schaub & Junkins, 2003)

2.2 Relative Motion Equations

The starting point for this analysis will be the equations developed by Schweighart and Sedwick (2002). They represent a set of linearized constant coefficient ordinary differential equations, similar to the Clohessy-Wiltshire equations, but include Earth oblateness (J_2) effects. These equations describe the relative motion of a spacecraft with respect to a J_2 perturbed reference circular orbit. Thus to obtain the relative motion of one spacecraft with respect to another, two sets of these equations are needed to propagate their individual motion, which is then differenced to obtain the spacecraft relative motion. These equations are given as follows:

$$\ddot{x} - 2(nc)\dot{y} - (5c^2 - 2)n^2 x = -3n^2 J_2 \left(R_e^2 / r_{ref}\right) \times \left\{ \frac{1}{2} - \left[3\sin^2 i_{ref} \sin^2(kt)/2\right] - \left[\left(1 + 3\cos 2i_{ref}\right)/8\right] \right\} + f_{Drag,x} \tag{2.4}$$

$$\ddot{y} + 2(nc)\dot{x} = -3n^2 J_2 \left(R_e^2 / r_{ref}\right) \sin^2 i_{ref} \sin(kt)\cos(kt) + f_{Drag,y} \tag{2.5}$$

$$\ddot{z} + q^2 z = 2lq\cos(qt + \varphi) + f_{Drag,z} \tag{2.6}$$

where the *x*-*y*-*z* terms represent the spacecraft coordinates in the Hill frame, R_e is the mean equatorial radius of the Earth, r_{ref} is the constant radius of the circular reference orbit, J_2 is the second spherical harmonic of the Earth's gravitational potential (a dimensionless quantity which is equal to 1.08263×10^{-3}), i_{ref} is the initial inclination of the reference orbit, t is the given time, and n is the mean orbital rate defined as:

$$n = \sqrt{\frac{\mu}{r_{ref}^3}} \tag{2.7}$$

where μ is the gravitational constant of the Earth which is equal to 3.986005×10^{14} m^3/s^2. The remaining constants specific to this formulation as well as other details about the Schweighart-Sedwick equations are summarized in Appendix B for reference.

The $f_{Drag,x}$, $f_{Drag,y}$, and $f_{Drag,z}$ terms represent the additional acceleration due to the aerodynamic drag in the radial, in-track, and cross-track directions, respectively. The specific aerodynamic force (i.e. force divided by mass or acceleration) acting on a spacecraft in orbit is as follows (Vallado, 2007):

$$\mathbf{f}_{Drag} = -\frac{1}{2}\frac{C_D A}{m}\rho\left\|\mathbf{v}_{spacecraft_{rel}}\right\|\mathbf{v}_{spacecraft_{rel}} \tag{2.8}$$

where C_D is the coefficient of drag of the spacecraft, A is the spacecraft's cross sectional area, m is the spacecraft's mass, ρ is the local atmospheric density, and $\mathbf{v}_{spacecraft_{rel}}$ is the relative velocity of the spacecraft with respect to the rotating atmosphere. The Earth's atmosphere has a mean motion due to the Earth's rotation and it is approximated by the rotation rate of the Earth. The velocity with respect to the rotating atmosphere $\mathbf{v}_{spacecraft_{rel}}$ is given by the following (Vallado, 2007):

$$\mathbf{v}_{spacecraft_{rel}} = \mathbf{v}_{spacecraft} - \boldsymbol{\omega}_e \times \mathbf{r}_{spacecraft} \tag{2.9}$$

where the $\mathbf{r}_{spacecraft}$ and $\mathbf{v}_{spacecraft}$ vectors represent the absolute position and velocity of the spacecraft with respect to the center of the Earth and $\boldsymbol{\omega}_e$ represents the angular velocity vector of the Earth. In order to describe these drag effects in terms of Hill coordinates, the $\mathbf{v}_{spacecraft_{rel}}$ term must be described in the Hill frame. A detailed derivation of this coordinate transformation is given in Appendix A. The final expression for the velocity of a spacecraft relative to the rotating atmosphere expressed in the Hill frame is as follows:

$$\mathbf{v}_{spacecraft_{rel}} = \begin{bmatrix} \dot{x} + \dot{r}_{ref} - y(\dot{\theta} - \omega_e \cos i) - z\,\omega_e \cos\theta \sin i \\ \dot{y} + (r_{ref} + x)(\dot{\theta} - \omega_e \cos i) + z\,\omega_e \sin\theta \sin i \\ \dot{z} + (r_{ref} + x)\,\omega_e \cos\theta \sin i - y\,\omega_e \sin\theta \sin i \end{bmatrix} \tag{2.10}$$

For the case where a circular reference orbit is used and the equations of motion are those given in the formulation by Schweighart and Sedwick (2002), the velocity of a spacecraft relative to the rotating atmosphere simplifies to:

$$\mathbf{v}_{spacecraft_{rel}} = \begin{bmatrix} \dot{x} - y(nc - \omega_e \cos i) - z\,\omega_e \cos\theta \sin i \\ \dot{y} + (r_{ref} + x)(nc - \omega_e \cos i) + z\,\omega_e \sin\theta \sin i \\ \dot{z} + (r_{ref} + x)\,\omega_e \cos\theta \sin i - y\,\omega_e \sin\theta \sin i \end{bmatrix} \tag{2.11}$$

where the $\dot{r}_{ref}$ term vanishes due to the fact that we are now dealing with a circular reference orbit, and the orbital rate $\dot{\theta}$ becomes nc, the constant orbital rate of the circular reference orbit used in the Schweighart-Sedwick equations.

2.3 Non-Dimensionalization of the Equations of Motion

In this section, the equations of motion described in the previous section will be non-dimensionalized. This will be done in part for computational efficiency when these equations are integrated numerically as well as for robustness of subsequent numerical results. The definition of dimensionless position and velocity parameters which are of the same order will also allow for a better understanding of the implications of these equations when drag is included in the final formulation.

2.3.1 Definition of Dimensionless Quantities

In this section, the non-dimensional quantities which will be used to non-dimensionalize the equations of motion will be defined.

First, a dimensionless time parameter τ will be defined:

$$\tau = n_0 t \tag{2.12}$$

where t is the given time and n_0 is the mean orbital rate of the initial circular reference orbit defined as:

$$n_0 = \sqrt{\frac{\mu}{r_{ref,0}^3}} \tag{2.13}$$

where $r_{ref,0}$ is the radius of the initial circular reference orbit and μ is the gravitational parameter of the Earth. The reason for this selection of n_0 is to avoid potential time scaling issues. Since a patched reference orbit method may be used in the analysis, the value of n will always be changing thus constantly re-scaling time if n itself were used. For simplicity, the initial value of orbital rate was selected to normalize the time variable. The reason for this patched reference orbit method will become clear when the numerical simulation results are presented. Essentially, the Schweighart-Sedwick equations were not intended to include drag in their original formulation. Thus, the addition of drag creates a large forcing primarily in the in-track direction which continuously pushes the two spacecraft away from the original reference orbit. With time, these distances can become large and the assumptions which where used in the derivation of these equations, i.e. that distances with respect to the reference frame are small, are no longer valid and thus the solution becomes erroneous. A way to reconcile this is to periodically 'reset' the reference orbit when distances become large. Although this was not done in this

thesis as a numerically stable algorithm to do so was not established, it is a possibility to consider for future work in this area. This merely limits the time period for which these simulations are valid and will be discussed further in the Numerical Simulations section.

Dimensionless distance quantities to replace the variables *x, y, z* will now be introduced. The variables *x, y, z* will be normalized with respect to a constant reference length parameter which for the time being will be defined as L_{ref}. These normalized variables $\hat{x}, \hat{y}, \hat{z}$ are defined as follows:

$$\hat{x} \equiv x / L_{ref} \tag{2.14}$$

$$\hat{y} \equiv y / L_{ref} \tag{2.15}$$

$$\hat{z} \equiv z / L_{ref} \tag{2.16}$$

Based on these definitions, the resulting velocity variables are:

$$\dot{x} \equiv \frac{dx}{dt} = n_0 \frac{dx}{d(n_0 t)} = n_0 \frac{dx}{d\tau} = n_0 x' = n_0 L_{ref} \hat{x}' \tag{2.17}$$

and similarly:

$$\dot{y} = n_0 L_{ref} \hat{y}' \tag{2.18}$$

$$\dot{z} = n_0 L_{ref} \hat{z}' \tag{2.19}$$

The resulting acceleration variables are:

$$\ddot{x} \equiv \frac{d^2 x}{dt^2} = n_0^2 \frac{d^2 x}{d(n_0 t)^2} = n_0^2 \frac{d^2 x}{d\tau^2} = n_0^2 x'' = n_0^2 L_{ref} \hat{x}'' \tag{2.20}$$

and similarly:

$$\ddot{y} = n_0^2 L_{ref} \hat{y}'' \tag{2.21}$$

$$\ddot{z} = n_0^2 L_{ref} \hat{z}'' \tag{2.22}$$

Notice that the units are consistent, namely $n_0 L_{ref}$ has units of velocity and $n_0^2 L_{ref}$ has units of acceleration.

If we choose $L_{ref} = d$ where d is a characteristic length associated with the relative motion geometry, such as the desired diameter of a projected circular formation or the desired constant offset distance in an in-track type formation, then the dimensionless distance variables $\hat{x}, \hat{y}, \hat{z}$ will be of the order of at most 1. Thus, d will replace L_{ref} in the above equations and this notation will be used for the remainder of this chapter.

2.3.2 Non-Dimensionalized Equations of Motion

In this section, the non-dimensionalized equations of motion will be presented. This will be done by re-defining the previously presented equations of motion in terms of the dimensionless parameters defined in the previous section via substitution and simplification.

First, the appropriate substitutions in order to transform these equations into functions of the newly defined dimensionless parameters $\hat{x}, \hat{y}, \hat{z}$, and τ will be made. Substituting these dimensionless quantities into the Schweighart-Sedwick equations results in:

$$n_0^2 d\,\hat{x}'' - 2(nc) n_0\, d\,\hat{y}' - (5c^2 - 2) n^2 d\,\hat{x} = -3n^2 J_2 \left(R_e^2 / r_{ref}\right) \times \left\{ \frac{1}{2} - \frac{3}{2} \sin^2 i_{ref} \sin^2 \left(k \frac{\tau}{n_0} \right) - \frac{1}{8} \left(1 + 3\cos 2 i_{ref}\right) \right\} + f_{Drag,x} \tag{2.23}$$

$$n_0^2\, d\,\hat{y}'' + 2(nc) n_0 d\,\hat{x}' = -3n^2 J_2 \left(R_e^2 / r_{ref}\right) \sin^2 i_{ref} \sin\left(k \frac{\tau}{n_0} \right) \cos\left(k \frac{\tau}{n_0} \right) + f_{Drag,y} \tag{2.24}$$

$$n_0^2 d\,\hat{z}'' + q^2 d\,\hat{z} = 2lq\cos\left(q\frac{\tau}{n_0}+\varphi\right) + f_{Drag,z} \tag{2.25}$$

where the drag terms $f_{Drag,x}$, $f_{Drag,y}$, and $f_{Drag,z}$ will be considered in more detail later on in this chapter. In order to obtain equations which have dimensionless coefficients, all three equations will be divided by $n_0^2 d$. The equations are now re-written as:

$$\begin{aligned}\hat{x}'' - 2\left(\frac{n}{n_0}\right)c\hat{y}' - (5c^2-2)\left(\frac{n}{n_0}\right)^2\hat{x} &= -3n^2 J_2\left(\frac{R_e^2}{r_{ref}}\right)\left(\frac{1}{n_0^2 d}\right) \\ &\times\left\{\frac{1}{2}-\frac{3}{2}\sin^2 i_{ref}\,\sin^2\left(\frac{k}{n_0}\tau\right)-\frac{1}{8}\left(1+3\cos 2i_{ref}\right)\right\}+\frac{f_{Drag,x}}{n_0^2\,d}\end{aligned} \tag{2.26}$$

$$\begin{aligned}&\hat{y}'' + 2\left(\frac{n}{n_0}\right)c\,\hat{x}' = \\ &-3n^2 J_2\left(\frac{R_e^2}{r_{ref}}\right)\left(\frac{1}{n_0^2 d}\right)\sin^2 i_{ref}\,\sin\left(\frac{k}{n_0}\tau\right)\cos\left(\frac{k}{n_0}\tau\right)+\frac{f_{Drag,y}}{n_0^2 d}\end{aligned} \tag{2.27}$$

$$\hat{z}'' + \left(\frac{q}{n_0}\right)^2\hat{z} = \left(\frac{1}{n_0^2 d}\right)2lq\cos\left(\frac{q}{n_0}\tau+\varphi\right)+\frac{f_{Drag,z}}{n_0^2\,d} \tag{2.28}$$

In order to simplify these expressions further, three new dimensionless quantities will be introduced:

$$\hat{n} \equiv n/n_0 \tag{2.29}$$

$$\hat{k} \equiv k/n_0 \tag{2.30}$$

$$\hat{q} \equiv q/n_0 \tag{2.31}$$

The non-dimensionalized equations of motion can now be written in their final form as follows:

$$\begin{aligned}\hat{x}'' - 2\hat{n}c\,\hat{y}' - (5c^2-2)\hat{n}^2\,\hat{x} &= -3\hat{n}^2 J_2\left(\frac{R_e^2}{r_{ref}d}\right) \\ &\times\left\{\frac{1}{2}-\frac{3}{2}\sin^2 i_{ref}\,\sin^2(\hat{k}\,\tau)-\frac{1}{8}\left(1+3\cos 2i_{ref}\right)\right\}+\frac{f_{Drag,x}}{n_0^2\,d}\end{aligned} \tag{2.32}$$

$$\hat{y}'' + 2\hat{n}c\,\hat{x}' = -3\hat{n}^2 J_2 \left(\frac{R_e^2}{r_{ref}\, d} \right) \sin^2 i_{ref}\, \sin(\hat{k}\,\tau) \cos(\hat{k}\,\tau) + \frac{f_{Drag,y}}{n_0^2\, d} \tag{2.33}$$

$$\hat{z}'' + \hat{q}^2 \hat{z} = 2 \left(\frac{l}{n_0 d} \right) \hat{q} \cos\left(\hat{q}\,\tau + \varphi\right) + \frac{f_{Drag,z}}{n_0^2\, d} \tag{2.34}$$

It can be seen from the above equations that the division by $n_0^2\, d$ has non-dimensionalized the drag terms. This will be considered in more detail in the next section.

2.3.3 Non-Dimensionalized Drag Terms

In this section, the dimensionless aerodynamic drag terms will be examined in more detail. The non-dimensionized drag terms are given by the following equation:

$$\hat{\mathbf{f}}_{Drag} \equiv \frac{\mathbf{f}_{Drag}}{n_0^2\, d} = -\frac{1}{2} \rho \left(\frac{1}{n_0^2\, d} \right) \frac{C_D A}{m} \left\| \mathbf{v}_{spacecraft_{rel}} \right\| \mathbf{v}_{spacecraft_{rel}} \tag{2.35}$$

where $\hat{\mathbf{f}}_{Drag}$ represents the non-dimensionalized equivalent of $\mathbf{f}_{Drag}$ and the remaining parameters of the equation were defined previously. Prior to the transformation of variables to dimensionless quantities the velocity of the spacecraft with respect to the rotating atmosphere expressed in the Hill frame is given by the following (refer to Appendix A):

$$\mathbf{v}_{spacecraft_{rel}} = \begin{bmatrix} \dot{x} - y(nc - \omega_e \cos i) - z\,\omega_e \cos\theta \sin i \\ \dot{y} + (r_{ref} + x)(nc - \omega_e \cos i) + z\,\omega_e \sin\theta \sin i \\ \dot{z} + (r_{ref} + x)\,\omega_e \cos\theta \sin i - y\,\omega_e \sin\theta \sin i \end{bmatrix} \tag{2.36}$$

where i and θ are functions of time and are given explicitly in the Schweighart-Sedwick formulation by the following equations (refer to Appendix B):

$$i(t) = i_{ref} - \frac{3}{2}\left(\frac{n}{k}\right) J_2 \left(\frac{R_e}{r_{ref}}\right)^2 \cos i_{ref} \sin i_{ref} \sin^2(kt) \tag{2.37}$$

$$\theta(t) = k\,t \tag{2.38}$$

Making the appropriate substitutions, the relative velocity is transformed to a function of the newly defined dimensionless variables $\hat{x}, \hat{y}, \hat{z}, \text{and } \tau$:

$$\mathbf{v}_{spacecraft_{rel}} = n_0 d \begin{bmatrix} \hat{x}' - \hat{y}\left(\dfrac{n}{n_0}c - \dfrac{\omega_e}{n_0}\cos i\right) - \hat{z}\dfrac{\omega_e}{n_0}\cos\theta \sin i \\ \hat{y}' + \left(\dfrac{r_{ref}}{d} + \hat{x}\right)\left(\dfrac{n}{n_0}c - \dfrac{\omega_e}{n_0}\cos i\right) + \hat{z}\dfrac{\omega_e}{n_0}\sin\theta \sin i \\ \hat{z}' + \left(\dfrac{r_{ref}}{d} + \hat{x}\right)\dfrac{\omega_e}{n_0}\cos\theta \sin i - \hat{y}\dfrac{\omega_e}{n_0}\sin\theta \sin i \end{bmatrix} \tag{2.39}$$

Now each of the terms inside the brackets is a dimensionless quantity. In order to simplify subsequent expressions, another dimensionless quantity will now be defined:

$$\hat{\omega}_e \equiv \omega_e / n_0 \tag{2.40}$$

The $\mathbf{v}_{spacecraft_{rel}}$ expression can now be written as:

$$\mathbf{v}_{spacecraft_{rel}} = n_0 d \begin{bmatrix} \hat{x}' - \hat{y}\left(\hat{n}c - \hat{\omega}_e \cos i\right) - \hat{z}\,\hat{\omega}_e \cos\theta \sin i \\ \hat{y}' + \left(\dfrac{r_{ref}}{d} + \hat{x}\right)\left(\hat{n}c - \hat{\omega}_e \cos i\right) + \hat{z}\,\hat{\omega}_e \sin\theta \sin i \\ \hat{z}' + \left(\dfrac{r_{ref}}{d} + \hat{x}\right)\hat{\omega}_e \cos\theta \sin i - \hat{y}\,\hat{\omega}_e \sin\theta \sin i \end{bmatrix} \tag{2.41}$$

The inclination i and argument of latitude θ can also be written as a function of τ as follows:

$$i(\tau) = i_{ref} - \frac{3}{2}\frac{J_2}{\hat{k}}\left(\frac{R_e}{r_{ref}}\right)^2 \cos i_{ref} \sin i_{ref} \sin^2(\hat{k}\,\tau) \tag{2.42}$$

$$\theta(\tau) = \hat{k}\,\tau \tag{2.43}$$

At this point, a new velocity parameter vector whose components are dimensionless will be defined:

$$\hat{\mathbf{v}}_{spacecraft_{rel}} = \begin{bmatrix} \hat{x}' - \hat{y}\left(\hat{n}c - \hat{\omega}_e \cos i\right) - \hat{z}\,\hat{\omega}_e \cos\theta \sin i \\ \hat{y}' + \left(\frac{r_{ref}}{d} + \hat{x}\right)\left(\hat{n}c - \hat{\omega}_e \cos i\right) + \hat{z}\,\hat{\omega}_e \sin\theta \sin i \\ \hat{z}' + \left(\frac{r_{ref}}{d} + \hat{x}\right)\hat{\omega}_e \cos\theta \sin i - \hat{y}\,\hat{\omega}_e \sin\theta \sin i \end{bmatrix} \tag{2.44}$$

where $\hat{\mathbf{v}}_{spacecraft_{rel}}$ can be thought of as the dimensionless $\hat{x}, \hat{y}, \hat{z}$ components of the spacecraft relative velocity expressed in the Hill frame. The non-dimensionalized aerodynamic drag equations can now be written as:

$$\hat{\mathbf{f}}_{Drag} = -\frac{1}{2}\rho\left(\frac{1}{n_0^2 d}\right)\frac{C_D A}{m}\left[n_0 d\left\|\hat{\mathbf{v}}_{spacecraft_{rel}}\right\|\right]\left[n_0 d\,\hat{\mathbf{v}}_{spacecraft_{rel}}\right] \tag{2.45}$$

which further simplifies to:

$$\hat{\mathbf{f}}_{Drag} = -\frac{1}{2}\left(\rho\frac{C_D A}{m}d\right)\left\|\hat{\mathbf{v}}_{spacecraft_{rel}}\right\|\hat{\mathbf{v}}_{spacecraft_{rel}} \tag{2.46}$$

Another dimensionless parameter will now be defined which can be thought of as a normalized ballistic coefficient β:

$$\beta = \left(\rho\frac{C_D A}{m}r_{ref}\right)^{-1} \tag{2.47}$$

Note that the ballistic coefficient B is classically defined as:

$$B = \left(\frac{C_D A}{m}\right)^{-1} \tag{2.48}$$

which has units of kg/m^2 in the SI system.

The final dimensionless drag expression can now be written in the following form:

$$\hat{\mathbf{f}}_{Drag} = -\frac{1}{2}\frac{1}{\beta}\left(\frac{d}{r_{ref}}\right)\left\|\hat{\mathbf{v}}_{spacecraft_{rel}}\right\|\hat{\mathbf{v}}_{spacecraft_{rel}} \tag{2.49}$$

where β and the components of $\hat{\mathbf{v}}_{spacecraft_{rel}}$ are all dimensionless quantities.

2.4 Linearizing the Dimensionless Drag Expression

In this section, the non-dimesionalized drag expression will be simplified and linearized. The physical reasons as to why the linearization is valid will be discussed during the process. From the previous section, the non-dimensionalized drag expression is given by the following:

$$\hat{\mathbf{f}}_{Drag} = -\frac{1}{2}\frac{1}{\beta}\left(\frac{d}{r_{ref}}\right)\left\|\hat{\mathbf{v}}_{spacecraft_{rel}}\right\|\hat{\mathbf{v}}_{spacecraft_{rel}} \tag{2.50}$$

In order to simplify this expression, the non-dimensionalized relative velocity term $\hat{\mathbf{v}}_{spacecraft_{rel}}$ will be split up into two vectors: one which contains all of the zeroeth order terms and another which contains all the first order terms in $\hat{x}, \hat{y}, \hat{z}, \hat{x}', \hat{y}', \hat{z}'$. Also, the subscript $spacecraft_{rel}$ will be dropped in this section for notational simplicity. Thus, the non-dimensionalized spacecraft velocity vector relative to the rotating atmosphere will be defined as:

$$\hat{\mathbf{v}}_{spacecraft_{rel}} \equiv \mathbf{v} \equiv \mathbf{v}_0 + \mathbf{v}_1 \tag{2.51}$$

where $\mathbf{v}_0$ and $\mathbf{v}_1$ represent the zeroth and first order terms in $\hat{x}, \hat{y}, \hat{z}, \hat{x}', \hat{y}', \hat{z}'$ respectively and are defined as follows:

$$\mathbf{v}_0 = \begin{bmatrix} 0 \\ \frac{r_{ref}}{d}\left(\hat{n}c - \hat{\omega}_e \cos i\right) \\ \frac{r_{ref}}{d}\hat{\omega}_e \cos\theta \sin i \end{bmatrix} \tag{2.52}$$

$$\mathbf{v}_1 = \begin{bmatrix} \hat{x}' - \hat{y}\left(\hat{n}c - \hat{\omega}_e \cos i\right) - \hat{z}\,\hat{\omega}_e \cos\theta \sin i \\ \hat{y}' + \hat{x}\left(\hat{n}c - \hat{\omega}_e \cos i\right) + \hat{z}\,\hat{\omega}_e \sin\theta \sin i \\ \hat{z}' + \hat{x}\,\hat{\omega}_e \cos\theta \sin i - \hat{y}\,\hat{\omega}_e \sin\theta \sin i \end{bmatrix} \tag{2.53}$$

In order to linearize the drag expression, we must linearize the $\|\mathbf{v}\|\mathbf{v}$ term. By definition, this term is given by:

$$\|\mathbf{v}\|\mathbf{v} \equiv \|\mathbf{v}_0 + \mathbf{v}_1\|(\mathbf{v}_0 + \mathbf{v}_1) \tag{2.54}$$

This expression can be expanded using the definition of the vector norm as follows:

$$\|\mathbf{v}_0 + \mathbf{v}_1\| = \left[(\mathbf{v}_0 + \mathbf{v}_1)\cdot(\mathbf{v}_0 + \mathbf{v}_1)\right]^{\frac{1}{2}}$$

$$\|\mathbf{v}_0 + \mathbf{v}_1\| = \left[\mathbf{v}_0 \cdot \mathbf{v}_0 + 2\,\mathbf{v}_0 \cdot \mathbf{v}_1 + \mathbf{v}_1 \cdot \mathbf{v}_1\right]^{\frac{1}{2}} \tag{2.55}$$

$$\|\mathbf{v}_0 + \mathbf{v}_1\| = \left[\,\|\mathbf{v}_0\|^2 + 2\,\mathbf{v}_0 \cdot \mathbf{v}_1 + \|\mathbf{v}_1\|^2\,\right]^{\frac{1}{2}}$$

The $\|\mathbf{v}\|\mathbf{v}$ expression can thus be re-written in the following form:

$$\|\mathbf{v}_0 + \mathbf{v}_1\|(\mathbf{v}_0 + \mathbf{v}_1) = \left[\,\|\mathbf{v}_0\|^2 + 2\mathbf{v}_0 \cdot \mathbf{v}_1 + \|\mathbf{v}_1\|^2\,\right]^{\frac{1}{2}}(\mathbf{v}_0 + \mathbf{v}_1) \tag{2.56}$$

A binomial series expansion will now be used in order to linearize the square root term. Recall that the binomial series expansion of $(1+\alpha)^k$ is given by the following:

$$(1+\alpha)^k = \sum_{n=0}^{\infty}\binom{k}{n}\alpha^n = 1 + k\alpha + \frac{k(k-1)}{2!}\alpha^2 + \ldots \tag{2.57}$$

First, the square root term must be written in the form $(1+\alpha)^k$:

$$\|\mathbf{v}_0 + \mathbf{v}_1\|(\mathbf{v}_0 + \mathbf{v}_1) = \|\mathbf{v}_0\|\left(1 + \frac{2\,\mathbf{v}_0 \cdot \mathbf{v}_1}{\|\mathbf{v}_0\|^2} + \frac{\|\mathbf{v}_1\|^2}{\|\mathbf{v}_0\|^2}\right)^{\frac{1}{2}}(\mathbf{v}_0 + \mathbf{v}_1) \tag{2.58}$$

Taking a binomial series expansion of the square root term results in the following:

$$\|\mathbf{v}_0+\mathbf{v}_1\|(\mathbf{v}_0+\mathbf{v}_1)\approx\|\mathbf{v}_0\|\left(1+\frac{\mathbf{v}_0\cdot\mathbf{v}_1}{\|\mathbf{v}_0\|^2}+\ldots\right)(\mathbf{v}_0+\mathbf{v}_1) \tag{2.59}$$

where the higher order terms are considered to be negligible. The physical reason as to why these terms are negligible is simple, the $\mathbf{v}_0$ is much larger in magnitude than the $\mathbf{v}_1$ term. Comparing the $\mathbf{v}_0$ to the $\mathbf{v}_1$ term is in effect comparing the absolute velocity of the Chief spacecraft with respect to the center of the Earth with the relative velocity of a Deputy spacecraft with respect to the Chief. Since both spacecraft are in similar orbits, we would expect relative velocities to be small in comparison to absolute velocities. Thus, multiplying out and again neglecting the higher order terms this simplifies to the following linear expression in *x-y-z* :

$$\|\mathbf{v}_0+\mathbf{v}_1\|(\mathbf{v}_0+\mathbf{v}_1)\approx\|\mathbf{v}_0\|\mathbf{v}_0+\|\mathbf{v}_0\|\mathbf{v}_1+\left(\frac{\mathbf{v}_0\cdot\mathbf{v}_1}{\|\mathbf{v}_0\|}\right)\mathbf{v}_0 \tag{2.60}$$

where each term will be examined and simplified individually:

First, the $\|\mathbf{v}_0\|$ term can be approximated as follows:

$$\|\mathbf{v}_0\|=\sqrt{{v_{0,y}}^2+{v_{0,z}}^2}$$

$$\|\mathbf{v}_0\|=\frac{r_{ref}}{d}\sqrt{(\hat{n}c-\hat{\omega}_e\cos i)^2+(\hat{\omega}_e\cos\theta\sin i)^2} \tag{2.61}$$

$$\|\mathbf{v}_0\|\approx\frac{r_{ref}}{d}(\hat{n}c-\hat{\omega}_e\cos i)=v_{0,y}$$

This approximation is based on the fact that the $(\hat{n}c-\hat{\omega}_e\cos i)$ term is of the order of 1 and the $(\hat{\omega}_e\cos\theta\sin i)$ term is on the order of maximum 10^{-2}. Also, $(\hat{n}c-\hat{\omega}_e\cos i)$ is always a positive quantity. Using this simplifying approximation, the remaining terms can be approximated as follows:

$$\|\mathbf{v}_0\|\mathbf{v}_0 \approx v_{0,y}\begin{bmatrix} 0 \\ v_{0,y} \\ v_{0,z} \end{bmatrix} \tag{2.62}$$

$$\|\mathbf{v}_0\|\mathbf{v}_1 \approx v_{0,y}\begin{bmatrix} v_{1,x} \\ v_{1,y} \\ v_{1,z} \end{bmatrix} \tag{2.63}$$

$$\left(\frac{\mathbf{v}_0 \cdot \mathbf{v}_1}{\|\mathbf{v}_0\|}\right)\mathbf{v}_0 \approx \frac{1}{v_{0,y}}(\mathbf{v}_0 \cdot \mathbf{v}_1)\mathbf{v}_0 = \begin{bmatrix} 0 \\ v_{0,y}\, v_{1,y} + v_{0,z}\, v_{1,z} \\ v_{0,z}\, v_{1,y} + \dfrac{v_{0,z}^2}{v_{0,y}} v_{1,z} \end{bmatrix} \tag{2.64}$$

Bringing all of these terms together, the linearized approximation of the $\|\mathbf{v}\|\mathbf{v}$ expression simplifies to:

$$\|\mathbf{v}\|\mathbf{v} \approx \begin{bmatrix} v_{0,y} v_{1,x} \\ v_{0,y}^2 + 2v_{0,y} v_{1,y} + v_{0,z}\, v_{1,z} \\ v_{0,y} v_{0,z} + \left(v_{0,y} + \dfrac{v_{0,z}^2}{v_{0,y}}\right) v_{1,z} + v_{0,z} v_{1,y} \end{bmatrix} \tag{2.65}$$

Factoring out $v_{0,y}$ results in:

$$\|\mathbf{v}\|\mathbf{v} \approx v_{0,y}\begin{bmatrix} v_{1,x} \\ v_{0,y} + 2v_{1,y} + \dfrac{v_{0,z}}{v_{0,y}} v_{1,z} \\ v_{0,z} + \left(1 + \dfrac{v_{0,z}^2}{v_{0,y}^2}\right) v_{1,z} + \dfrac{v_{0,z}}{v_{0,y}} v_{1,y} \end{bmatrix} \tag{2.66}$$

As discussed earlier, the $v_{0,y}$ is much larger than the $v_{0,z}$, thus to simplify the expression, terms multiplied by $v_{0,z}/v_{0,y}$ will be neglected. This allows us to approximate $\|\mathbf{v}\|\mathbf{v}$ as follows:

$$\|\mathbf{v}\|\mathbf{v} \approx v_{0,y}\begin{bmatrix} v_{1,x} \\ v_{0,y}+2v_{1,y} \\ v_{0,z}+v_{1,z} \end{bmatrix} \tag{2.67}$$

The resulting linearized drag expression can now be written as:

$$\hat{\mathbf{f}}_{Drag} \approx -\frac{1}{2}\frac{1}{\beta}\frac{d}{r_{ref}}v_{0,y}\begin{bmatrix} v_{1,x} \\ v_{0,y}+2v_{1,y} \\ v_{0,z}+v_{1,z} \end{bmatrix} \tag{2.68}$$

For notational simplicity, the following parameters will be defined and non-dimensionalized:

$$\begin{aligned} \sigma &\equiv nc - \omega_e \cos i \\ \hat{\sigma} &\equiv \sigma/n_0 = \hat{n}c - \hat{\omega}_e \cos i \end{aligned} \tag{2.69}$$

and

$$\begin{aligned} \varsigma &\equiv \omega_e \sin i \\ \hat{\varsigma} &\equiv \varsigma/n_0 = \hat{\omega}_e \sin i \end{aligned} \tag{2.70}$$

When all variable substitutions are made, the final expression for linearized drag is obtained:

$$\hat{\mathbf{f}}_{Drag} \approx -\frac{1}{2}\frac{1}{\beta}\left(\frac{d}{r_{ref}}\right)\hat{\sigma}\begin{bmatrix} \hat{x}' - \hat{y}\,\hat{\sigma} - \hat{z}\,\hat{\varsigma}\cos\theta \\ \frac{r_{ref}}{d}\hat{\sigma} + 2\left(\hat{y}' + \hat{x}\,\hat{\sigma} + \hat{z}\,\hat{\varsigma}\sin\theta\right) \\ \frac{r_{ref}}{d}\hat{\varsigma}\cos\theta + \hat{z}' + \hat{x}\,\hat{\varsigma}\cos\theta - \hat{y}\,\hat{\varsigma}\sin\theta \end{bmatrix} \tag{2.71}$$

2.5 Final Equations of Motion

In this section, the final linearized equations of motion which are valid for circular orbits will be presented. The linearized aerodynamic drag expression determined in the previous section will be included in the Schweighart-Sedwick equations and the resulting equations of the linear dynamic system will be determined in matrix-vector form.

The first step in this analysis is to examine the relative linearized drag equation. The linearized aerodynamic drag expression given in the previous section describes the drag effect on a particular spacecraft with respect to an unperturbed circular reference orbit, i.e. a reference orbit which is not disturbed by aerodynamic drag effects. In order to model the relative drag effects between two spacecraft, their equations of motion with respect to the reference orbit must be differenced. Thus, the relative drag effects are given by the following:

$$\Delta\hat{\mathbf{f}}_{Drag} = \hat{\mathbf{f}}_{Drag,Deputy} - \hat{\mathbf{f}}_{Drag,Chief} \tag{2.72}$$

Using the result obtained in the previous section, this may be approximated as:

$$\Delta\hat{\mathbf{f}}_{Drag} \approx -\frac{1}{2}\frac{d}{r_{ref}} v_{0,y} \left\{ \left(\frac{1}{\beta} \begin{bmatrix} v_{1,x} \\ v_{0,y} + 2v_{1,y} \\ v_{0,z} + v_{1,z} \end{bmatrix} \right)_{Deputy} - \left(\frac{1}{\beta} \begin{bmatrix} v_{1,x} \\ v_{0,y} + 2v_{1,y} \\ v_{0,z} + v_{1,z} \end{bmatrix} \right)_{Chief} \right\} \tag{2.73}$$

where the parameters which define the normalized ballistic coefficient β, i.e. physical spacecraft characteristics as well as local atmospheric density are not necessarily the same.

The first case that will be considered is when both spacecraft share the same physical parameters and thus the same normalized ballistic coefficient β. The assumption that ρ is approximately the same for both spacecraft will be made in

order to simplify the analysis. When circular orbits of the same radii are considered, the altitudes of the two spacecraft are the same and theoretically speaking local density should also be the same (refer to Appendix C for the exponential atmospheric density model). Although there are several other factors which determine local density, such and solar and geomagnetic activity levels, when spacecraft formations are in close proximity density differences are likely small and this approximation can be applicable in many situations. For this special case, the above linearized differential drag expression simplifies to:

$$\Delta\hat{\mathbf{f}}_{Drag} \approx -\frac{1}{2}\frac{1}{\beta}\left(\frac{d}{r_{ref}}\right) v_{0,y} \begin{bmatrix} \Delta v_{1,x} \\ 2\Delta v_{1,y} \\ \Delta v_{1,z} \end{bmatrix} \tag{2.74}$$

where the constant terms cancel out and the Δv terms are defined as follows:

$$\Delta v_{1,x} = \Delta\hat{x}' - \Delta\hat{y}\left(\hat{n}c - \hat{\omega}_e \cos i\right) - \Delta\hat{z}\,\hat{\omega}_e \cos\theta \sin i \tag{2.75}$$

$$\Delta v_{1,y} = \Delta\hat{y}' + \Delta\hat{x}\left(\hat{n}c - \hat{\omega}_e \cos i\right) + \Delta\hat{z}\,\hat{\omega}_e \sin\theta \sin i \tag{2.76}$$

$$\Delta v_{1,z} = \Delta\hat{z}' + \Delta\hat{x}\,\hat{\omega}_e \cos\theta \sin i - \Delta\hat{y}\,\hat{\omega}_e \sin\theta \sin i \tag{2.77}$$

where $\Delta\hat{x} = \hat{x}_{Deputy} - \hat{x}_{Chief}$, $\Delta\hat{y} = \hat{y}_{Deputy} - \hat{y}_{Chief}$, and so on.

The next step is to add this linearized differential drag model into the relative motion equations given by Schweighart and Sedwick (2002). This will result in a set of linearized differential equations which describe the relative motion between two spacecraft while taking into account the effects of both J_2 and aerodynamic drag perturbations which are valid for circular reference orbits. These relative motion equations are given by:

$$\Delta\hat{x}'' - 2\hat{n}c\,\Delta\hat{y}' - (5c^2 - 2)\hat{n}^2\Delta\hat{x} - \Delta f_{Drag_{N.D.},x} = 0 \tag{2.78}$$

$$\Delta\hat{y}'' + 2\hat{n}c\,\Delta\hat{x}' - \Delta f_{Drag_{N.D.},y} = 0 \tag{2.79}$$

$$\Delta\hat{z}'' + \hat{q}^2\Delta\hat{z} - \Delta f_{Drag_{N,D},z} = 2\hat{q}\left(\frac{l}{n_0\, d}\right)\cos\left(\hat{q}\tau + \varphi\right) \tag{2.80}$$

The resulting system of linear differential equations can be written in matrix form as follows:

$$\mathbf{M}\,\Delta\hat{\mathbf{x}}'' + \mathbf{C}\,\Delta\hat{\mathbf{x}}' + \mathbf{K}\,\Delta\hat{\mathbf{x}} = \mathbf{f} \tag{2.81}$$

where

$$\Delta\hat{\mathbf{x}} \equiv \begin{bmatrix} \Delta\hat{x} \\ \Delta\hat{y} \\ \Delta\hat{z} \end{bmatrix} \tag{2.82}$$

$$\mathbf{f} = \begin{bmatrix} 0 \\ 0 \\ 2\hat{q}\left(\dfrac{l}{n_0\, d}\right)\cos\left(\hat{q}\,\tau + \varphi\right) \end{bmatrix} \tag{2.83}$$

the generalized inertia matrix $\mathbf{M}$ is in this case the identity matrix $\mathbf{I}$:

$$\mathbf{M} = \mathbf{I} \equiv \begin{bmatrix} 1 & 0 & 0 \\ 0 & 1 & 0 \\ 0 & 0 & 1 \end{bmatrix} \tag{2.84}$$

the stiffness matrix $\mathbf{K}$ is found to be:

$$\mathbf{K} = \begin{bmatrix} -(5c^2 - 2)\hat{n}^2 & -\dfrac{1}{2}\dfrac{1}{\beta}\hat{\sigma}^2 & -\dfrac{1}{2}\dfrac{1}{\beta}\hat{\sigma}\hat{\varsigma}\cos\theta \\ \dfrac{1}{\beta}\hat{\sigma}^2 & 0 & \dfrac{1}{\beta}\hat{\sigma}\hat{\varsigma}\sin\theta \\ \dfrac{1}{2}\dfrac{1}{\beta}\hat{\sigma}\hat{\varsigma}\cos\theta & -\dfrac{1}{2}\dfrac{1}{\beta}\hat{\sigma}\hat{\varsigma}\sin\theta & \hat{q}^2 \end{bmatrix} \tag{2.85}$$

and the damping matrix $\mathbf{C}$ is found to be:

$$\mathbf{C} = \begin{bmatrix} \frac{1}{2}\frac{1}{\beta}\hat{\sigma} & -2\hat{n}c & 0 \\ 2\hat{n}c & \frac{1}{\beta}\hat{\sigma} & 0 \\ 0 & 0 & \frac{1}{2}\frac{1}{\beta}\hat{\sigma} \end{bmatrix} \tag{2.86}$$

It should be noted that this system can be easily written in state-space form as follows:

$$\Delta\mathbf{X}' = \mathbf{A}\,\Delta\mathbf{X} + \mathbf{W} \tag{2.87}$$

where

$$\Delta\mathbf{X} = \begin{bmatrix} \Delta\mathbf{x} \\ \Delta\mathbf{x}' \end{bmatrix} \tag{2.88}$$

$$\mathbf{A} = \begin{bmatrix} \mathbf{0}_{3\times3} & \mathbf{M} \\ -\mathbf{K} & -\mathbf{C} \end{bmatrix} \tag{2.89}$$

$$\mathbf{W} = \begin{bmatrix} \mathbf{0}_{3\times1} \\ \mathbf{f} \end{bmatrix} \tag{2.90}$$

2.6 Stability Analysis

One of the objectives of this thesis is to assess the capability of drag as a means of formation maintenance and control. Although such a control law will not be developed here, a preliminary stability analysis for the case where the two spacecraft can change their effective drag area will be carried out. This analysis will make use of the linear dynamic model developed in the previous sections.

2.6.1 Differential Drag Analysis

In this section, the case where the Chief and Deputy spacecraft can have different effective drag areas will be considered. Here, the two spacecraft physical parameters are assumed to be nominally the same. In other words, each spacecraft will be of the same mass m, drag coefficient C_D, and baseline drag area A_0. The Chief and Deputy will also be assumed to be sufficiently close such that the value of local atmospheric density ρ can be assumed to be essentially the same for both spacecraft.

Each spacecraft has a minimum baseline drag area of A_0 as well as the capability of rotating some aerodynamic panels to increase its effective drag area by an amount δA. The drag areas of the Chief and Deputy spacecraft will thus be defined as follows:

$$A_C \equiv A_0 + \delta A_C \tag{2.91}$$

$$A_D \equiv A_0 + \delta A_D \tag{2.92}$$

where the subscripts C and D denote Chief and Deputy respectively.

In order to model the relative drag effects between two spacecraft, their equations of motion with respect to the reference orbit must be differenced. Thus, as discussed in the previous section, the relative dimensionless drag effects are given by the following:

$$\Delta\hat{\mathbf{f}}_{Drag} = \hat{\mathbf{f}}_{Drag,Deputy} - \hat{\mathbf{f}}_{Drag,Chief} \tag{2.93}$$

This may be approximated using the linearized drag model developed previously in this chapter as follows:

$$\Delta\hat{\mathbf{f}}_{Drag} \approx -\frac{1}{2}\left(\frac{d}{r_{ref}}\right)v_{0,y}\left\{\frac{1}{\beta_D}\begin{bmatrix} v_{1,x_D} \\ v_{0,y}+2v_{1,y_D} \\ v_{0,z}+v_{1,z_D}\end{bmatrix} - \frac{1}{\beta_C}\begin{bmatrix} v_{1,x_C} \\ v_{0,y}+2v_{1,y_C} \\ v_{0,z}+v_{1,z_C}\end{bmatrix}\right\} \tag{2.94}$$

Using the new definitions of A_C and A_D, the above differential drag expression can be written as:

$$\begin{aligned}\Delta\hat{\mathbf{f}}_{Drag} \approx & -\frac{1}{2}\left(\frac{d}{r_{ref}}\right)v_{0,y}\left(\frac{\rho C_D r_{ref}}{m}\right) \\ & \times\left\{A_0\begin{bmatrix}\Delta v_{1,x} \\ 2\Delta v_{1,y} \\ \Delta v_{1,z}\end{bmatrix} + \delta A_D\begin{bmatrix} v_{1,x_D} \\ v_{0,y}+2v_{1,y_D} \\ v_{0,z}+v_{1,z_D}\end{bmatrix} - \delta A_C\begin{bmatrix} v_{1,x_C} \\ v_{0,y}+2v_{1,y_C} \\ v_{0,z}+v_{1,z_C}\end{bmatrix}\right\}\end{aligned} \tag{2.95}$$

It is advantageous to control the δA terms in such a way that they are related to the state vector of the particular spacecraft with respect to the reference orbit. The scalar δA terms are thus assumed to be related to the state vector of the spacecraft via a control gain matrix $\mathbf{G}$ as follows:

$$\delta A = \mathbf{G}\begin{bmatrix}\mathbf{x} \\ \dot{\mathbf{x}}\end{bmatrix} \tag{2.96}$$

where $\mathbf{G}$ will be of the form:

$$\mathbf{G} = \begin{bmatrix} g_1 & g_2 & g_3 & g_4 & g_5 & g_6\end{bmatrix} \tag{2.97}$$

In order to relate the change in area to dimensionless state variables, the δA expression can be written as follows:

$$\delta A = \mathbf{G}\begin{bmatrix}(d)\hat{\mathbf{x}} \\ (n_0 d)\hat{\mathbf{x}}'\end{bmatrix} \tag{2.98}$$

These constants can be absorbed into the gain matrix $\mathbf{G}$ and a new gain matrix $\mathbf{G}'$ can be defined:

$$\begin{aligned}\mathbf{G}' &= d\begin{bmatrix} g_1 & g_2 & g_3 & n_0\, g_4 & n_0\, g_5 & n_0\, g_6\end{bmatrix} \\ \mathbf{G}' &= \begin{bmatrix} g_1' & g_2' & g_3' & g_4' & g_5' & g_6'\end{bmatrix}\end{aligned} \tag{2.99}$$

Therefore, the increase in area δA can be related to the dimensionless state variables as follows:

$$\delta A = \mathbf{G}' \begin{bmatrix} \hat{\mathbf{x}} \\ \hat{\mathbf{x}}' \end{bmatrix} \tag{2.100}$$

With this knowledge of the form of the δA expressions, substituting into the $\Delta\hat{\mathbf{f}}_{Drag}$ equation and linearizing results in the following:

$$\Delta\hat{\mathbf{f}}_{Drag} = -\frac{1}{2}\left(\frac{d}{r_{ref}}\right) v_{0,y} \left(\frac{\rho C_D r_{ref}}{m}\right) \left\{ A_0 \begin{bmatrix} \Delta v_{1,x} \\ 2\Delta v_{1,y} \\ \Delta v_{1,z} \end{bmatrix} + \left(\delta A_D - \delta A_C\right) \begin{bmatrix} 0 \\ v_{0,y} \\ v_{0,z} \end{bmatrix} \right\} \tag{2.101}$$

and in terms of gain matrices this can also be written as:

$$\begin{aligned} \Delta\hat{\mathbf{f}}_{Drag} = & -\frac{1}{2}\left(\frac{d}{r_{ref}}\right) v_{0,y} \left(\frac{\rho C_D r_{ref}}{m}\right) \\ & \times \left\{ A_0 \begin{bmatrix} \Delta v_{1,x} \\ 2\Delta v_{1,y} \\ \Delta v_{1,z} \end{bmatrix} + \left(\mathbf{G}'_D \begin{bmatrix} \hat{\mathbf{x}}_D \\ \hat{\mathbf{x}}'_D \end{bmatrix} - \mathbf{G}'_C \begin{bmatrix} \hat{\mathbf{x}}_C \\ \hat{\mathbf{x}}'_C \end{bmatrix} \right) \begin{bmatrix} 0 \\ v_{0,y} \\ v_{0,z} \end{bmatrix} \right\} \end{aligned} \tag{2.102}$$

If the gain matrices for both the Chief and Deputy spacecraft are assumed to be the same, then the differential area between the two spacecraft can be written in terms of the relative state vector as follows:

$$\Delta\hat{\mathbf{f}}_{Drag} = -\frac{1}{2}\left(\frac{d}{r_{ref}}\right) v_{0,y} \left(\frac{\rho C_D r_{ref}}{m}\right) \left\{ A_0 \begin{bmatrix} \Delta v_{1,x} \\ 2\Delta v_{1,y} \\ \Delta v_{1,z} \end{bmatrix} + \left(\mathbf{G}' \begin{bmatrix} \Delta\hat{\mathbf{x}} \\ \Delta\hat{\mathbf{x}}' \end{bmatrix} \right) \begin{bmatrix} 0 \\ v_{0,y} \\ v_{0,z} \end{bmatrix} \right\} \tag{2.103}$$

which can also be written as:

$$\Delta\hat{\mathbf{f}}_{Drag} = -\frac{1}{2}\left(\frac{d}{r_{ref}}\right) \frac{1}{\beta_0} v_{0,y} \left\{ \begin{bmatrix} \Delta v_{1,x} \\ 2\Delta v_{1,y} \\ \Delta v_{1,z} \end{bmatrix} + \left(\frac{\delta A_D - \delta A_C}{A_0}\right) \begin{bmatrix} 0 \\ v_{0,y} \\ v_{0,z} \end{bmatrix} \right\} \tag{2.104}$$

where β_0 represents the normalized ballistic coefficient corresponding to the baseline area A_0. The first vector in the brackets summarizes the linearized drag

effect on the formation and the second vector represents a control input variable which acts in the in-track and cross-track directions only. It should be noted, however, that the input from the in-track direction is much larger than that of the cross-track direction for a given difference of area $\delta A_D - \delta A_C$.

2.6.2 Eigenvalue Analysis

In this section, the eigenvalues of the controlled system presented in the last section will be determined for the special case of a marginally stable system.

When control gains are included in the equations of motion, the matrices **C** and **K** will have additional terms included in them related to control gain matrix terms. The **M** matrix will remain unchanged as the 3×3 identity matrix. In order to simplify subsequent expressions, the following parameters related to the control variables will be defined:

$$\kappa_y \equiv \frac{1}{2}\frac{1}{\beta_0}\frac{1}{A_0}\hat{\sigma}^2\left(\frac{r_{ref}}{d}\right) \tag{2.105}$$

$$\kappa_z \equiv \frac{1}{2}\frac{1}{\beta_0}\frac{1}{A_0}\hat{\sigma}\hat{\varsigma}\left(\frac{r_{ref}}{d}\right) \tag{2.106}$$

The controlled stiffness matrix **K** is now found to be:

$$\mathbf{K} = \begin{bmatrix} -(5c^2-2)\hat{n}^2 & -\frac{1}{2}\frac{1}{\beta_0}\hat{\sigma}^2 & -\frac{1}{2}\frac{1}{\beta_0}\hat{\sigma}\hat{\varsigma}\cos\theta \\ \frac{1}{\beta_0}\hat{\sigma}^2 + g_1'\kappa_y & g_2'\kappa_y & \frac{1}{\beta_0}\hat{\sigma}\hat{\varsigma}\sin\theta + g_3'\kappa_y \\ \frac{1}{2}\frac{1}{\beta_0}\hat{\sigma}\hat{\varsigma}\cos\theta + g_1'\kappa_z & -\frac{1}{2}\frac{1}{\beta_0}\hat{\sigma}\hat{\varsigma}\sin\theta + g_2'\kappa_z & \hat{q}^2 + g_3'\kappa_z \end{bmatrix} \tag{2.107}$$

and the controlled damping matrix **C** is:

$$\mathbf{C} = \begin{bmatrix} \frac{1}{2}\frac{1}{\beta_0}\hat{\sigma} & -2\hat{n}c & 0 \\ 2\hat{n}c + g_4'\kappa_y & \frac{1}{\beta_0}\hat{\sigma} + g_5'\kappa_y & g_6'\kappa_y \\ g_4'\kappa_z & g_5'\kappa_z & \frac{1}{2}\frac{1}{\beta_0}\hat{\sigma} + g_6'\kappa_z \end{bmatrix} \tag{2.108}$$

What will be considered here is the in-plane (x-y) problem. The terms coupling of the in-plane (x-y) with the out-of-plane equations (z-equation) are small in comparison to the other terms in the matrices and will thus be neglected in this analysis. Since this is the case, in the stiffness matrix $\mathbf{K}$ the g_3' term can thus simply be set equal to zero and similarly for the damping matrix $\mathbf{C}$ the g_6' term will also be set equal to zero. The effect that a change in area will have on the z motion will be small in comparison to that on the y due to the difference in magnitudes of $v_{0,y}$ and $v_{0,z}$. For the in-plane case, the stiffness matrix $\mathbf{K}$ is top right 2×2 matrix of the full $\mathbf{K}$ matrix:

$$\mathbf{K} = \begin{bmatrix} -(5c^2 - 2)\hat{n}^2 & -\frac{1}{2}\frac{1}{\beta_0}\hat{\sigma}^2 \\ \frac{1}{\beta_0}\hat{\sigma}^2 + g_1'\kappa_y & g_2'\kappa_y \end{bmatrix} \tag{2.109}$$

and similarly, the damping matrix $\mathbf{C}$ is:

$$\mathbf{C} = \begin{bmatrix} \frac{1}{2}\frac{1}{\beta_0}\hat{\sigma} & -2\hat{n}c \\ 2\hat{n}c + g_4'\kappa_y & \frac{1}{\beta_0}\hat{\sigma} + g_5'\kappa_y \end{bmatrix} \tag{2.110}$$

The solution to this system of linear differential equations is known to take the following form:

$$\Delta\mathbf{x} = \mathbf{u}e^{\lambda t} \tag{2.111}$$

where $\Delta\mathbf{x}$ represents the relative position vector of the Deputy with respect to the Chief, $e^{(\cdot)}$ denotes the exponential function, λ is in general a constant complex

number, t is the given time, and $\mathbf{u}$ is a 3×1 vector of constants. Substituting this solution into this linear system results in the following:

$$\begin{aligned}\mathbf{M}\lambda^2\mathbf{u}e^{\lambda t}+\mathbf{C}\lambda\mathbf{u}e^{\lambda t}+\mathbf{K}\mathbf{u}e^{\lambda t}&=\mathbf{0}\\ \left(\mathbf{M}\lambda^2+\mathbf{C}\lambda+\mathbf{K}\right)\mathbf{u}&=\mathbf{0}\end{aligned} \tag{2.112}$$

The above equation represents a set of linear homogeneous equations. For non-trivial solution, the determinant of the coefficients of $\mathbf{u}$ must vanish. We therefore have:

$$\left|\mathbf{M}\lambda^2+\mathbf{C}\lambda+\mathbf{K}\right|=0 \tag{2.113}$$

which is the characteristic equation of the system. The roots of this equation are the eigenvalues of the linear system. To simplify this expression, we can write it as:

$$\begin{aligned}\left|\begin{bmatrix}1&0\\0&1\end{bmatrix}\lambda^2+\begin{bmatrix}A&B\\C&D\end{bmatrix}\lambda+\begin{bmatrix}E&F\\G&H\end{bmatrix}\right|&=0\\ \begin{vmatrix}\lambda^2+A\lambda+E & B\lambda+F\\ C\lambda+G & \lambda^2+D\lambda+H\end{vmatrix}&=0\end{aligned} \tag{2.114}$$

which results in the following characteristic polynomial:

$$\begin{aligned}\lambda^4+(D+A)\lambda^3+(H+AD+E-BC)\lambda^2\\ +(DE-CF-GB+AH)\lambda+(HE-GF)=0\end{aligned} \tag{2.115}$$

Asymptotic stability occurs when the general complex roots of this equation include a negative real part since this represents exponential decay. However, the full closed form solution to this equation is not so straight forward and thus makes finding such roots analytically very difficult. However, marginal stability (purely complex roots) can be achieved if the third and first order terms of the polynomial are set to zero using the control gain matrix terms. This essentially results in reducing the solution of the quartic equation to that of a more manageable quadratic equation and will thus be the case considered in this analysis.

Setting the third order coefficient to zero requires the following:

$$\begin{gathered}\left(D+A\right)=0\\ \left(\frac{1}{\beta_0}\hat{\sigma}+g_5'\kappa_y+\frac{1}{2}\frac{1}{\beta_0}\hat{\sigma}\right)=0\end{gathered} \tag{2.116}$$

which yields the following expression for g_5':

$$g_5'=-3A_0\frac{d}{\hat{\sigma}\,r_{ref}} \tag{2.117}$$

Thus, g_5 is determined as:

$$\begin{gathered}g_5=\frac{g_5'}{n_0 d}\\ g_5=-3A_0\frac{1}{r_{ref}}\frac{1}{\left(nc-\omega_e\cos i\right)}\end{gathered} \tag{2.118}$$

From the first order term, we require the following:

$$\begin{gathered}\left(DE-CF-GB+AH\right)=0\\ \left[\frac{1}{\beta_0}\hat{\sigma}+g_5'\kappa_y\right]\left[-(5c^2-2)\hat{n}^2\right]\\ \quad+\frac{1}{2}\frac{1}{\beta_0}\hat{\sigma}^2\left[2\hat{n}c+g_4'\kappa_y\right]+2\hat{n}c\left[\frac{1}{\beta_0}\hat{\sigma}^2+g_1'\kappa_y\right]\\ \quad+\left[-\left(5c^2-2\right)\hat{n}^2\,g_2'\,\kappa_y\right]=0\end{gathered} \tag{2.119}$$

which simplifies to:

$$g_4'\kappa_y\hat{\sigma}^2+4\,\hat{n}\,c\,g_1'\,\beta_0\kappa_y=-\hat{\sigma}(5c^2-2)\hat{n}^2-6\hat{n}c\hat{\sigma}^2 \tag{2.120}$$

In this case, selection of the gain values is not so straight forward. Essentially, if we set one of these two unknowns equal to zero we can choose either a proportional response g_1' or a derivative response g_4'. Choosing a proportional response, we set g_4' to be equal to zero. From this, a value for g_1' can be determined:

$$g_1' = -\frac{A_0}{2\hat{n}c\hat{\sigma}}\frac{d}{r_{ref}}\left[(5c^2-2)\hat{n}^2 + 6\hat{n}c\hat{\sigma}\right] \tag{2.121}$$

Using this, we can find an expression for g_1:

$$\begin{aligned} g_1 &= \frac{g_1'}{d} \\ g_1 &= -\frac{A_0}{(2nc^2 - 2c\omega_e\cos i)}\frac{1}{r_{ref}}\left[11nc^2 - 2n - 6c\omega_e\cos i\right] \end{aligned} \tag{2.122}$$

This leaves us with one more proportional control gain related to the relative y displacement (g_2) to be determined. With the other gains now specified, the characteristic polynomial becomes:

$$\lambda^4 + \left(H + AD + E - BC\right)\lambda^2 + \left(HE - GF\right) = 0 \tag{2.123}$$

where

$$\left(H + AD + E - BC\right) = g_2'\kappa_y - \frac{1}{4}\frac{1}{\beta_0^2}\hat{\sigma}^2 - (c^2-2)\,\hat{n}^2 \tag{2.124}$$

and

$$\begin{aligned} &\left(HE - GF\right) = \\ &\left[g_2'\kappa_y + \frac{\hat{\sigma}}{4\hat{n}c\beta_0}\right]\left[\frac{1}{2}\frac{1}{\beta_0}\hat{\sigma} - (5c^2-2)\hat{n}^2\right] + \frac{\hat{\sigma}^2}{4\hat{n}c\beta_0}\left[\frac{1}{2}\frac{1}{\beta_0} - 6\hat{n}c\right] \end{aligned} \tag{2.125}$$

With marginal stability, the characteristic polynomial will have the following pairs of purely complex roots:

$$\lambda_{1,2} = \pm\frac{j}{\sqrt{2}}\sqrt{\left(H + AD + E - BC\right) + \sqrt{\left(H + AD + E - BC\right)^2 - 4\left(HE - GF\right)}} \tag{2.126}$$

$$\lambda_{3,4} = \pm\frac{j}{\sqrt{2}}\sqrt{\left(H + AD + E - BC\right) - \sqrt{\left(H + AD + E - BC\right)^2 - 4\left(HE - GF\right)}} \tag{2.127}$$

where $j = \sqrt{-1}$. This does give some range as to what the value of g_2 should take as the following condition must hold to ensure purely complex roots:

$$\left(H + AD + E - BC\right)^2 - 4\left(AH + HE - GF\right) > 0 \tag{2.128}$$

With this, all of the necessary gains can be determined. A summary of the entries of the control gain matrix is given below:

$$
\begin{aligned}
g_1 &= -\frac{A_0}{(2nc^2 - 2c\omega_e \cos i)} \frac{1}{r_{ref}} \left[11nc^2 - 2n - 6c\omega_e \cos i\right] \\
g_3 &= 0 \\
g_4 &= 0 \\
g_5 &= -3A_0 \frac{1}{r_{ref}} \frac{1}{(nc - \omega_e \cos i)} \\
g_6 &= 0
\end{aligned}
\tag{2.129}
$$

The remaining g_2 gain is determined in part from the condition given in equation 2.128 where $H = g_2' \kappa_y$ and is the only term which contains g_2'. Different values for this may need to tried and tested for effectiveness but all other gains have been specified.

Chapter 3 - Numerical Simulations for Circular Reference Orbits

In this section, numerical simulation results based on the equations developed in Chapter 2 will be presented. For these simulations, the Schweighart-Sedwick formulation with additional non-linear drag terms was used. This was done in order to increase modeling accuracy and to obtain results which can used as an accurate baseline for comparison in later chapters. The non-dimensionalized formulation developed in Chapter 2 was used for computational efficiency and robustness of numerical results.

These numerical simulations were performed using MATLAB©. The non-linear differential equations of motion were solved using MATLAB©'s `ode45` numerical integration function. This method employs an adaptive mixed $4^{\text{th}}/5^{\text{th}}$ order Runge-Kutta method which is known as the Dormand-Price method.

In all of these simulations, the local atmospheric density of each spacecraft was computed using the method described in Appendix C. This exponential atmospheric model, computes densities above an ellipsoidal model of the Earth to increase modeling accuracy.

3.1 Spacecraft Physical Parameters

In order to perform numerical simulations, values of spacecraft physical parameters must be specified in order to characterize drag effects. For this study, three different sets of spacecraft physical parameters were selected. Two were selected from actual formation flying and rendezvous mission designs and the other

is an invented set of parameters which was selected to showcase a more pronounced drag effect for a given altitude. These parameters will now be presented.

3.1.1 TECSAS Physical Parameters

The TECSAS mission was intended to be a technology demonstration mission which would validate hardware and software solutions needed in order to accomplish on-orbit satellite servicing missions (refer to Figure 3-1).

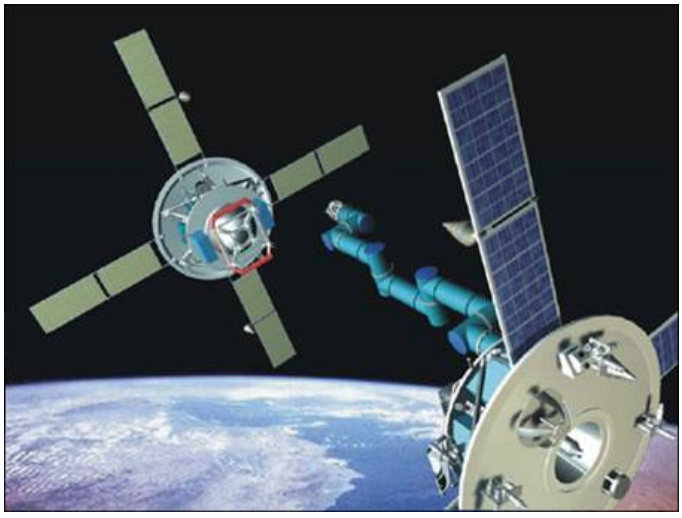

Figure 3-1: An artist's rendering of the TECSAS spacecraft (on-orbit servicing website)

This mission was scheduled for launch in 2009, and was a collaborative effort between the Canadian Space Agency (CSA), the German Space Center (DLR), and the Russian Babakin Space Center. Unfortunately, the program was cut and the TECSAS mission never flew. However, the design characteristics of this spacecraft make it ideal for analysis purposes since it represents a realistic set of physical

parameters which were intended to be used in a formation flying mission (refer to Table 3-1).

TECSAS Spacecraft Physical Parameters		
Parameter	**Value**	**Units**
mass	175	[kg]
Area	2.22	[m^2]
C_d	2.3	[-]
Ballistic Coeff.	34.27	[kg/m^2]

Table 3-1: TECSAS spacecraft physical parameters

3.1.2 JC2Sat Physical Parameters

As was mentioned earlier, JC2Sat is a collaborative formation flying mission between the Canadian Space Agency (CSA) and the Japan Aerospace Exploration Agency (JAXA) (refer to Figure 1-1 and 1-2). This technology demonstration mission plans to use differential drag as the primary means of formation maintenance and control, and it is slated to be launched in 2010.

The physical characteristics of JC2Sat given used here are based on the design documents released for the mission in August of 2009 (Shankar Kumar & Ng, 2009). These parameters are thus only approximate values and are summarized in Table 3-2 below:

JC2Sat Spacecraft Physical Parameters		
Parameter	**Value**	**Units**
mass	20	[kg]
Area	0.09	[m^2]
C_d	2.2	[-]
Ballistic Coeff.	202.02	[kg/m^2]

Table 3-2: JC2Sat spacecraft physical parameters

3.1.3 TEST Physical Parameters

Although, there is no clever name associated with this invented spacecraft, its physical parameters were designed in such a way as to increase the effect due to drag for a given altitude compared to JC2Sat and TECSAS. The TEST spacecraft physical parameters are given in Table 3-3 below:

TEST Spacecraft Physical Parameters		
Parameter	**Value**	**Units**
mass	175	[kg]
Area	4	[m^2]
C_d	2.25	[-]
Ballistic Coeff.	19.44	[kg/m^2]

Table 3-3: Test spacecraft physical parameters

Based on these three sets of spacecraft physical parameters, we would expect that that for a given orbit altitude the effects due to drag would be greatest for the TEST spacecraft, followed by TECSAS, and would be least for JC2Sat.

3.2 Projected Circular Formation

In this section, simulation results for a projected *y-z* (in-track/cross-track) circular formation will be presented. For this type of formation, the orbits of the Chief and Deputy spacecraft are setup in such a way that their relative motion becomes a circle when it is projected on to the *y-z* (in-track/cross-track) plane (please refer to Figure 3-2 for formation geometry). This type of formation is useful for Earth sensing missions because the distance between the two satellites is maintained constant in this plane.

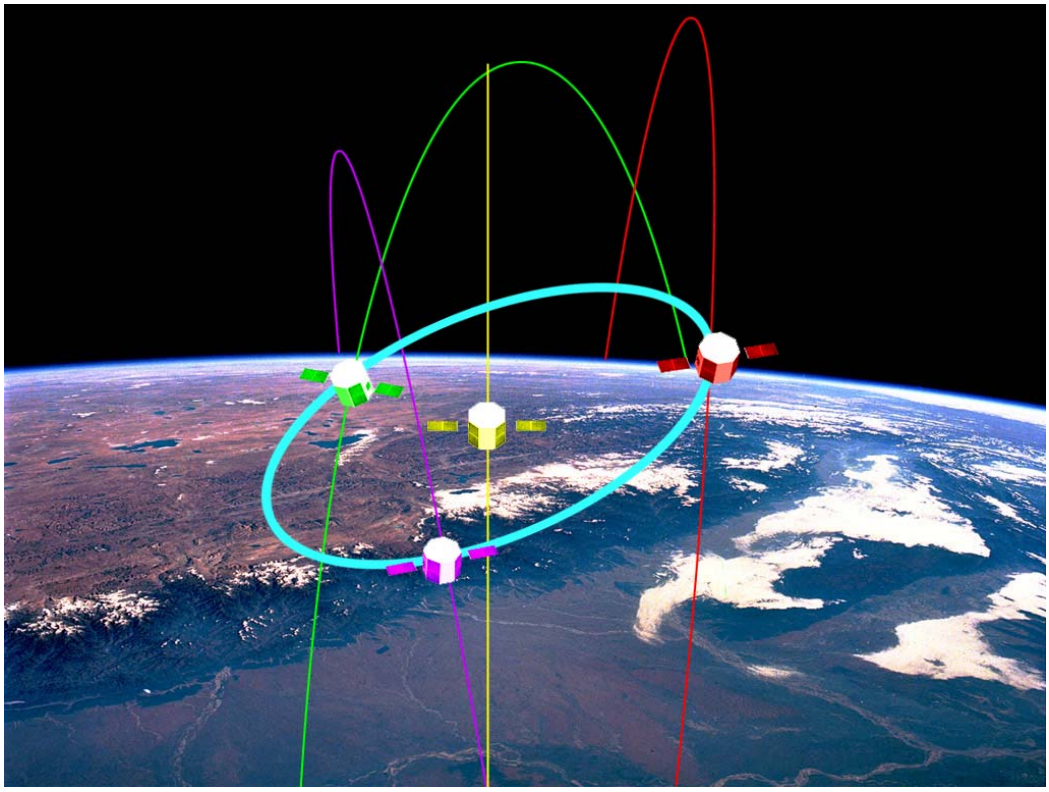

Figure 3-2: Geometry of a projected y-z circular formation

The motion in the *y-z* plane must satisfy the following constraint:

$$y^2 + z^2 = r^2 \tag{3.1}$$

where r is the desired radius of the formation. Initial conditions to generate this type of motion can be created by examining the Clohessy-Wilshire equations. Based on this, Sabol et al. (2001) designed the following initial conditions to create this type of formation geometry:

$$\begin{aligned} \Delta x_0 &= (r/2)\cos\alpha \\ \Delta \dot{x}_0 &= (r\,n/2)\sin\alpha \\ \Delta y_0 &= 2\Delta \dot{x}_0 / n \\ \Delta \dot{y}_0 &= -2n\Delta x_0 \\ \Delta z_0 &= 2\Delta x_0 \\ \Delta \dot{z}_0 &= 2\Delta \dot{x}_0 \end{aligned} \tag{3.2}$$

where r is the radius of the reference orbit, n is the mean orbital rate of this circular reference orbit, and α is the initial spacecraft phasing angle in the *y-z* plane. However, since these initial conditions are based on the Clohessy-Wiltshire equations, a secular drift may be present due to the fact that orbital perturbations are not accounted for. To account for J_2 perturbations, the following initial conditions for the Chief and the Deputy can be used in the context of the Schweighart-Sedwick equations (Landry, 2005). It should be noted that α was set equal to zero for simplicity:

$$\begin{aligned} x_{0,Deputy} &= r/2 \\ y_{0,Deputy} &= 0 \\ z_{0,Deputy} &= r \\ \dot{x}_{0,Deputy} &= 0 \\ \dot{y}_{0,Deputy} &= -2x_{0,Deputy}\,n\sqrt{1+s} + \frac{3}{4}\frac{n}{\hat{k}}J_2\frac{R_e^2}{r_{ref}}\sin^2 i_{ref} \end{aligned} \tag{3.3}$$

$$\dot{z}_{0,Deputy} = 0$$

and for the Chief:

$$\begin{aligned} x_{0,Chief} &= 0 \\ y_{0,Chief} &= 0 \\ z_{0,Chief} &= 0 \\ \dot{x}_{0,Chief} &= 0 \\ \dot{y}_{0,Chief} &= \frac{3}{4}\frac{n}{\hat{k}} J_2 \frac{R_e^2}{r_{ref}} \sin^2 i_{ref} \\ \dot{z}_{0,Chief} &= 0 \end{aligned} \tag{3.4}$$

The constant term that appears in the in the in-track velocity terms is specific to the Schweighart-Sedwick formulation and is present to eliminate secular drift with respect to the circular reference orbit used in that particular formulation (refer to Appendix B for further details on this formulation).

3.2.1 Results for TECSAS

First the results for the case where the Chief and Deputy spacecraft are assumed to have identical ballistic coefficients will be presented. It should be noted that ballistic coefficient in this sense refers only to the spacecraft physical characteristics and does not include local atmospheric density as it does in the dimensionless ballistic coefficient. In this case, density is independently calculated for each spacecraft using the method described in Appendix C.

The parameters of the circular reference orbit used in this preliminary analysis were selected as being those of the TECSAS mission (given in Table 3-4).

This was done so that the obtained numerical results could be compared to an analysis which has been done on the TECSAS mission (Landry, 2005) in order to validate these numerical results. This is why the results for the TECSAS physical parameters will be presented first.

Circular Reference Orbit Parameters		
Parameter	**Value**	**Units**
e	0	[-]
i	78	[deg]
Ω	320	[deg]

Table 3-4: Initial simulation reference orbit parameters

First, the ideal Clohessy-Wiltshire equations were solved to produce the idealized motion for this type of projected circular formation, i.e. with no perturbation forces taken into account. This will act as the baseline for comparison for all other projected circular formations simulations presented in this thesis. For a radius of 100 meters (used in all projected circular simulations in this thesis), the ideal motion is given in Figure 3-3 below. Please note that this result is independent of spacecraft physical parameters or reference orbit altitude.

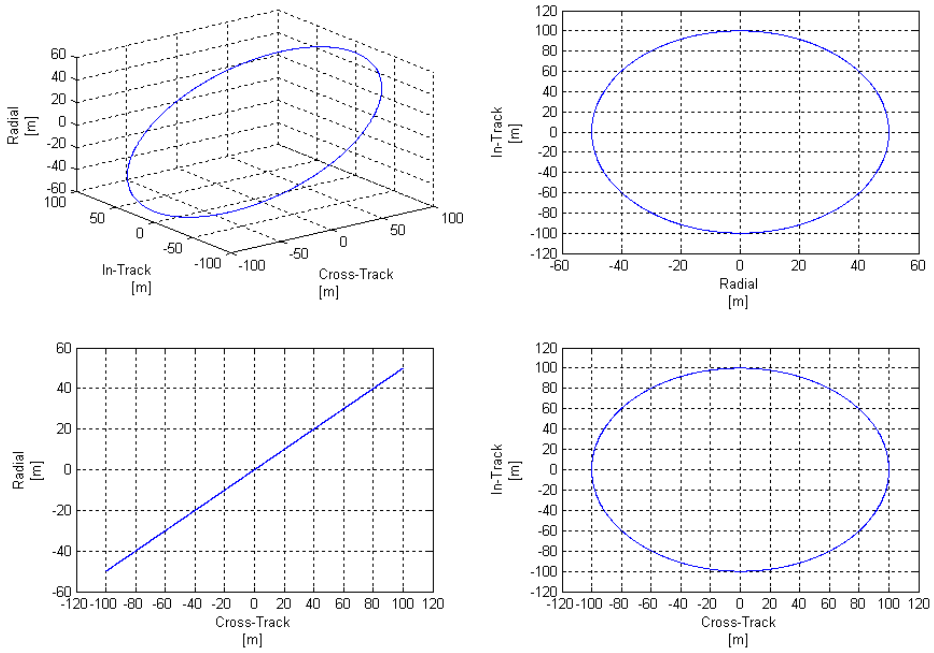

Figure 3-3: Unperturbed ideal motion for a projected y-z circular formation - 78^0 inclination

In order to emphasize the effects of drag, an altitude range of 250 to 500 km was selected for analysis. When J_2 effects are included in the numerical simulations in this altitude range, a significant drift in the cross-track motion develops. For a 24 hour simulation time, these results are shown in Figure 3-4. The results shown here are also valid for JC2Sat as well as the TEST parameters since the J_2 effects are independent of mass and all other physical spacecraft parameters. These results are representative of J_2 effects in altitudes in the range of 250 to 500 km over a 24 hour period and will thus be the baseline for comparison for assessing the effects of drag at a given altitude in this range. It should be noted that there no visible effect due to J_2 on the in-plane (x-y) motion in this case.

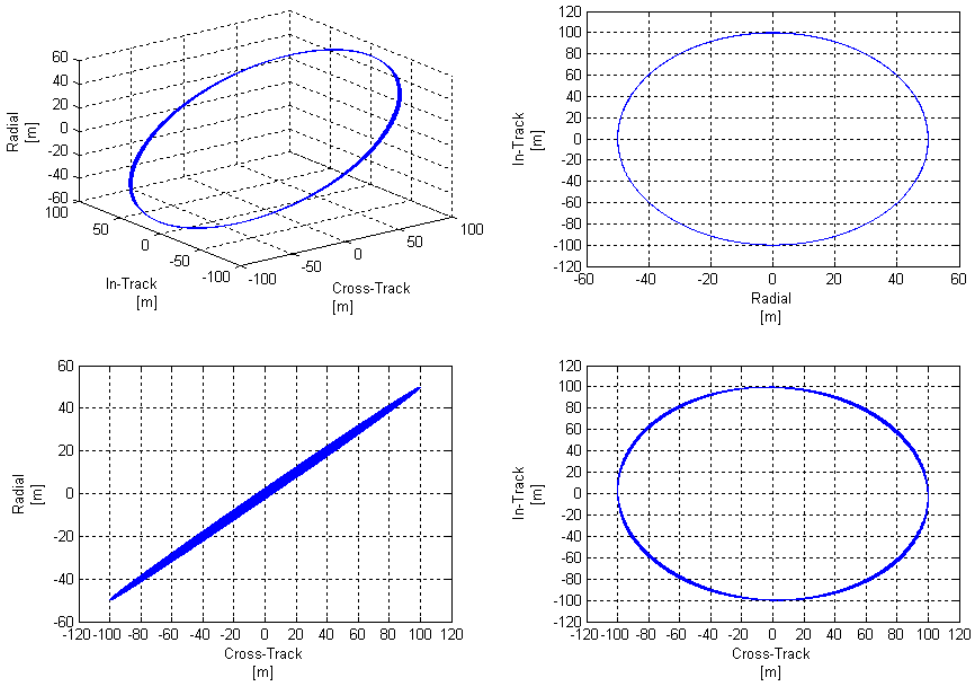

Figure 3-4: Projected y-z circular formation - J_2 perturbations only – 250 km to 500 km altitude – 78° inclination – 24 hour simulation

The TECSAS spacecraft was intended to operate in approximately a 500 km altitude orbit (Landry, 2005). When J_2 and atmospheric drag perturbations are included at this altitude in the simulation, the results obtained are shown in Figure 3-5. These results agree very well with the results obtained by Landry (2005) in his analysis of the TECSAS mission. From this result, it is clear that drag does not have a significant effect on the relative motion at this altitude for the period of time under consideration. Thus, J_2 is the predominant factor in this case.

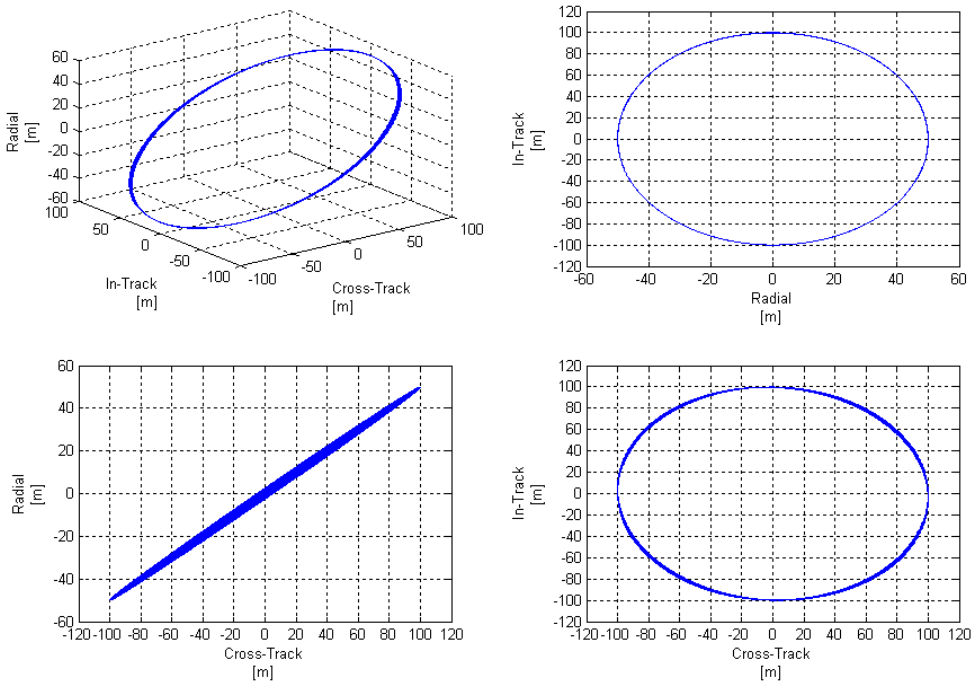

Figure 3-5: Projected y-z circular formation - J_2 and drag perturbations – 500 km altitude – 78° inclination – TECSAS Physical Parameters – 24 hour simulation

A lower altitude was considered next to see what effect drag can have on the formation geometry when these effects become as large as the J_2 effects. The results shown in Figure 3-6 represent an altitude of 300 km. Here, the drag effects are obvious when compared to Figure 3-4. Drag appears to primarily have an in-plane (in-track/radial) effect on the relative motion. Drag has seemingly two main effects on the in-plane motion, namely an in-track drift and an apparent damping of the motion or a shrinking of the projected in-plane ellipse. This makes sense as the damping matrix **C** clearly shows two off diagonal terms which represent non-dissipative gyroscopic damping, which are present due to the description of motion in a rotating frame, and the diagonal terms represent dissipative damping on the system. The cause of the in-track drift is not obvious and will be discussed later after more numerical simulation results have been presented.

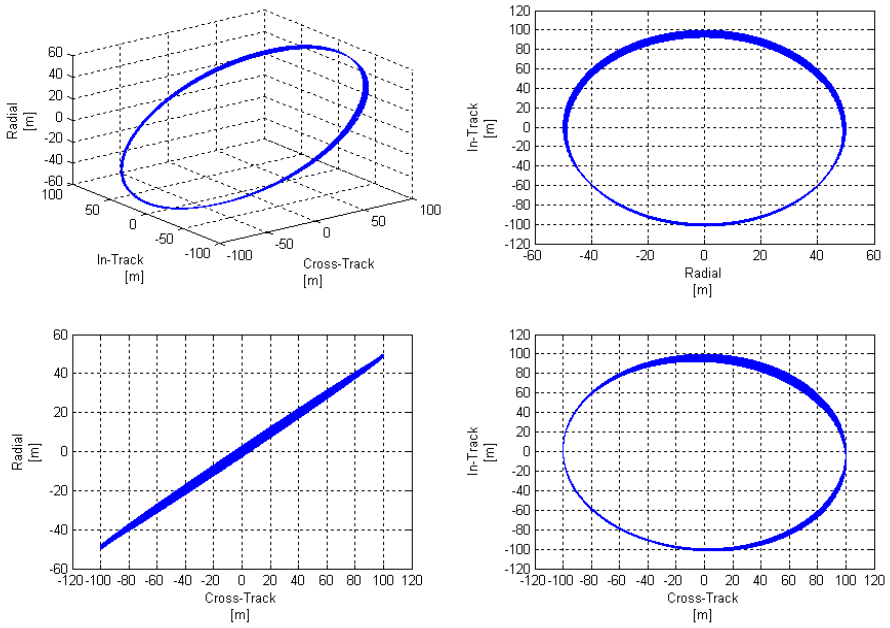

Figure 3-6: Projected y-z circular formation - J_2 and drag perturbations – 300 km altitude – 78° inclination – TECSAS Physical Parameters – 24 hour simulation

The next situation considered was that of a 250 km altitude (results shown in Figure 3-7). In this case, we see a similar trend only the effect is much more pronounced. Thus, a pattern appears to be emerging.

To try and isolate the cause of the in-track drift, a few more situations were considered. Figure 3-8 shows the same result as Figure 3-7 only with no J_2 effects included. In this case, the in-track drift does not occur, but the in-plane damping is evident. Also, in this extreme case we do see some cross-track drift due to drag though it is smaller in comparison to the in-plane effects. It would appear that it is the coupling with J_2 which causes the in-track drift. As such, we would expect this J_2 effect to be very small for inclinations which are very low since the variations of the Earth's gravity field will not substantial in this case. Figure 3-9 shows the same result as Figure 3-7, namely a 250 km altitude orbit, only here a 15° inclination was used.

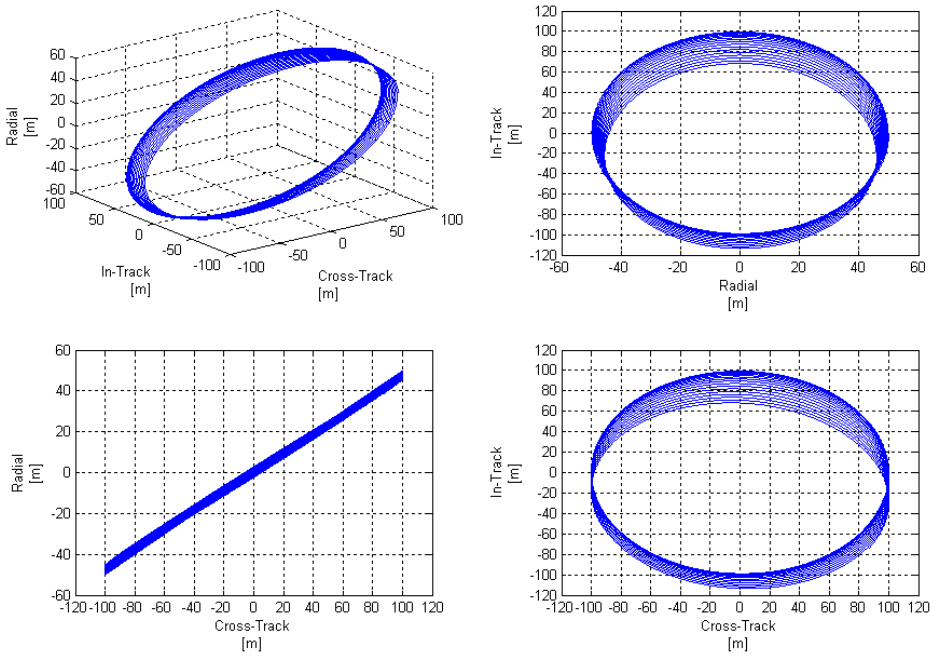

Figure 3-7: Projected y-z circular formation - J_2 and drag perturbations – 250 km altitude – 78° inclination – TECSAS Physical Parameters – 24 hour simulation

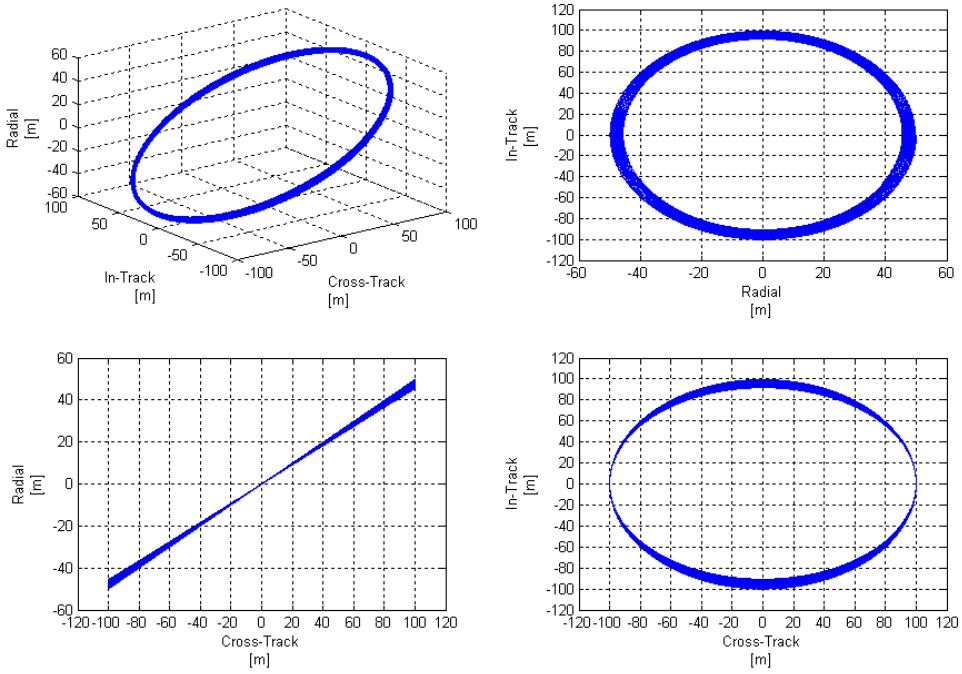

Figure 3-8: Projected y-z circular formation – Drag perturbations only – 250 km altitude – 78° inclination – TECSAS Physical Parameters – 24 hour simulation

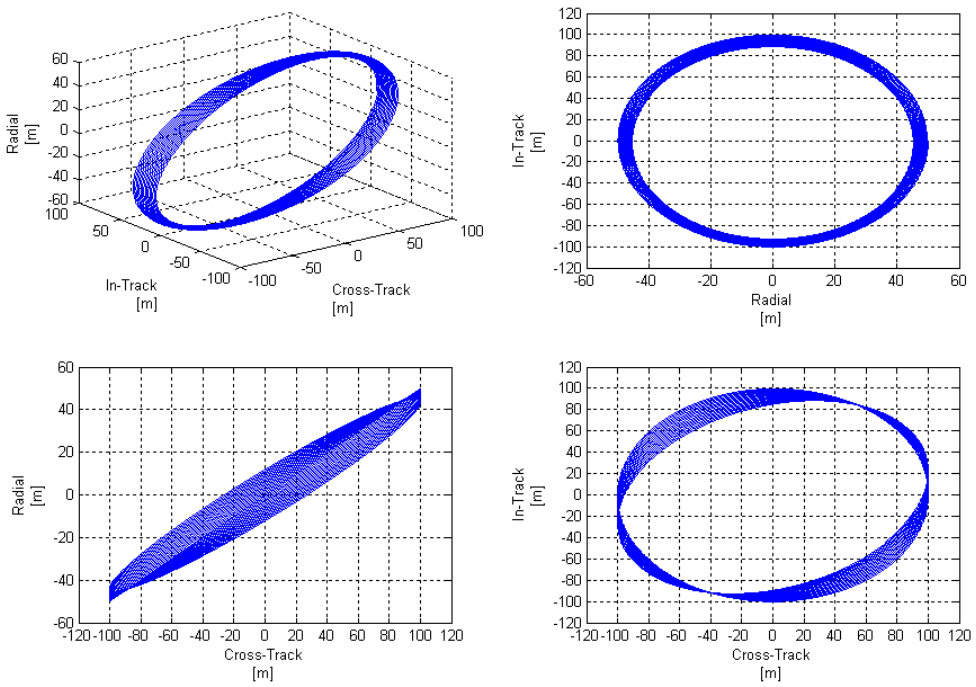

Figure 3-9: Projected y-z circular formation - J_2 and drag perturbations – 250 km altitude – 15° inclination – TECSAS Physical Parameters – 24 hour simulation

The results for the in-plane effects in Figure 3-9 are very similar to the results shown in Figure 3-8. This supports the idea that, at least in this case, for this set of initial conditions, the in-track drift is due to coupling between J_2 and drag effects.

It is now interesting to consider whether this in-track drift can be compensated for by using differential drag. For this, we considered the 300 km altitude case (uncompensated results shown in Figure 3-6). By trial and error, an increase in area of the Deputy by an amount of 0.0025% of the nominal value was found to compensate for the previously found drift over a period of 24 hours (the configuration is shown schematically in Figure 3-11). It should be emphasized that this is only a trial and error approach and that a control law has yet to be developed. However, this result demonstrates the feasibility of using drag as means

of formation keeping at least in this situation. This very small increase in area demonstrates how large this differential drag force can be at low altitudes and also how sensitive this will be when attempts are made to use differential drag as a control variable.

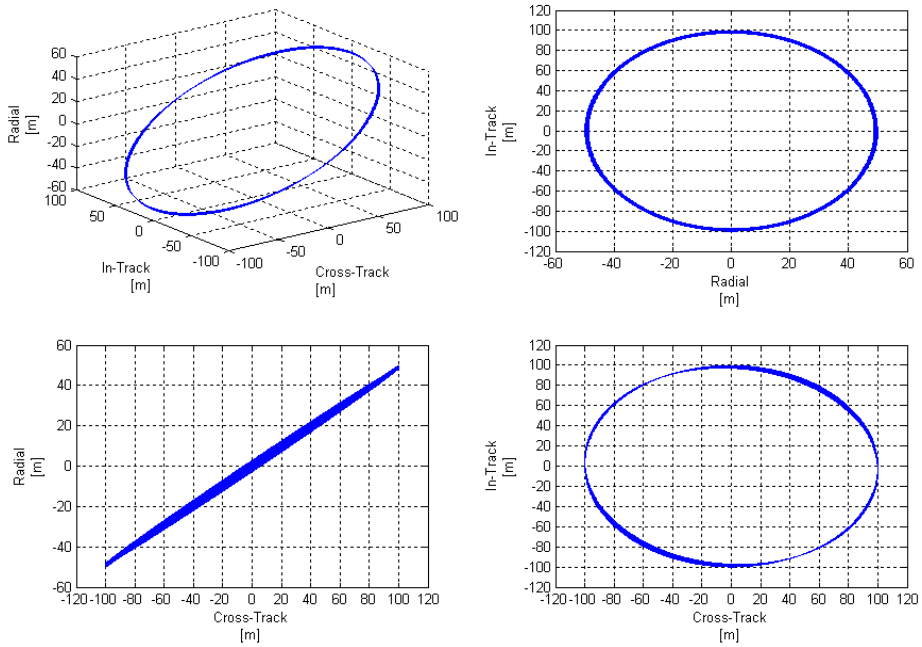

Figure 3-10: Projected y-z circular formation - J_2 and drag perturbations with differential drag drift compensation – 300 km altitude – 78° inclination – TECSAS Physical Parameters – 24 hour simulation

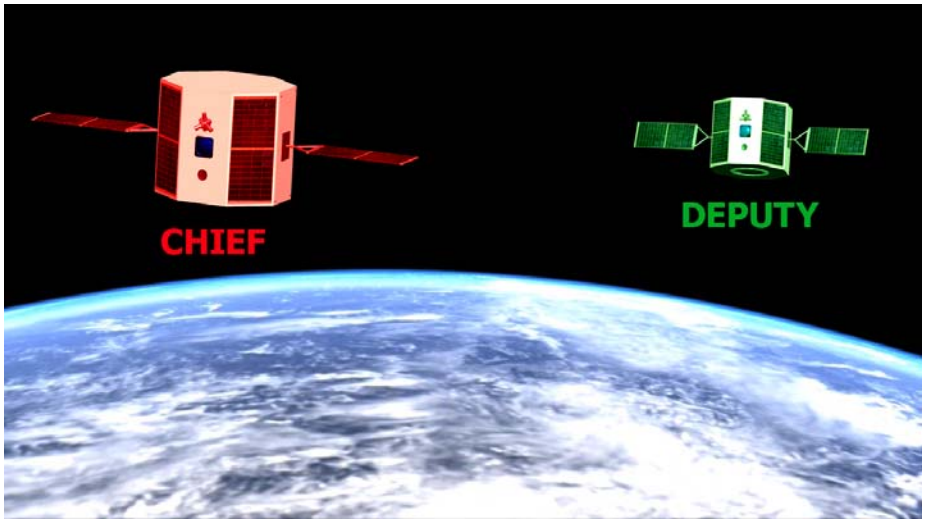

Figure 3-11: Artist rendering of differential drag configuration used

3.2.2 Results for JC2Sat

In this section, the results obtained for JC2Sat will be presented. The simulations performed to assess the effect of drag on the formation will be the same as those considered for the TECSAS spacecraft in the previous section. As was mentioned earlier, the baseline for comparison for assessing the magnitude of drag effects will be the results shown in Figure 3-4 as this result demonstrates the effect of J_2 perturbations alone in the altitude range under consideration.

The first reference orbit considered was that of a 500 km altitude (results shown in Figure 3-12). The results in this case are the same as those found for the TECSAS parameters, namely no significant effect on the relative motion. The results for a 300 km altitude are shown in Figure 3-13. In this case we see a similar response as was found for TECSAS. Although the effect is not as large, there is a noticeable in-track drift and reduction in the size of the in-plane ellipse. This is also found for the 250 km case shown in Figure 3-14.

The results are as expected since the physical parameters of JC2Sat are such that the effects due to drag at a given altitude will be less compared to TECSAS.

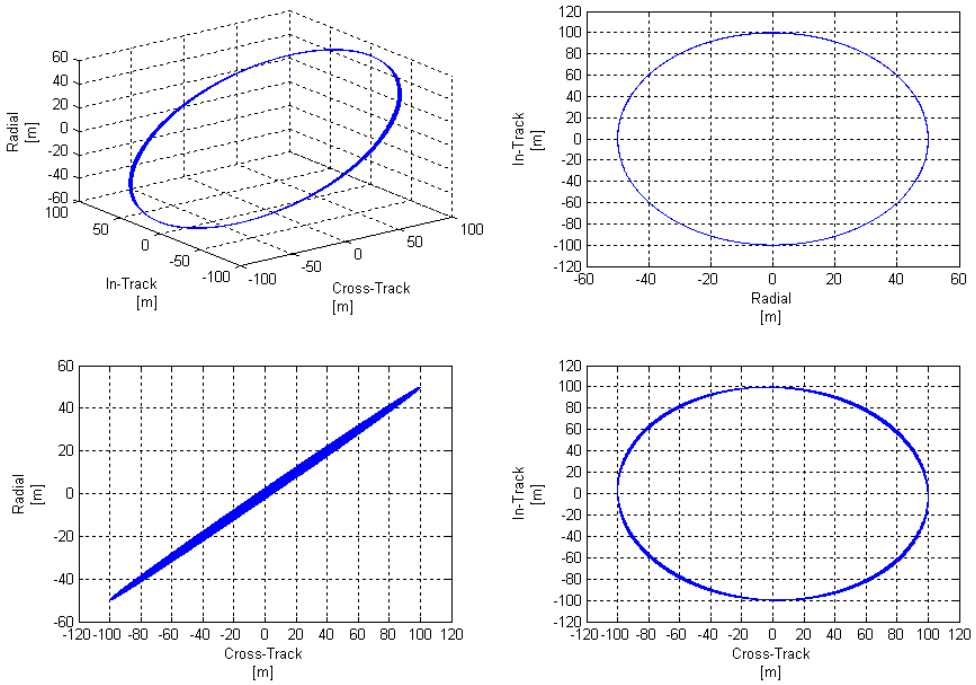

Figure 3-12: Projected y-z circular formation - J_2 and drag perturbations – 500 km altitude – 78º inclination – JC2Sat Physical Parameters – 24 hour simulation

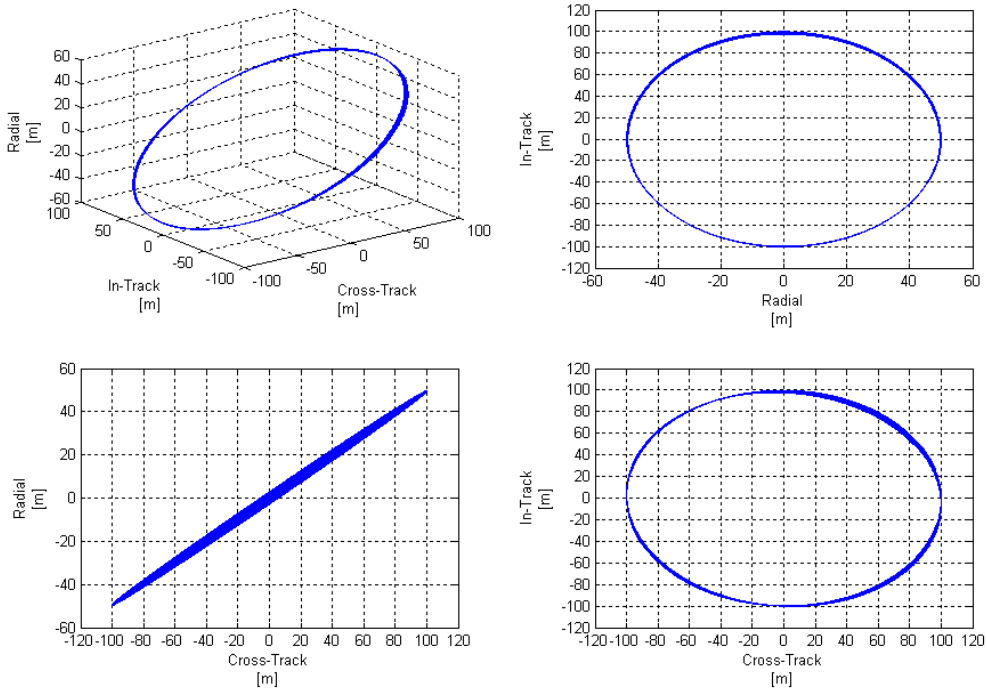

Figure 3-13: Projected y-z circular formation - J_2 and drag perturbations – 300 km altitude – 78º inclination – JC2Sat Physical Parameters – 24 hour simulation

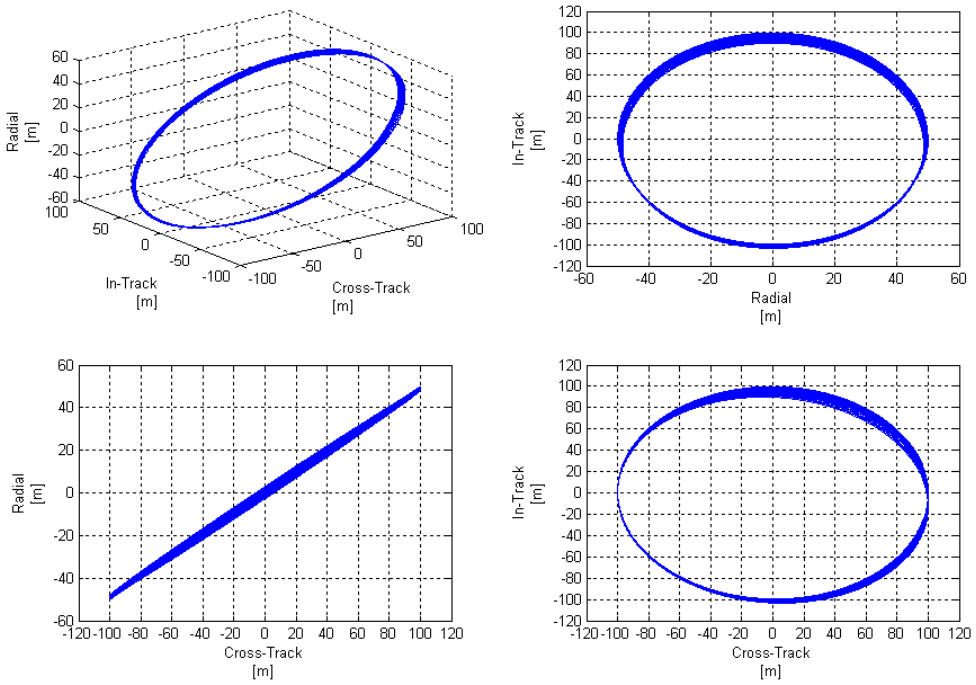

Figure 3-14: Projected y-z circular formation - J_2 and drag perturbations – 250 km altitude – 78° inclination – JC2Sat Physical Parameters – 24 hour simulation

The 250 km altitude case was considered for evaluating the effectiveness of using differential drag to compensate for the in-track drift. It was found that a similar increase in area of the Deputy spacecraft was again able to compensate for the in-track drift over this 24 hour period. The result is shown in Figure 3-15.

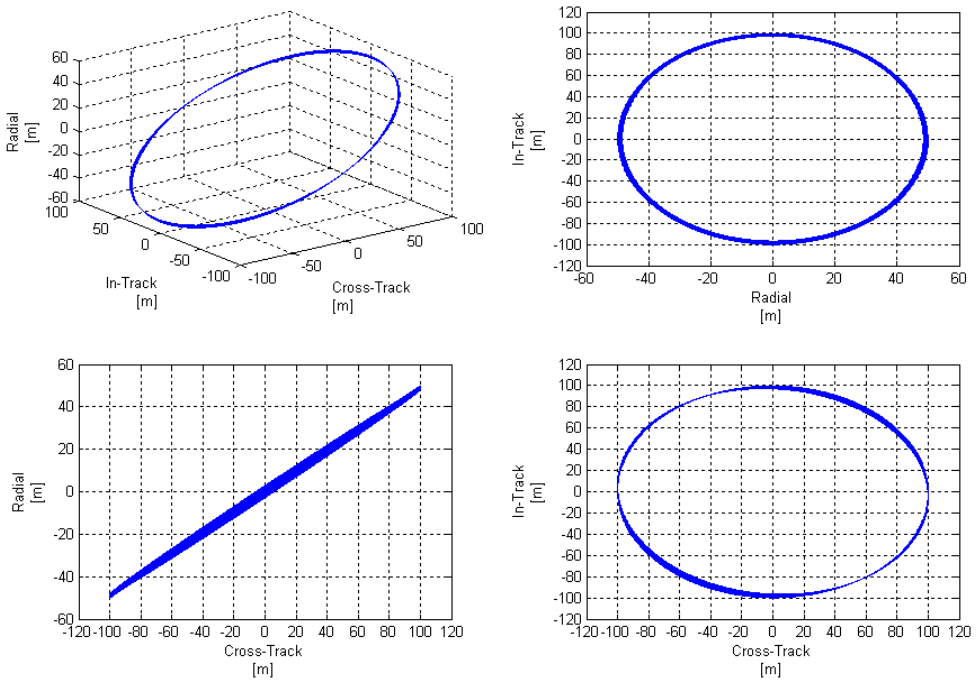

Figure 3-15: Projected y-z circular formation - J_2 and drag perturbations with differential drag drift compensation – 300 km altitude – 78° inclination – JC2Sat Physical Parameters – 24 hour simulation

3.2.3 Results for the TEST Parameters

In this section, the results for the TEST spacecraft parameters will be presented. The same reference orbit and altitudes will be considered for comparison with the TECSAS and JC2Sat results.

For the 500 km altitude case, the result is the same as that of JC2Sat and TECSAS, namely no significant effect over the 24 hour period. For the 300 km altitude case, the effects due to drag are similar to TECSAS and JC2Sat but are much more pronounced due to the nature of the TEST physical characteristics

(results shown in Figure 3-16). The same is true for the 250 km altitude case shown in Figure 3-17. For this case, the drift due to drag is very pronounced and to emphasize this drift the axes are plotted as functions of time in Figure 3-18. The damping of the motion is now very easy to see especially in the radial direction.

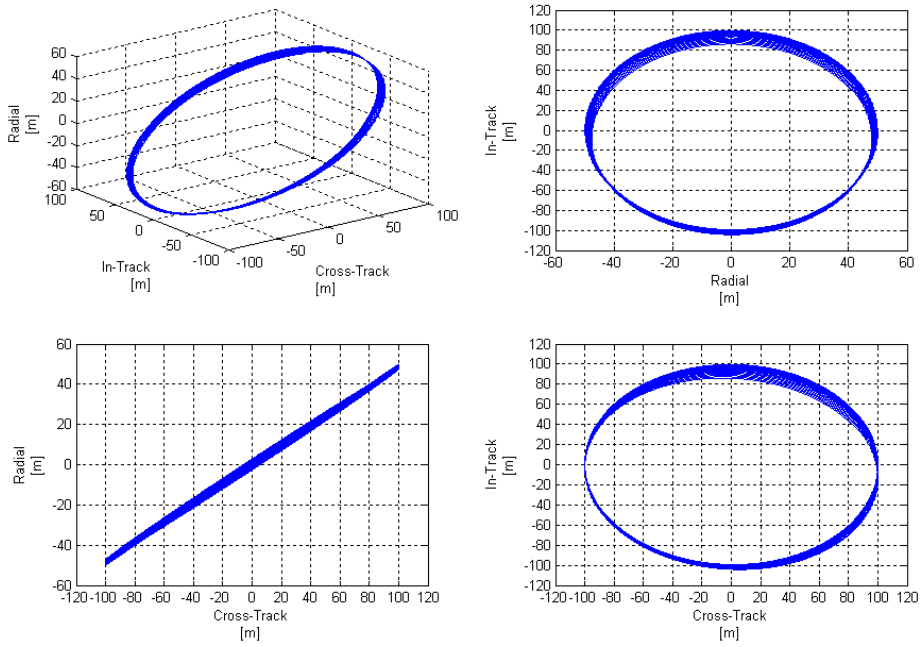

Figure 3-16: Projected y-z circular formation - J_2 and drag perturbations – 300 km altitude – 78° inclination – TEST Spacecraft Physical Parameters – 24 hour simulation

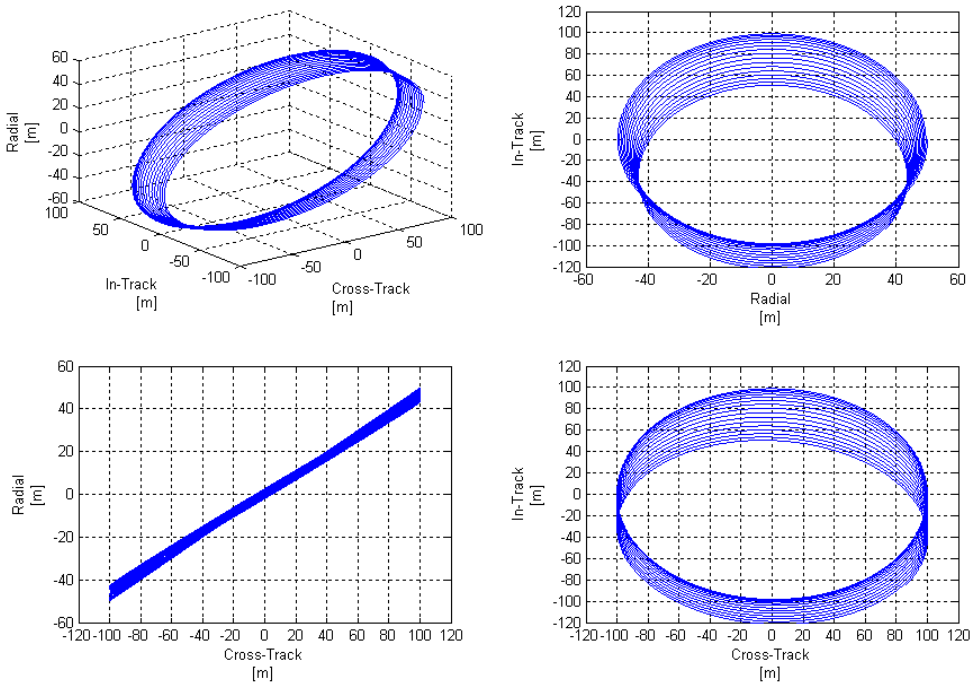

Figure 3-17: Projected y-z circular formation - J_2 and drag perturbations – 300 km altitude – 78° inclination – TEST Spacecraft Physical Parameters – 24 hour simulation

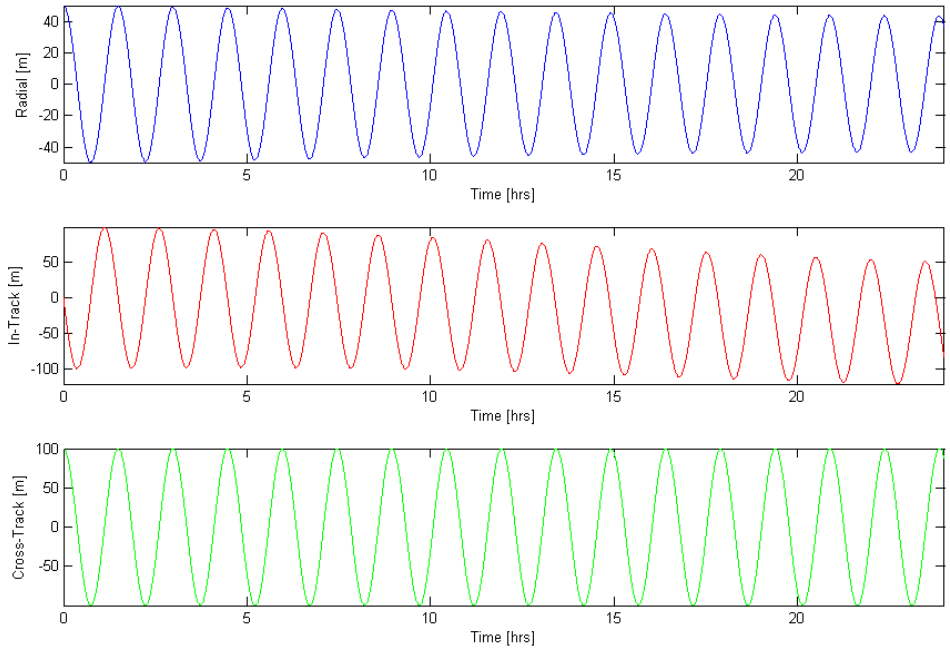

Figure 3-18: Projected y-z circular formation - J_2 and drag perturbations – 300 km altitude – 78° inclination – TEST Spacecraft Physical Parameters – 24 hour simulation – Components as a function of time

The results obtained for these three sets of physical parameters are consistent and seem to indicate that an in-track drift as well as an in-plane damping of the oscillatory motion will result due to drag effects on this type of formation. The results are also consistent with logic that as the ballistic coefficients of the Chief and Deputy increase the effects due to drag will decrease which was as predicted.

It should be noted that there is a major drawback with the current numerical propagator. The limitation is that for extreme drag cases, namely low altitudes, the time frame over which the solution is valid is somewhat limited. This is simply due to the fact that the Schweighart-Sedwick equations were not designed to handle the additional drag forces. An equation of motion is needed to be solved for each the Chief and the Deputy spacecraft with respect to a reference orbit in order to propagate the relative motion. However, the circular reference orbit used in the Schweighart-Sedwick formulation is perturbed by J_2 effects only. Thus, the added force caused by drag effects is continuously pushing each spacecraft further and further away from the reference orbit primarily in the in-track direction. Although the relative motion does not necessarily grow large, their individual motion with respect the reference orbit will grow unboundedly with time due to this additional forcing. One assumption in deriving these relative motion equations is that the relative distances are small compared to the radius of the reference orbit. When this is no longer the case, the obtained solution will become erroneous. As an example, consider the TEST spacecraft parameters and the case of a 300 km altitude. The individual motion of the Chief and Deputy spacecraft with respect to the reference orbit when only J_2 perturbations are considered is given in Figure 3-19. Comparing this result to the case where both J_2 and drag are considered

(shown in Figure 3-20) the in-track drift with respect to the reference orbit is clear. This presents a further motivation for the development of equations which are designed to account for drag and will be discussed further in Chapter 4.

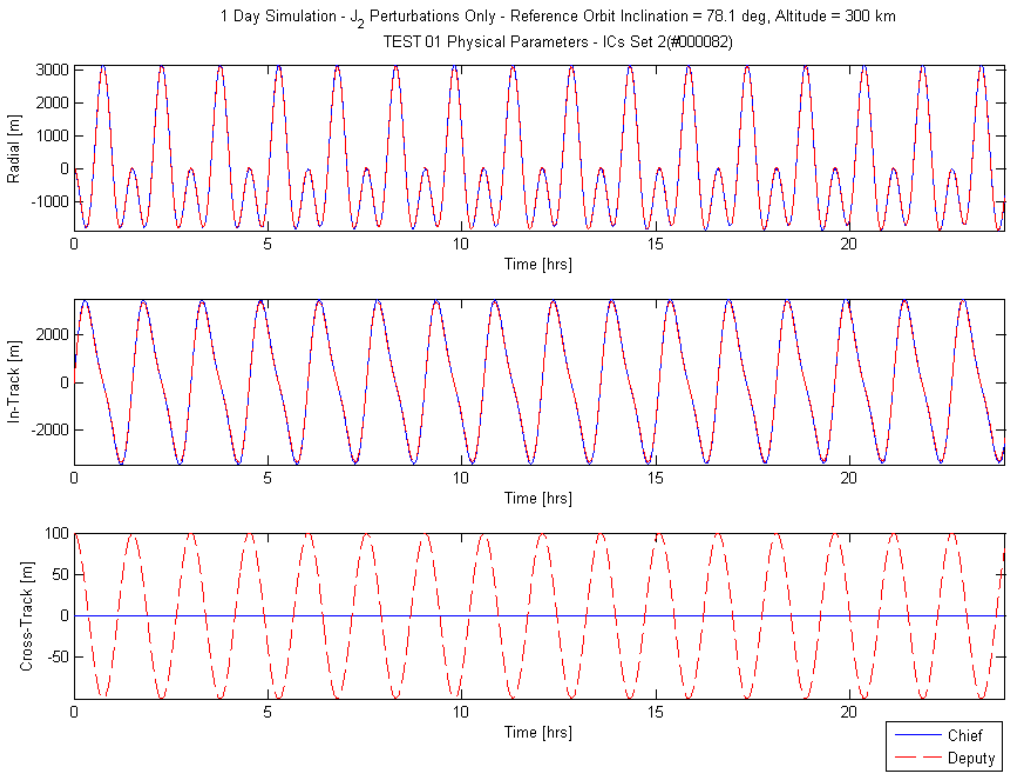

Figure 3-19: Projected y-z circular formation - J_2 perturbations only – 300 km altitude – 78° inclination – TEST Spacecraft Physical Parameters – 24 hour simulation – Chief and Deputy motion with respect to the circular reference orbit

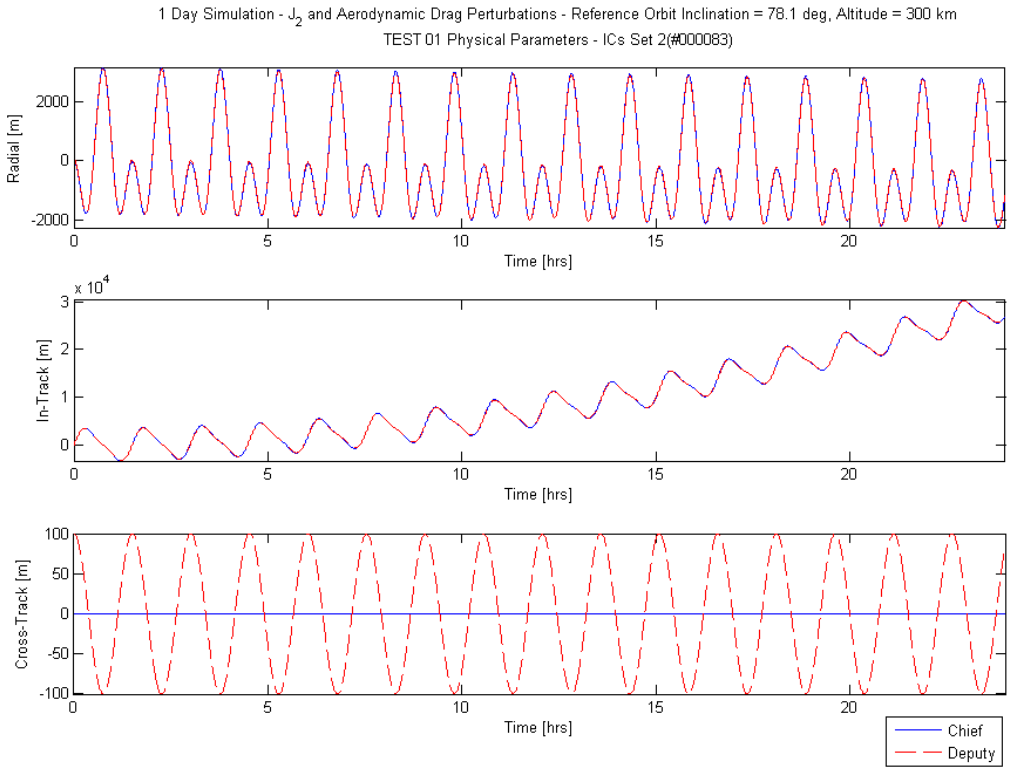

Figure 3-20: Projected y-z circular formation - J_2 and drag perturbations – 300 km altitude – 78° inclination – TEST Spacecraft Physical Parameters – 24 hour simulation – Chief and Deputy motion with respect to the circular reference orbit

3.3 In-Track Formation

In this section, simulation results for an in-track formation will be presented. In this type of formation, both spacecraft will share the same ground track (refer to Figure 3-21 for a schematic of an in-track formation). To share the same groundtrack, the Chief and Deputy satellites have to be in slightly different orbital planes separated by right ascension of the ascending node $\Delta\Omega$ which accounts for the rotation of the Earth (Sabol et al., 2001). The repeated groundtrack permits temporal measurements to be made faster than in the case of a single spacecraft mission.

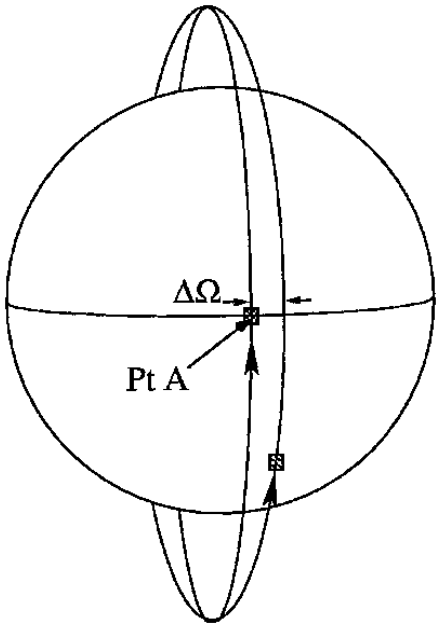

Figure 3-21: Schematic of an In-Track formation (Sabol et al., 2001)

The initial conditions needed to generate this type of formation are given by Sabol et al. (2001) and modified slightly by Landry (2005). These are as follows:

$$\begin{aligned} \Delta x_0 &= 0 \\ \Delta y_0 &= d \\ \Delta z_0 &= -\frac{\omega_e}{nc}\Delta y_0 \sin i \\ \Delta \dot{x}_0 &= 0 \\ \Delta \dot{y}_0 &= 0 \\ \Delta \dot{z}_0 &= 0 \end{aligned} \tag{3.5}$$

where d is the desired in-track separation distance determined by operational constraints, ω_e is the rotation rate of the Earth, n is the mean orbital rate of the

circular reference orbit, and c is the constant used in the Schweighart-Sedwick formulation (refer to Appendix B). In the case of the Schweighart-Sedwick formulation, the initial conditions for the Deputy with respect to the reference orbit are given by:

$$\begin{aligned} x_{0,Deputy} &= 0 \\ y_{0,Deputy} &= d \\ z_{0,Deputy} &= -\frac{\omega_e}{nc} d \sin i_{ref} \\ \dot{x}_{0,Deputy} &= 0 \\ \dot{y}_{0,Deputy} &= \frac{3}{4} \frac{n}{\hat{k}} J_2 \frac{R_e^2}{r_{ref}} \sin^2 i_{ref} \\ \dot{z}_{0,Deputy} &= 0 \end{aligned} \tag{3.6}$$

and for the Chief:

$$\begin{aligned} x_{0,Chief} &= 0 \\ y_{0,Chief} &= 0 \\ z_{0,Chief} &= 0 \\ \dot{x}_{0,Chief} &= 0 \\ \dot{y}_{0,Chief} &= \frac{3}{4} \frac{n}{\hat{k}} J_2 \frac{R_e^2}{r_{ref}} \sin^2 i_{ref} \\ \dot{z}_{0,Chief} &= 0 \end{aligned} \tag{3.7}$$

where the constant term in the in-track velocity is again specific to the Schweighart-Sedwick formulation. The initial condition for $\dot{x}_{0,Chief}$ and $\dot{x}_{0,Deputy}$ are set to zero in this case in order to maintain a constant offset in-track position between the two spacecraft.

For a preliminary analysis and validation of results, the results obtained from our numerical model for an in-track formation was compared to the results obtained by Shankar Kumar and Ng (2007) in a study using Analytical Graphics Inc's (AGI) Satellite Tool Kit (STK) High Precision Orbit Propagator (HPOP). This study by Shankar Kumar and Ng (2007) was to assess the magnitude of the drift caused by differential drag at different altitudes and was done as part of a preliminary feasibility study for the upcoming JC2Sat mission. The spacecraft physical parameters used in this study were as follows:

Spacecraft Physical Parameters Used by Shankar Kumar and Ng (2007)		
Parameter	**Value**	**Units**
mass	8	[kg]
Area	0.09	[m^2]
C_d	2.0	[-]

Table 3-5: Spacecraft physical parameters used in the study by Shankar Kumar and Ng (2007)

A 600 km altitude, sun synchronous orbit is the situation considered here for comparison. When the Chief spacecraft is assumed to have an increase in drag area of 10%, the resulting in-track drift for various levels of solar activity using STK is shown in Figure 3-22. The result obtained using the Schweighart-Sedwick equations with added non-linear drag for the same set of circumstances is given Figure 3-23. It is clear that our result for in-track drift agrees very well with the result obtained using STK for an average amount of solar activity (f10.7 = 150). The drift in the radial direction for this situation was reported to be 1.2 meters for STK which also agrees very closely with our results. This gives added confidence to the results obtained using our simplified numerical model.

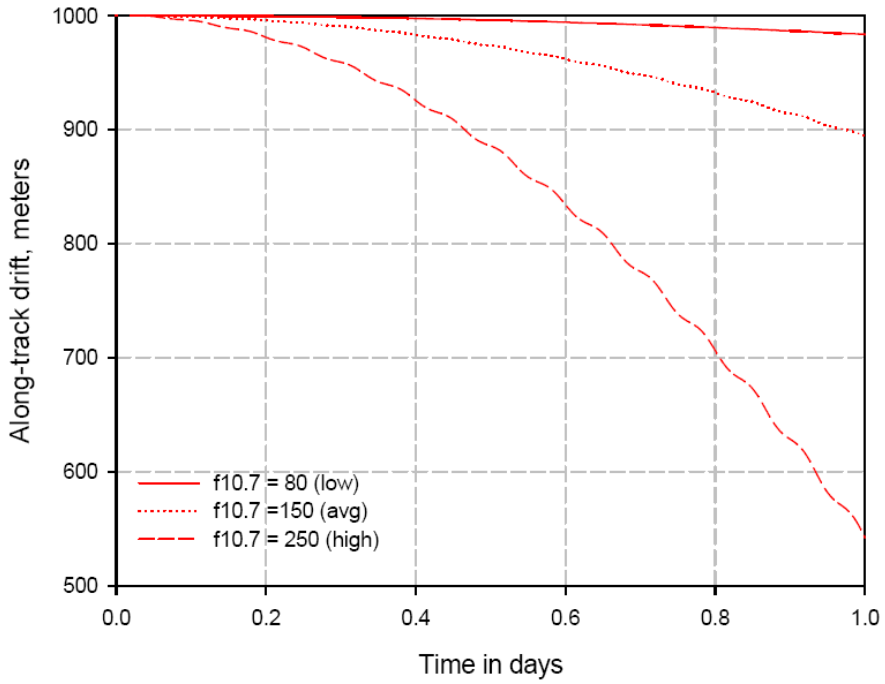

Figure 3-22: In-track drift due to a 10% differential drag area - results obtained by Shankar Kumar and Ng (2007) using Satellite Tool Kit for different amounts of solar activity – Sun Synchronous – 600 km altitude

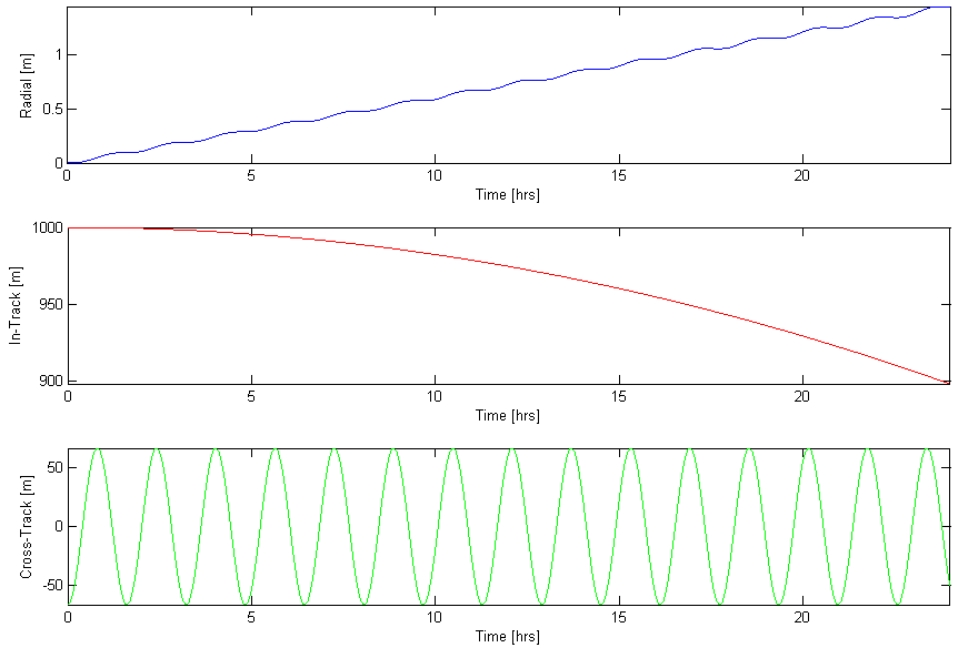

Figure 3-23: In-track drift due to a 10% differential drag area - results obtained using Schweighart-Sedwick equations with added non-linear drag – Sun Synchronous – 600 km altitude

The reference orbit that will be considered for the remaining simulations in this section will be the same as the one considered for the projected circular formation (see Table 3-4). A 100 meter in-track separation distance will be considered for consistency with the 100 meter radius projected circular formation considered in the previous section. For this type of formation, it is more meaningful to plot the components as a function of time for this type of motion rather than to show a 3-D plot. When the ideal unperturbed motion is considered for any altitude in the range under consideration here, the following result is obtained:

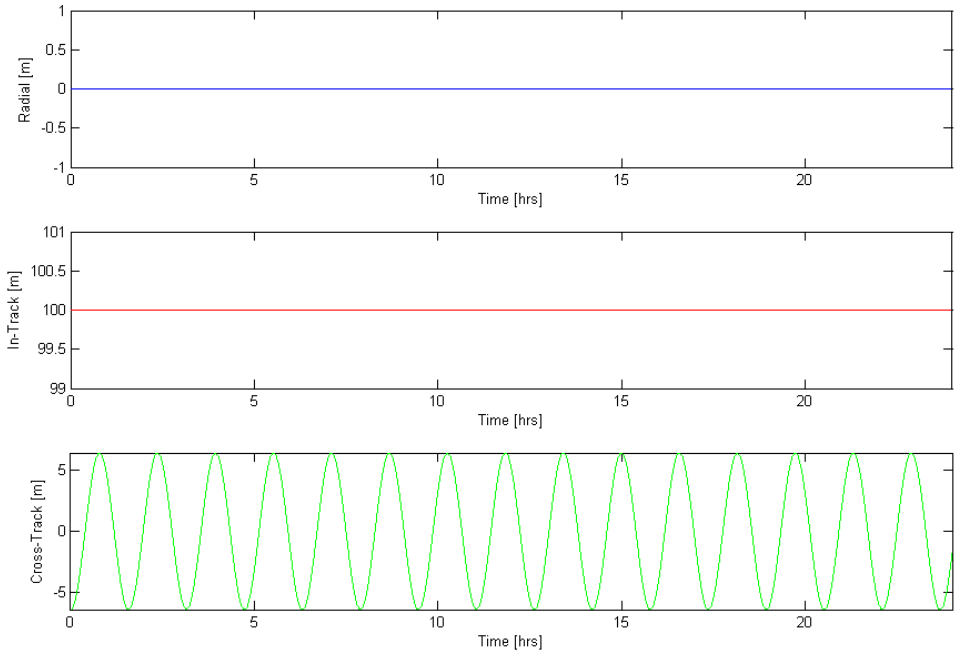

Figure 3-24: Idealized In-track formation – No perturbations – 500 km altitude – 78° inclination – 24 hour simulation

The result shown in Figure 3-24 will be used as the baseline for comparison in this section. It turns out that for a circular orbit, J_2 effects do not cause a noticeable effect over a 24 hour period. Thus, the result shown in Figure 3-24 is representative

of the motion obtained when J_2 perturbations are included in the simulation for the altitudes considered here and will be used to assess the effect of drag on the formation for a given altitude. In this section results for only the TECSAS parameters will be presented to avoid being repetitive. The trends related to drag effects and the magnitude of ballistic coefficient is similar to that of the projected circular case and is why it will not be repeated here.

3.3.1 Results for TECSAS

As with the projected circular formation, the first case that will be considered is that of a 500 km altitude. The result for this scenario where both J_2 and drag effects are included and both spacecrafts have the same physical characteristics is given in Figure 3-25 below:

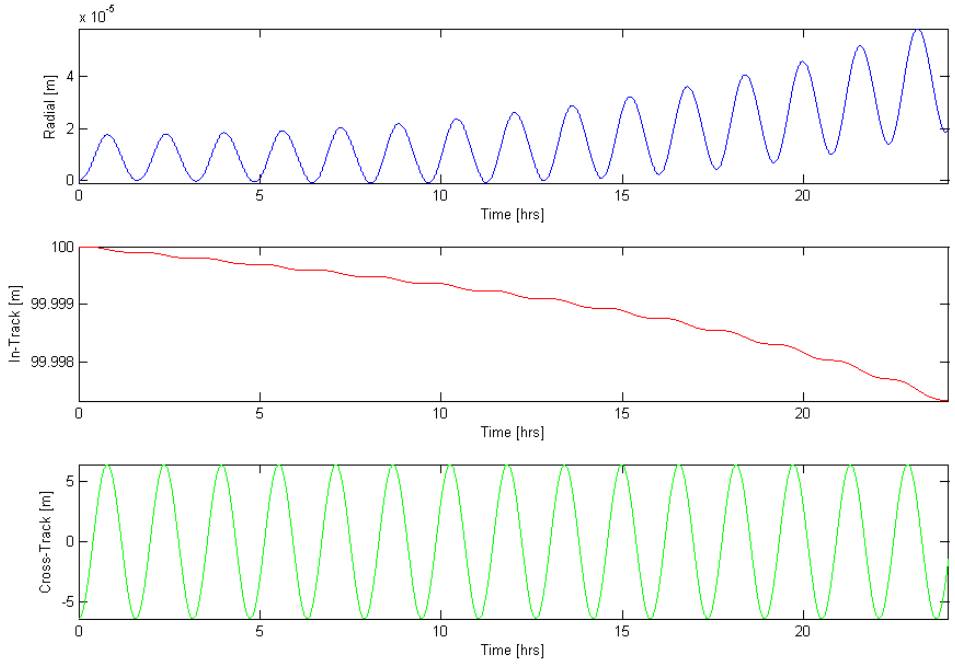

Figure 3-25: In-track formation - J_2 and drag perturbations – 500 km altitude – 78° inclination – TECSAS Spacecraft Physical Parameters – 24 hour simulation

As in the case of the projected circular formation there is an in-track drift present in the relative motion. Although it is small in this case, the in-track drift becomes significantly larger at lower altitudes. The result for a 300 km altitude orbit is shown in Figure 3-26 and that for a 250 km altitude is shown in Figure 3-27. We see similar type of in-track drift developing as we did in the case of a projected circular formation. The small drift in the radial direction is likely due to the coupling of the radial and in-track equations.

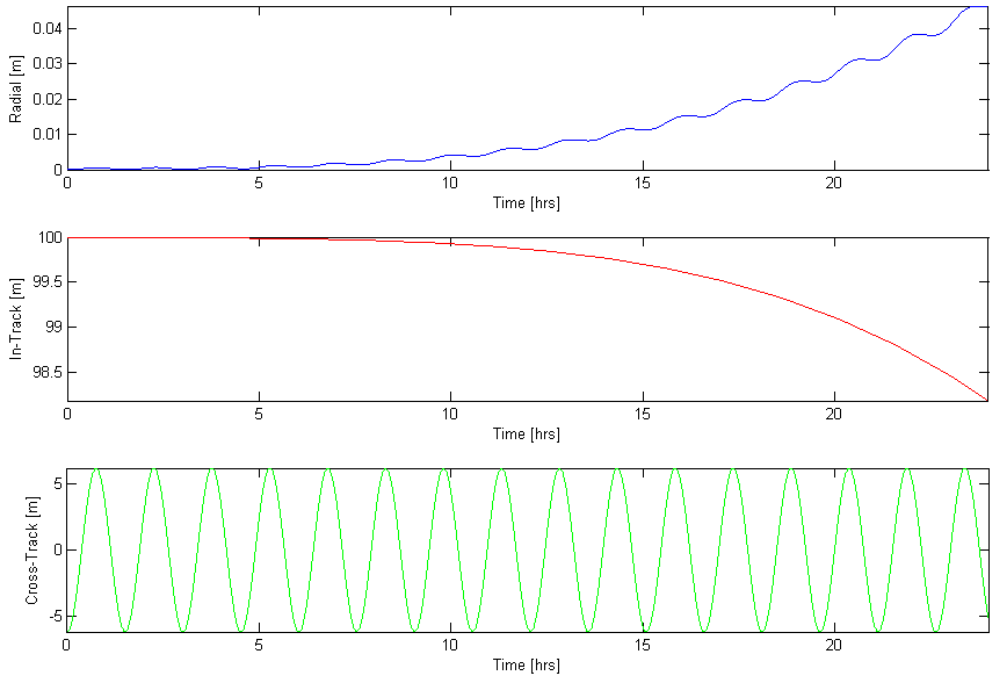

Figure 3-26: In-track formation - J_2 and drag perturbations – 300 km altitude – 78° inclination – TECSAS Spacecraft Physical Parameters – 24 hour simulation

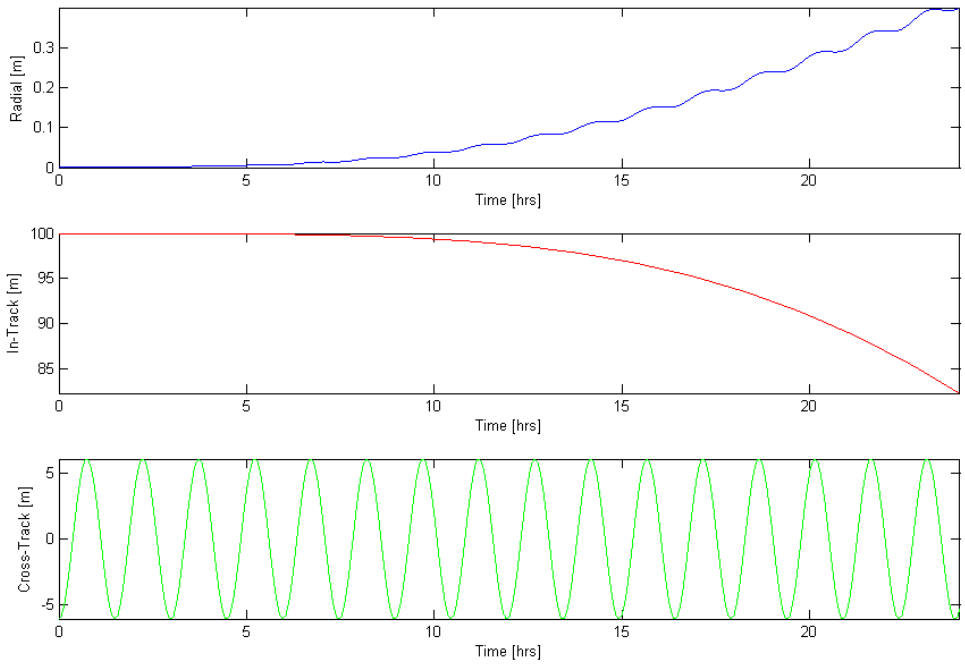

Figure 3-27: In-track formation - J_2 and drag perturbations – 250 km altitude – 78° inclination – TECSAS Spacecraft Physical Parameters – 24 hour simulation

3.4 Conclusions

The results obtained appear to be consistent with the effects that J_2 and drag perturbation forces are known to have on individual spacecraft orbits. For instance, in circular orbits J_2 effects cause a precession of the orbital plane, an example of this is shown in Figure 3-28. Thus, when two spacecraft are in slightly different orbits two slightly different precession rates would occur. As a result of this, we would expect a drift predominately in the cross-track relative motion. Drag, however, cases a dissipation of the individual orbits and is primarily an in-plane effect. A classic example of the in-plane effect of drag is shown in Figure 3-29. In-plane effects correspond to the in-track and radial directions in the Hill

frame and are where we see the predominant effects due to drag on the relative motion.

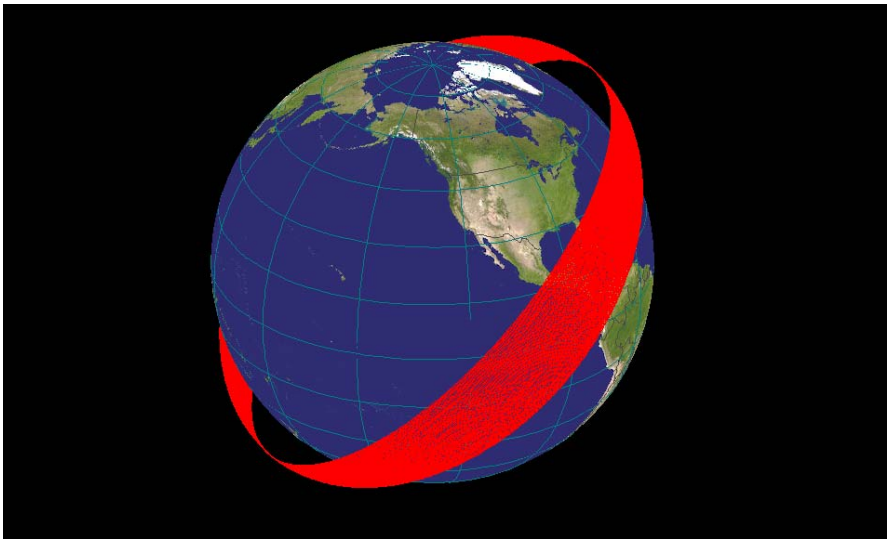

Figure 3-28: MATLAB© simulation demonstrating J_2 effects in LEO - 800 km altitude orbit – Inclination of 45° – 1 week simulation time

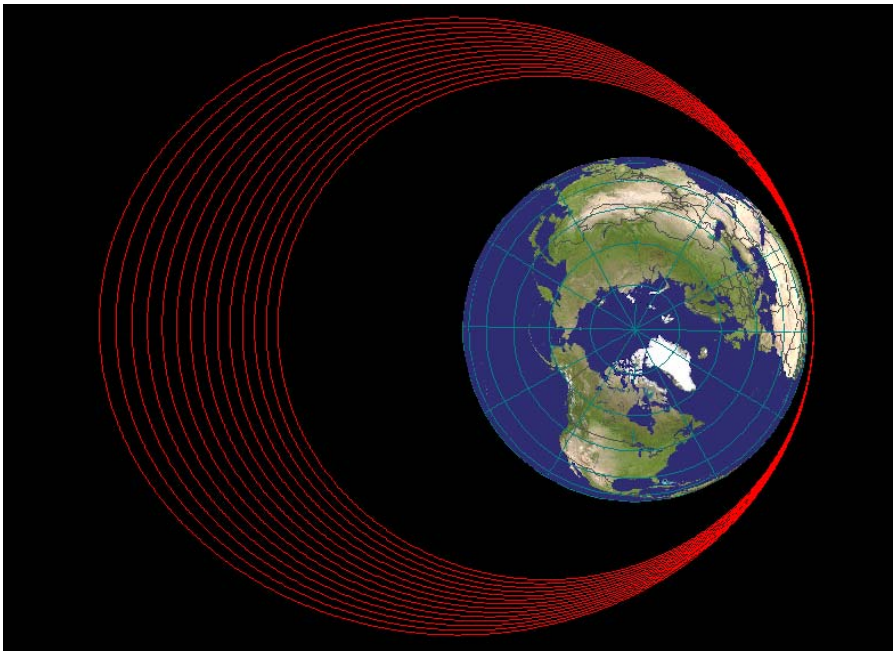

Figure 3-29: MATLAB© simulation demonstrating aerodynamic drag effects in LEO - simulation for an initial radius of perigee of 300 km – Inclination of 5° – initial eccentricity of 0.5 – 2 day simulation time

Chapter 4 - Relative Motion Equations for Elliptical Orbits

In this chapter, the relative motion equations with respect to an elliptical reference orbit will be developed. More precisely, the goal of this chapter is to develop relative motion equations which incorporate the effects of both J_2 potential and aerodynamic drag which are valid for elliptical reference orbits while at the same time maintain the simplicity and linearity of the equations developed in the previous chapter.

4.1 Relative Motion Equations

In this section, the relative motion equations which are valid for elliptical reference orbits will be presented. The starting point for this analysis will be the linearized general relative motion equations (Schaub & Junkins, 2003) which places no restrictions on the eccentricity of the reference orbit. These equations are given by:

$$\begin{aligned}
&\ddot{x} - 2\dot{\theta}\dot{y} - \ddot{\theta}y - \left(\dot{\theta}^2 + \frac{2\mu}{r_{ref}^3}\right)x = \Delta a_{J_2,x} + \Delta a_{Drag,x} \\
&\ddot{y} + 2\dot{\theta}\dot{x} - \ddot{\theta}x - \left(\dot{\theta}^2 - \frac{\mu}{r_{ref}^3}\right)y = \Delta a_{J_2,y} + \Delta a_{Drag,y} \\
&\ddot{z} + \frac{\mu}{r_{ref}^3}z = \Delta a_{J_2,z} + \Delta a_{Drag,z}
\end{aligned} \tag{4.1}$$

where $\dot{\theta}$ is the instantaneous angular rate of the Hill frame and r_{ref} is the instantaneous radial distance from the center of the Earth. Furthermore, the Δa_{J_2} and Δa_{Drag} terms represent the differential J_2 and differential atmospheric drag

perturbations respectively. The examination and simplification of these relative perturbation terms will be the subject of the remainder of this chapter.

4.1.1 Elliptical Reference Orbit

The elliptical reference orbit must be corrected in order to account for J_2 and atmospheric drag perturbations. Without such a correction, a secular drift would always be present in the relative motion and the spacecraft in question would be continuously drifting away from the given reference orbit. Not making any correction would result in perhaps simpler equations of relative motion but these equations would have a limited time window of validity as distances with respect to the reference orbit would grow rapidly.

One way to take into account these perturbations is to use Gauss' Planetary Equations (also known as the Gaussian form of Variation of Parameters of the orbital elements). These equations allow non-conservative perturbation forces such as drag to be taken into account as well as conservative forces such as J_2. The proposed equations represent a set of six first order ode's and are used to propagate the orbital elements of the reference orbit under consideration. These equations are given generally by (Battin, 1987):

$$\begin{aligned}
\frac{da}{dt} &= \frac{2a^2}{h}\left[e\sin f\ a_r + \frac{p}{r_{ref}}\ a_\theta\right] \\
\frac{di}{dt} &= \frac{r_{ref}\cos\theta}{h}\ a_z \\
\frac{d\Omega}{dt} &= \frac{r_{ref}\sin\theta}{h\sin i}\ a_z
\end{aligned} \tag{4.2}$$

$$\frac{de}{dt} = \frac{1}{h}\left[p\sin f\ a_r + \left[(p + r_{ref})\cos f + r_{ref}e\right]a_\theta\right]$$

$$\frac{d\omega}{dt} = \frac{1}{he}\left[-p\cos f\ a_r + (p + r_{ref})\sin f\ a_\theta\right] - \frac{r_{ref}\sin\theta\cos i}{h\sin i}a_z$$

$$\frac{dM}{dt} = n + \frac{\sqrt{1-e^2}}{he}\left[\left(p\cos f - 2r_{ref}e\right)a_r - (p + r_{ref})\sin f\ a_\theta\right]$$

where p is the semi-latus rectum, h is the magnitude of the specific angular moment vector of the reference orbit, and r_{ref} is the instantaneous radial distance from the center of the Earth. These parameters are related to the orbital elements by the following:

$$p = a(1-e^2) \tag{4.3}$$

$$h = \sqrt{\mu a(1-e^2)} \tag{4.4}$$

$$r_{ref} = \frac{a(1-e^2)}{1 + e\cos f} \tag{4.5}$$

The a_r, a_θ, and a_z terms in Gauss' planetary equations represent the perturbative accelerations in the r, θ, and z directions respectively. This coordinate system is equivalent to the Hill frame where the r direction is the x direction aligned with the radial vector, the z direction is denoted by the same symbol in both systems and is aligned with the orbit normal, and the θ or transverse direction is the y direction which completes the right handed coordinate system. These acceleration terms will include effects due to both atmospheric drag and J_2 perturbations and will discussed in the following sections.

The true anomaly f is also required to solve these equations. This can be determined by solving Kepler's equation which requires the solution of the following two identities which relate the mean anomaly M to the eccentric anomaly E and the eccentric anomaly E to the true anomaly f:

$$M = E - e\sin E \quad \text{and} \quad \tan\frac{f}{2} = \sqrt{\frac{1+e}{1-e}}\tan\frac{E}{2} \tag{4.6}$$

These equations can be solved by a number of iterative methods. One method of solution is described by (Vallado, 2007) in Algorithms 2 and 6.

The equations in their current form require numerical integration; however, simplifications will be made in the following sections to reduce the complexity of these equations to gain a better understanding of the drifts in these orbital elements caused by individual perturbations.

4.1.2 Small Eccentricity Assumption

In order to simplify the analysis, only orbits of small eccentricity will be considered. In other words, higher than first order eccentricity terms will be neglected when compared to numbers of order 1. As such, several simplifications will be made based on values of small eccentricity which will arise frequently and will thus be shown in this section. First, the semi-latus rectum p can be approximated as:

$$p = a(1-e^2) \approx a \tag{4.7}$$

Similarly for the specific angular momentum h:

$$h = \sqrt{\mu a(1-e^2)} \approx \sqrt{\mu a} = \sqrt{(n^2a^3)a} = na^2 \tag{4.8}$$

Another quantity which arises often is higher powers of r_{ref} . The first simplification is made using the approximation of p shown above. General powers of r_{ref} can be expanded binomially as follows:

$$r_{ref}^k = \left(\frac{p}{1+e\cos f}\right)^k \approx a^k(1+e\cos f)^{-k} \approx a^k(1-k\,e\cos f) \tag{4.9}$$

where higher than first order eccentricity terms are neglected in the expansion.

4.1.3 J_2 Perturbation Forces

In this section, the simplified perturbation accelerations due to J_2 effects in the r, θ, and z directions will be developed. The J_2 perturbation force expressed in the Hill frame is given generally by (Schweighart & Sedwick, 2002):

$$\mathbf{a}_{J_2} = -\frac{3}{2}\frac{J_2 \mu R_e^2}{r_{ref}^4}\begin{bmatrix} 1-3\sin^2 i \sin^2\theta \\ 2\sin^2 i \sin\theta\cos\theta \\ 2\sin i \cos i \sin\theta \end{bmatrix} \tag{4.10}$$

where θ denotes the argument of latitude and $\mathbf{a}_{J_2}$ is defined as:

$$\mathbf{a}_{J_2} \equiv \begin{bmatrix} a_r & a_\theta & a_z \end{bmatrix}^T \equiv \begin{bmatrix} a_x & a_y & a_z \end{bmatrix}^T \tag{4.11}$$

This can be simplified using the small eccentricity assumption which also takes into account the dependence of the radial distance r_{ref} on the true anomaly f. This results in:

$$\mathbf{a}_{J_2} \approx -\frac{3}{2}\frac{J_2 \mu R_e^2}{a^4}(1+4e\cos f)\begin{bmatrix} 1-3\sin^2 i \sin^2\theta \\ 2\sin^2 i \sin\theta\cos\theta \\ 2\sin i \cos i \sin\theta \end{bmatrix} \tag{4.12}$$

4.1.4 Atmospheric Drag Perturbation Forces

It has been previously shown that the perturbative acceleration due to aerodynamic drag effects is given by:

$$\mathbf{a}_{Drag} = -\frac{1}{2}\rho\frac{C_D A}{m} v_{spacecraft_{rel}} \mathbf{v}_{spacecraft_{rel}} \tag{4.13}$$

where $\mathbf{v}_{spacecraft_{rel}}$ is the velocity of the spacecraft with respect to the rotating atmosphere. It has been shown in Appendix A that the velocity of a spacecraft relative to the rotating atmosphere can be expressed in the Hill frame as:

$$\mathbf{v}_{spacecraft_{rel}} = \begin{bmatrix} \dot{r}_{ref} \\ r_{ref}\,(\dot{f} - \omega_e \cos i) \\ r_{ref}\ \omega_e \cos\theta \sin i \end{bmatrix} \tag{4.14}$$

where in this case we are considering a fictitious spacecraft which lies in and follows the reference orbit and thus, the relative *x-y-z* positions and velocity terms in the equations given in Appendix A are set to zero to obtain the above result.

The terms of this vector can be related to the orbital elements by the following relations (Vallado, 2007):

$$\dot{r}_{ref} \equiv \frac{dr_{ref}}{dt} = \frac{dr_{ref}}{df}\frac{df}{dt} = \frac{pe\sin f}{(1+e\cos f)^2}\frac{h}{r^2} = \frac{h}{p}e\sin f \tag{4.15}$$

$$\dot{f} = \frac{h}{r^2} = \sqrt{\mu a(1-e^2)}\,\frac{(1+e\cos f)^2}{a^2(1-e^2)^2} = \frac{n}{(1-e^2)^{3/2}}(1+e\cos f)^2 \tag{4.16}$$

which can be approximated using the small eccentricity assumption as:

$$\dot{r}_{ref} = \frac{h}{p}e\sin f \approx nae\sin f \tag{4.17}$$

$$\dot{f} = \frac{n}{(1-e^2)^{3/2}}(1+e\cos f)^2 \approx n(1+2e\cos f) \tag{4.18}$$

We now need to determine a simplified expression for the relative speed $v_{spacecraft_{rel}}$ of the spacecraft which is given by:

$$v_{spacecraft_{rel}} = \sqrt{\dot{r}_{ref}^2 + r_{ref}^2\,(\dot{f} - \omega_e \cos i)^2 + r_{ref}^2\ \omega_e^2 \cos^2\theta \sin^2 i} \tag{4.19}$$

Each of the terms under the square root will now be expanded in terms of the orbital elements and simplified under the small eccentricity assumption. Starting with the radial component, we obtain:

$$\dot{r}_{ref}^2 \approx (an)^2 e^2 \sin^2 f \approx 0 \tag{4.20}$$

Similarly for the transverse component:

$$\left[r_{ref}\left(\dot{f} - \omega_e \cos i\right)\right]^2 \approx (an)^2 \left\{(1 - e\cos f)\left[1 + 2e\cos f - \hat{\omega}_e \cos i\right]\right\}^2 \tag{4.21}$$

Here, n has been factored out and the definition of the previously defined normalized $\hat{\omega}_e$ parameter will be employed. This parameter is also small, on the order of the eccentricities under consideration. Thus, higher powers of this parameter will also be considered negligible when compared to 1 as well. Using this assumption, the above expression can be simplified to:

$$\left[r_{ref}\left(\dot{f} - \omega_e \cos i\right)\right]^2 \approx (an)^2 \left[1 + e\cos f - \hat{\omega}_e \cos i\right]^2 \tag{4.22}$$

Expanding this expression binomially yields:

$$\left[r_{ref}\left(\dot{f} - \omega_e \cos i\right)\right]^2 \approx (an)^2 \left[1 + 2e\cos f - 2\hat{\omega}_e \cos i\right] \tag{4.23}$$

Finally, for the z-component:

$$\begin{gathered}\left[r_{ref}\ \omega_e \cos\theta \sin i\right]^2 \approx \left[a(1 - e\cos f)\ \omega_e \cos\theta \sin i\right]^2 \\ \left[r_{ref}\ \omega_e \cos\theta \sin i\right]^2 \approx (an)^2 \left[(1 - e\cos f)\ \hat{\omega}_e \cos\theta \sin i\right]^2 \approx 0\end{gathered} \tag{4.24}$$

This term is also negligible since it is on the order of $\hat{\omega}_e^2$.

With these simplifying assumptions, the $v_{spacecraft_{rel}}$ term may be approximated as follows:

$$v_{spacecraft_{rel}} = (an)\left[1 + 2e\cos f - 2\hat{\omega}_e \cos i\right]^{1/2} \tag{4.25}$$

This expression can be expanded binomially as:

$$v_{spacecraft_{rel}} = (an)\left[1 + e\cos f - \hat{\omega}_e \cos i\right] \tag{4.26}$$

The resulting expression can be easily recognized as merely the simplified transverse component of the relative velocity. The physical meaning for this is that the reference orbit is considered to be nearly circular and thus we would expect its

transverse component of relative velocity to be significantly larger than the radial or normal components.

Now, the drag effect will be further simplified by examining each component of relative velocity separately. For the radial component:

$$a_{Drag,r} = -\frac{1}{2}\rho\frac{C_D A}{m} v_{spacecraft_{rel}}\left[\dot{r}_{ref}\right]$$

$$a_{Drag,r} \approx -\frac{1}{2}\rho\frac{C_D A}{m}(an)^2\left[1+e\cos f-\hat{\omega}_e\cos i\right]\left[e\sin f\right] \tag{4.27}$$

$$a_{Drag,r} \approx -\frac{1}{2}\rho\frac{C_D A}{m}(an)^2 e\sin f$$

Similarly for the transverse component:

$$a_{Drag,\theta} = -\frac{1}{2}\rho\frac{C_D A}{m} v_{spacecraft_{rel}}\left[r_{ref}\left(\dot{f}-\omega_e\cos i\right)\right] \tag{4.28}$$

Substituting the previously obtained simplifications for these expressions results in:

$$a_{Drag,\theta} \approx -\frac{1}{2}\rho\frac{C_D A}{m}(an)^2\left[1+e\cos f-\hat{\omega}_e\cos i\right]^2 \tag{4.29}$$

which can be expanded binomially as:

$$a_{Drag,\theta} \approx -\frac{1}{2}\rho\frac{C_D A}{m}(an)^2\left[1+2e\cos f-2\hat{\omega}_e\cos i\right] \tag{4.30}$$

Finally for the normal component:

$$a_{Drag,z} = -\frac{1}{2}\rho\frac{C_D A}{m} v_{spacecraft_{rel}}\left[r_{ref}\ \omega_e\cos\theta\sin i\right]$$

$$\begin{aligned} a_{Drag,z} \approx -\frac{1}{2}\rho\frac{C_D A}{m}(an)^2&\left[1+e\cos f-\hat{\omega}_e\cos i\right] \\ &\times\left[\left(1-e\cos f\right)\left(\hat{\omega}_e\cos\theta\sin i\right)\right] \end{aligned} \tag{4.31}$$

$$a_{Drag,z} \approx -\frac{1}{2}\rho\frac{C_D A}{m}(an)^2\hat{\omega}_e\cos\theta\sin i$$

Bringing all of this information together yields the final simplified expression which describes the aerodynamic drag perturbation accelerations:

$$\mathbf{a}_{Drag} \approx -\frac{1}{2}\rho\frac{C_D A}{m}(an)^2\begin{bmatrix} e\sin f \\ 1+2e\cos f-2\hat{\omega}_e\cos i \\ \hat{\omega}_e\cos\theta\sin i \end{bmatrix} \tag{4.32}$$

4.1.5 Reference Orbit Propagation

In this section, the final equations which describe the reference elliptical orbit will be presented. The semi-analytical method of averaging is used to develop simplified equations which can be used to propagate the orbital elements with time. In this way, both the reference orbit and the spacecraft which moves with respect to that orbit would both be perturbed by orbit-averaged perturbation forces. Averaging these perturbations will capture the secular drift effects and not the short term periodic variations. In this context, secular drift refers to long term effects. This averaging will be done using the following method (Schaub & Junkins, 2003):

$$\left(\frac{d\xi}{dt}\right)_{\text{sec}} \equiv \frac{d\bar{\xi}}{dt} = \frac{(1-e^2)^{3/2}}{2\pi}\int_0^{2\pi}(1+e\cos f)^{-2}\frac{d\xi}{dt}df \tag{4.33}$$

where the subscript sec refers to the secular component of the drift.

For the J_2 effects, these orbit-averaged expressions are well known and are given generally by (Schaub & Junkins, 2003):

$$\begin{aligned} \frac{d\bar{a}}{dt} &= 0 \\ \frac{d\bar{i}}{dt} &= 0 \\ \frac{d\bar{\Omega}}{dt} &= -\frac{3}{2}J_2 n\left(\frac{R_e}{p}\right)^2\cos i \\ \frac{d\bar{e}}{dt} &= 0 \end{aligned} \tag{4.34}$$

$$\frac{d\overline{\omega}}{dt} = \frac{3}{4} J_2 n \left(\frac{R_e}{p} \right)^2 \left(5\cos^2 i - 1 \right)$$

$$\frac{d\overline{M}}{dt} = n + \frac{3}{4} J_2 n \left(\frac{R_e}{p} \right)^2 \sqrt{1-e^2} \left(3\cos^2 i - 1 \right)$$

We now need to develop simplified expressions for the time rates of change of the orbital elements which are due to drag effects. With these expressions, we can orbit-average them and combine them with a simplified version of the above drift rates due to J_2 to obtain the final combined expressions. Substituting the simplified expression for the drag force and simplifying using the small eccentricity and small $\hat{\omega}_e$ assumption yields the following:

$$\begin{aligned}
\frac{da}{dt} &\approx -\rho \frac{C_D A}{m} (a^2 n) \left[1 + 3e\cos f - 2\hat{\omega}_e \cos i \right] \\
\frac{di}{dt} &\approx -\frac{1}{2} \rho \frac{C_D A}{m} (a\, n)\, \hat{\omega}_e \cos^2 \theta \sin i \\
\frac{d\Omega}{dt} &\approx -\frac{1}{2} \rho \frac{C_D A}{m} (a\, n)\, \hat{\omega}_e \sin\theta \cos\theta \\
\frac{de}{dt} &\approx -\rho \frac{C_D A}{m} (a\, n) \left[(1 - 2\hat{\omega}_e \cos i)\cos f + e\,(1 + \cos^2 f) \right] \\
\frac{d\omega}{dt} &\approx -\rho \frac{C_D A}{m} \left(\frac{a\, n}{e} \right) \sin f \left[1 + e\cos f - 2\hat{\omega}_e \cos i \right] \\
\frac{dM}{dt} &\approx n + \rho \frac{C_D A}{m} \left(\frac{a\, n}{e} \right) \sin f \left[1 + e\cos f - 2\hat{\omega}_e \cos i \right]
\end{aligned} \tag{4.35}$$

Recall that a dimensionless ballistic coefficient was previously defined. This definition will now be generalized for use in elliptic orbits as:

$$\beta \equiv \left(\rho \frac{C_D A}{m} a \right)^{-1} \tag{4.36}$$

This will allow for the final equations to be written in a more condensed form. In order to orbit-average these expressions, the small eccentricity assumption allows equation 4.33 to be approximated as follows:

$$\left(\frac{d\xi}{dt}\right)_{\text{sec}} \equiv \frac{d\bar{\xi}}{dt} \approx \frac{1}{2\pi}\int_0^{2\pi}(1-2e\cos f)\frac{d\xi}{dt}df \tag{4.37}$$

Orbit-averaging the drift rates of the orbital elements due to drag and combining with them with the simplified J_2 rates results in the final secular drift rates:

$$\begin{aligned}
\frac{d\bar{a}}{dt} &= -\frac{1}{\beta}a\,n\left[1-2\hat{\omega}_e\cos i\right] \\
\frac{d\bar{i}}{dt} &= -\frac{1}{4}\frac{1}{\beta}n\,\hat{\omega}_e\sin i \\
\frac{d\overline{\Omega}}{dt} &= -\frac{3}{2}J_2 n\left(\frac{R_e}{a}\right)^2\cos i \\
\frac{d\bar{e}}{dt} &= -\frac{1}{2}\frac{1}{\beta}e\,n \\
\frac{d\overline{\omega}}{dt} &= \frac{3}{4}J_2 n\left(\frac{R_e}{a}\right)^2\left[5\cos^2 i-1\right] \\
\frac{d\overline{M}}{dt} &= n+\frac{3}{4}J_2 n\left(\frac{R_e}{a}\right)^2\left[3\cos^2 i-1\right]
\end{aligned} \tag{4.38}$$

These six first order ordinary differential equations describe the mean secular drift of the reference orbital elements. These equations do not consider the short periodic variations of the actual osculating elements but rather account for the mean secular drifts and can thus be used to estimate the mean orbital elements with time. Integrating these equations numerically allows for the propagation of the reference orbit.

In order to validate these equations, some numerical simulation results will be presented. These simulations compare the full time derivative expressions given in equations 3.2 with the developed secular drift equations which are valid only for reference orbits of small eccentricity only. This simulation numerically integrated both sets of six first order differential equations using the MATLAB© `ode45` function. In order to perform these simulations, a set of spacecraft physical parameters was needed. Those selected were those of the TECSAS spacecraft which are given in Table 4-1:

TECSAS Spacecraft Physical Parameters		
Parameter	**Value**	**Units**
mass	175	[kg]
Area	2.22	[m^2]
C_d	2.3	[-]
Ballistic Coeff.	34.27	[kg/m^2]

Table 4-1: TECSAS Spacecraft Physical Parameters

The initial orbital elements selected were those of a sun-synchronous orbit and of approximately a 300km altitude and are summarized in Table 4-2. For the simulation considered here, the density was calculated at the beginning of the simulation to be the density at the point above the ellipsoidal Earth at time zero. This density was then assumed to be a constant throughout the simulation. Although this is not a good approximation in practice, the point of this simulation was to show that the trends of the two sets of equations were the same. Thus, we wanted to eliminate errors in local density estimation due to the orbit-averaged nature of the orbital elements.

Elliptical Reference Orbit Initial Orbital Elements			
Parameter	**Symbol**	**Value**	**Units**
Radius of Perigee	r_p	6678.137	[km]
Semi-Major Axis	a	6814.426	[km]
Iniclination	i	97.13523	[deg]
RAAN	Ω	0	[deg]
Eccentricity	e	0.02	[-]
Argument of Perigee	ω	0	[deg]
Mean Anomaly	M	0	[deg]
Initial Density	ρ	2.42E-11	[kg/m^3]

Table 4-2: Elliptical Reference Orbit Initial Orbital Elements

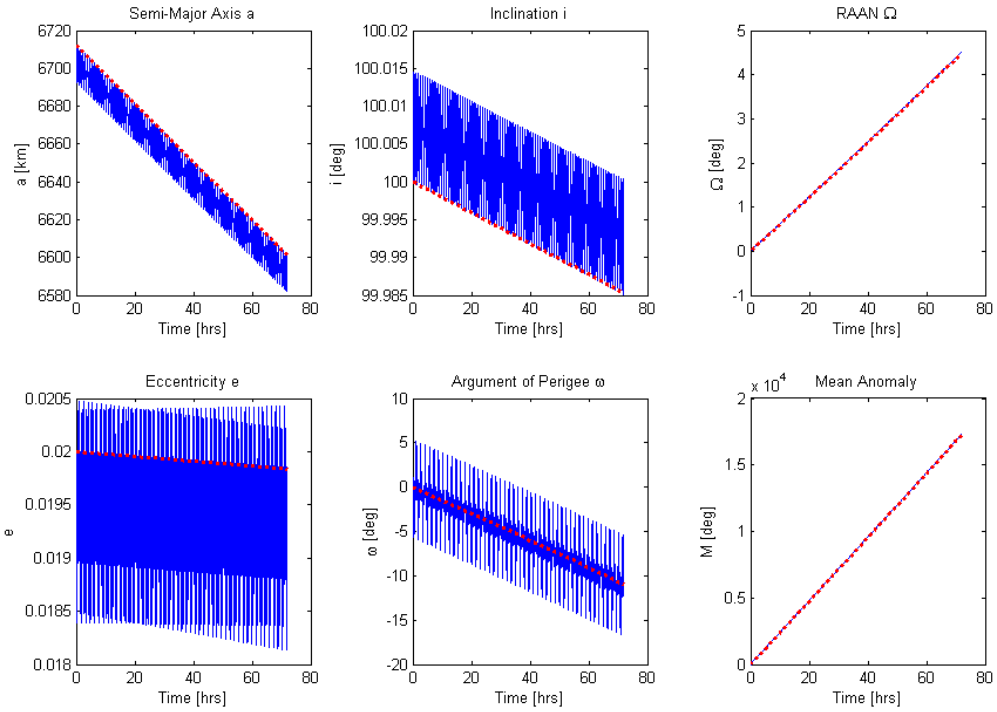

Figure 4-1: Simulation results which compare actual drift to the simplified mean secular drift of the orbital elements

The results of the simulation (shown in Figure 4-1) indicate that the developed simplified equations follow the mean drift rates of the orbital elements at least for the set of simulation parameters considered. It can be seen that the actual

osculating orbital elements (shown in blue) follow a general drift direction which is followed very closely by the simplified mean drift of the orbital elements (shown in red). The difference between the two is the actual osculating elements also have short term period variations.

4.2 Relative Perturbations

In this section, the perturbation effects acting on the spacecraft with respect to the reference orbit will be developed for both J_2 and aerodynamic drag effects.

4.2.1 Relative J_2 Perturbations

The relative J_2 effects are modeled using the gradient of the J_2 potential field. This is based on the method used by (Schweighart & Sedwick, 2002). The linear relative J_2 disturbance is found by multiplying the relative position vector expressed in the Hill frame by the J_2 gradient matrix written as:

$$\Delta\mathbf{a}_{J_2} = \nabla\mathbf{J}_2(\mathbf{r}_{ref})\mathbf{x} \tag{4.39}$$

where the J_2 gradient matrix is given by:

$$\nabla\mathbf{J}_2(r,\theta,i) = \frac{6\mu J_2 R_e^2}{r_{ref}^5}\begin{bmatrix} \left(1-3\sin^2 i\sin^2\theta\right) & \sin^2 i\sin 2\theta & \sin 2i\sin\theta \\ \sin^2 i\sin 2\theta & -\frac{1}{4}-\sin^2 i\left(\frac{1}{2}-\frac{7}{4}\sin^2\theta\right) & -(\sin 2i\cos\theta)/4 \\ \sin 2i\sin\theta & -(\sin 2i\cos\theta)/4 & -\frac{3}{4}+\sin^2 i\left(\frac{1}{2}+\frac{5}{4}\sin^2\theta\right) \end{bmatrix} \tag{4.40}$$

In order to simplify this expression, the J_2 gradient matrix will be time averaged over the orbit. This is done using the following integral, essentially we are taking the average value:

$$\frac{1}{2\pi}\int_0^{2\pi} \nabla \mathbf{J}_2(\mathbf{r}_{ref})\, d\theta \tag{4.41}$$

In order to obtain this integral, the dependence of r_{ref} on θ must be taken into account. This is done using the definition of the argument of latitude θ:

$$\theta = f + \omega \tag{4.42}$$

Using the small eccentricity assumption, we can approximate the dependence of r_{ref} on θ as follows:

$$\frac{1}{r_{ref}^5} \approx \frac{1}{a^5}(1 + 5e\cos f) = \frac{1}{a^5}(1 + 5e\cos(\theta - \omega)) \tag{4.43}$$

Substituting this expression into the J_2 gradient matrix and performing the integration results in the following:

$$\frac{1}{2\pi}\int_0^{2\pi} \nabla \mathbf{J}_2(\mathbf{r}_{ref})\, d\theta = \frac{\mu}{a^3}\mathbf{Q} + e\frac{\mu}{a^3}\tilde{\mathbf{Q}} \tag{4.44}$$

which can be written as:

$$\frac{1}{2\pi}\int_0^{2\pi} \nabla \mathbf{J}_2(\mathbf{r}_{ref})\, d\theta = \frac{\mu}{a^3}\begin{bmatrix} 4s & 0 & 0 \\ 0 & -s & 0 \\ 0 & 0 & -3s \end{bmatrix} + e\frac{\mu}{a^3}\begin{bmatrix} \tilde{q}_{11} & \tilde{q}_{12} & \tilde{q}_{13} \\ \tilde{q}_{12} & \tilde{q}_{22} & \tilde{q}_{23} \\ \tilde{q}_{13} & \tilde{q}_{23} & \tilde{q}_{33} \end{bmatrix} \tag{4.45}$$

where s is a dimensionless parameter defined by:

$$s \equiv \frac{3}{8} J_2 \left(\frac{R_e}{a}\right)^2 (1 + 3\cos 2i) \tag{4.46}$$

and all the remaining terms in the symmetric $\tilde{\mathbf{Q}}$ matrix are related to the eccentricity and argument of perigee. The diagonal terms of this matrix are given by:

$$\tilde{q}_{11} = -15\left(\frac{J_2 R_e^2}{2\pi a^2}\right)\left(\sin(2i - \omega) - \sin(2i + \omega) - 2\sin\omega + 4\sin\omega\cos^2 i\right) = 0 \tag{4.47}$$

$$\tilde{q}_{22} = -5\left(\frac{J_2 R_e^2}{2\pi a^2}\right)\left(\sin(2i-\omega) - \sin(2i+\omega) - 2\sin\omega + 4\sin\omega\cos^2 i\right) = 0$$

$$\tilde{q}_{33} = 10\left(\frac{J_2 R_e^2}{2\pi a^2}\right)\left(\sin(2i-\omega) - \sin(2i+\omega) - 2\sin\omega + 4\sin\omega\cos^2 i\right) = 0$$

For the off diagonal terms, we have:

$$\tilde{q}_{12} = 0$$

$$\tilde{q}_{13} = 15\,J_2\left(\frac{R_e}{a}\right)^2 \sin 2i \sin\omega \tag{4.48}$$

$$\tilde{q}_{23} = -\frac{15}{4}J_2\left(\frac{R_e}{a}\right)^2 \sin 2i \cos\omega$$

If we define another dimensionless parameter:

$$\tilde{s} \equiv \frac{15}{4}J_2\left(\frac{R_e}{a}\right)^2 \sin 2i \tag{4.49}$$

The time-averaged integral of the J_2 gradient matrix can now be written as:

$$\frac{1}{2\pi}\int_0^{2\pi} \nabla \mathbf{J}_2(\mathbf{r}_{ref})\, d\theta = n^2 \begin{bmatrix} 4s & 0 & 4e\tilde{s}\sin\omega \\ 0 & -s & -e\tilde{s}\cos\omega \\ 4e\tilde{s}\sin\omega & -e\tilde{s}\cos\omega & -3s \end{bmatrix} \tag{4.50}$$

This time averaged expression is consistent with that obtained by (Schweighart & Sedwick, 2002) which is valid for circular orbits. Letting eccentricity equal to zero, we obtain the same result.

4.2.2 Relative Drag Perturbations

In this section the relative drag effects will be determined. Recall the previously derived expression for the velocity of a spacecraft with respect to the rotating atmosphere expressed in the Hill frame (please refer to Appendix A):

$$\mathbf{v}_{spacecraft_{rel}} = \begin{bmatrix} \dot{x} + \dot{r}_{ref} - y\,(\dot{f} - \omega_e \cos i) - z\;\omega_e \cos\theta\;\sin i \\ \dot{y} + (r_{ref} + x)(\dot{f} - \omega_e \cos i) + z\;\omega_e \sin\theta\;\sin i \\ \dot{z} + (r_{ref} + x)\;\omega_e \cos\theta \sin i - y\;\omega_e \sin\theta\;\sin i \end{bmatrix} \tag{4.51}$$

The method of linearization of the drag expression will be similar to that employed earlier in chapter 2. This will be redone in the context of the small eccentricity approximation for verification. First, separate the relative velocity vector into its zeroeth and first order terms in $x,\ y,\ z$:

$$\mathbf{v}_{spacecraft_{rel}} \equiv \mathbf{v} \equiv \mathbf{v}_0 + \mathbf{v}_1 \tag{4.52}$$

where subscript zero denotes zeroth order terms and subscript 1 denotes first order terms in $x,\ y,\ z$. These are given by:

$$\mathbf{v}_0 = \begin{bmatrix} \dot{r}_{ref} \\ r_{ref}\,(\dot{f} - \omega_e \cos i) \\ r_{ref}\;\omega_e \cos\theta \sin i \end{bmatrix} \approx an \begin{bmatrix} e \sin f \\ 1 + e\cos f - \hat{\omega}_e \cos i \\ \hat{\omega}_e \cos\theta \sin i \end{bmatrix} \tag{4.53}$$

$$\begin{aligned} \mathbf{v}_1 &= \begin{bmatrix} \dot{x} - y\,(\dot{f} - \omega_e \cos i) - z\;\omega_e \cos\theta\;\sin i \\ \dot{y} + x(\dot{f} - \omega_e \cos i) + z\;\omega_e \sin\theta\;\sin i \\ \dot{z} + x\;\omega_e \cos\theta \sin i - y\;\omega_e \sin\theta\;\sin i \end{bmatrix} \\ \mathbf{v}_1 &\approx \begin{bmatrix} \dot{x} - y\,n\,(1 + e\cos f - \hat{\omega}_e \cos i) - z\,n\,\hat{\omega}_e \cos\theta \sin i \\ \dot{y} + x\,n\,(1 + e\cos f - \hat{\omega}_e \cos i) + z\,n\,\hat{\omega}_e \sin\theta \sin i \\ \dot{z} + x\,n\,\hat{\omega}_e \cos\theta \sin i - y\,n\,\hat{\omega}_e \sin\theta \sin i \end{bmatrix} \end{aligned} \tag{4.54}$$

In order to linearize the drag expression, we need to linearize and simplify the following:

$$\|\mathbf{v}\|\mathbf{v} \equiv \|\mathbf{v}_0 + \mathbf{v}_1\|(\mathbf{v}_0 + \mathbf{v}_1) \tag{4.55}$$

First, expand this using the definition of the scalar (dot) product:

$$\begin{aligned} \|\mathbf{v}_0 + \mathbf{v}_1\| &= \left[(\mathbf{v}_0 + \mathbf{v}_1)\cdot(\mathbf{v}_0 + \mathbf{v}_1)\right]^{\frac{1}{2}} \\ \|\mathbf{v}_0 + \mathbf{v}_1\| &= \left[\mathbf{v}_0 \cdot \mathbf{v}_0 + 2\mathbf{v}_0 \cdot \mathbf{v}_1 + \mathbf{v}_1 \cdot \mathbf{v}_1\right]^{\frac{1}{2}} \\ \|\mathbf{v}_0 + \mathbf{v}_1\| &= \left[\,\|\mathbf{v}_0\|^2 + 2\mathbf{v}_0 \cdot \mathbf{v}_1 + \|\mathbf{v}_1\|^2\,\right]^{\frac{1}{2}} \end{aligned} \tag{4.56}$$

The $\|\mathbf{v}\|\mathbf{v}$ expression can thus be rewritten as:

$$\|\mathbf{v}_0 + \mathbf{v}_1\|(\mathbf{v}_0 + \mathbf{v}_1) = \left[\|\mathbf{v}_0\|^2 + 2\mathbf{v}_0 \cdot \mathbf{v}_1 + \|\mathbf{v}_1\|^2\right]^{\frac{1}{2}}(\mathbf{v}_0 + \mathbf{v}_1) \tag{4.57}$$

We now want to eliminate the square root term. We can re-write the above expression as follows:

$$\|\mathbf{v}_0 + \mathbf{v}_1\|(\mathbf{v}_0 + \mathbf{v}_1) = \|\mathbf{v}_0\|\left(1 + \frac{2\mathbf{v}_0 \cdot \mathbf{v}_1}{\mathbf{v}_0 \cdot \mathbf{v}_0} + \frac{\|\mathbf{v}_1\|^2}{\|\mathbf{v}_0\|^2}\right)^{\frac{1}{2}}(\mathbf{v}_0 + \mathbf{v}_1) \tag{4.58}$$

The remaining terms under the square root are small compared to 1. This is due to the fact that the velocity of the reference frame is much larger than that of the relative velocity of the spacecraft with respect to the reference frame. Thus, higher order terms can be neglected and this can be expanded binomially as:

$$\|\mathbf{v}_0 + \mathbf{v}_1\|(\mathbf{v}_0 + \mathbf{v}_1) \approx \|\mathbf{v}_0\|\left[1 + \frac{1}{2}\left(\frac{2\mathbf{v}_0 \cdot \mathbf{v}_1}{\|\mathbf{v}_0\|^2} + \frac{\|\mathbf{v}_1\|^2}{\|\mathbf{v}_0\|^2}\right)\right](\mathbf{v}_0 + \mathbf{v}_1) \tag{4.59}$$

The second order terms of $\mathbf{v}_1$ can also be neglected due to the fact that they are being divided by $\|\mathbf{v}_0\|^2$. Thus, these terms are very small. This now simplifies to:

$$\begin{aligned} \|\mathbf{v}_0 + \mathbf{v}_1\|(\mathbf{v}_0 + \mathbf{v}_1) &\approx \|\mathbf{v}_0\|\left(1 + \frac{\mathbf{v}_0 \cdot \mathbf{v}_1}{\|\mathbf{v}_0\|^2}\right)(\mathbf{v}_0 + \mathbf{v}_1) \\ \|\mathbf{v}_0 + \mathbf{v}_1\|(\mathbf{v}_0 + \mathbf{v}_1) &\approx \underbrace{\|\mathbf{v}_0\|\mathbf{v}_0}_{I} + \underbrace{\|\mathbf{v}_0\|\mathbf{v}_1}_{II} + \underbrace{\left(\frac{\mathbf{v}_0 \cdot \mathbf{v}_1}{\|\mathbf{v}_0\|}\right)\mathbf{v}_0}_{III} \end{aligned} \tag{4.60}$$

This formulation now requires knowledge of the $\|\mathbf{v}_0\|$ term. As shown previously, this term can be approximated as:

$$\|\mathbf{v}_0\| = v_{spacecraft_{rel}} \approx r_{ref}(\dot{f} - \omega_e \cos i) \approx an(1 + e\cos f - \hat{\omega}_e \cos i) \tag{4.61}$$

Each of the three terms above (*I,II,III*) will be simplified individually using the small eccentricity assumption. The first term (*I*) in the above expression was determined previously to be:

$$\|\mathbf{v}_0\|\mathbf{v}_0 \approx (an)^2 \begin{bmatrix} e\sin f \\ 1+2e\cos f - 2\hat{\omega}_e \cos i \\ \hat{\omega}_e \cos\theta \sin i \end{bmatrix} \tag{4.62}$$

Orbit-averaging this term using the same method used in the relative J_2 effects section yields:

$$\frac{1}{2\pi}\int_0^{2\pi} \|\mathbf{v}_0\|\mathbf{v}_0 df \approx \frac{(an)^2}{2\pi}\int_0^{2\pi} \begin{bmatrix} e\sin f \\ 1+2e\cos f - 2\hat{\omega}_e \cos i \\ \hat{\omega}_e \cos\theta \sin i \end{bmatrix} df \tag{4.63}$$

This results in:

$$\frac{1}{2\pi}\int_0^{2\pi} \|\mathbf{v}_0\|\mathbf{v}_0 df \approx (an)^2 \begin{bmatrix} 0 \\ 1-2\hat{\omega}_e \cos i \\ 0 \end{bmatrix} \tag{4.64}$$

The second term (*II*) can be written as:

$$\|\mathbf{v}_0\|\mathbf{v}_1 \approx r_{ref}(\dot{f} - \omega_e \cos i) \begin{bmatrix} \dot{x} - y(\dot{f} - \omega_e \cos i) - z\,\omega_e \cos\theta \sin i \\ \dot{y} + x(\dot{f} - \omega_e \cos i) + z\,\omega_e \sin\theta \sin i \\ \dot{z} + x\,\omega_e \cos\theta \sin i - y\,\omega_e \sin\theta \sin i \end{bmatrix} \tag{4.65}$$

Which can be expanded as:

$$\begin{aligned} \|\mathbf{v}_0\|\mathbf{v}_1 \approx\ & an\,(1 + e\cos f - \hat{\omega}_e \cos i) \begin{bmatrix} \dot{x} \\ \dot{y} \\ \dot{z} \end{bmatrix} \\ & + an^2\,(1 + e\cos f - \hat{\omega}_e \cos i) \begin{bmatrix} -y\,(1 + 2e\cos f - \hat{\omega}_e \cos i) - z\,\hat{\omega}_e \cos\theta \sin i \\ x(1 + 2e\cos f - \hat{\omega}_e \cos i) + z\,\hat{\omega}_e \sin\theta \sin i \\ x\,\hat{\omega}_e \cos\theta \sin i - y\,\hat{\omega}_e \sin\theta \sin i \end{bmatrix} \end{aligned} \tag{4.66}$$

Multiplying out and neglecting higher powers of $\hat{\omega}_e$ and e results in:

$$\begin{aligned}\|\mathbf{v}_0\|\mathbf{v}_1 \approx an\,(1+e\cos f-\hat{\omega}_e\cos i)&\begin{bmatrix}\dot{x}\\ \dot{y}\\ \dot{z}\end{bmatrix}\\ +an^2&\begin{bmatrix}-y\,(1+3e\cos f-2\hat{\omega}_e\cos i)-z\,\hat{\omega}_e\cos\theta\sin i\\ x\,(1+3e\cos f-2\hat{\omega}_e\cos i)+z\,\hat{\omega}_e\sin\theta\sin i\\ x\,\hat{\omega}_e\cos\theta\sin i-y\,\hat{\omega}_e\sin\theta\sin i\end{bmatrix}\end{aligned} \tag{4.67}$$

Orbit-averaging this term gives the following:

$$\frac{1}{2\pi}\int_0^{2\pi}\|\mathbf{v}_0\|\mathbf{v}_1 df \approx an\,(1-\hat{\omega}_e\cos i)\begin{bmatrix}\dot{x}\\ \dot{y}\\ \dot{z}\end{bmatrix}+an^2\begin{bmatrix}-y\,(1-2\hat{\omega}_e\cos i)\\ x\,(1-2\hat{\omega}_e\cos i)\\ 0\end{bmatrix} \tag{4.68}$$

The final term (*III*) is slightly more complicated, and thus will be simplified in segments for clarity. Firstly, the scalar (dot) product of the zeroeth and first order terms will be simplified component by component. For the x-component:

$$\begin{aligned}v_{0,x}v_{1,x} &\approx a\,n\,e\sin f\left[\dot{x}-y\,n\,(1+e\cos f-\hat{\omega}_e\cos i)-z\,n\,\hat{\omega}_e\cos\theta\sin i\right]\\ v_{0,x}v_{1,x} &\approx a\,n\,e\sin f\,(\dot{x}-y\,n)\end{aligned} \tag{4.69}$$

For the y –component:

$$\begin{aligned}v_{0,y}v_{1,y} &\approx an\,(1+e\cos f-\hat{\omega}_e\cos i)\\ &\quad\times\left[\dot{y}+x\,n\,(1+e\cos f-\hat{\omega}_e\cos i)+z\,n\,\hat{\omega}_e\sin\theta\sin i\right]\\ v_{0,y}v_{1,y} &\approx an\left\{\begin{array}{l}\dot{y}(1+e\cos f-\hat{\omega}_e\cos i)\\ \quad+x\,n\,(1+2e\cos f-2\hat{\omega}_e\cos i)+z\,n\,\hat{\omega}_e\sin\theta\sin i\end{array}\right\}\end{aligned} \tag{4.70}$$

For the z -component:

$$\begin{aligned}v_{0,z}v_{1,z} &\approx an(\hat{\omega}_e\cos\theta\sin i)(\dot{z}+x\,n\,\hat{\omega}_e\cos\theta\sin i-y\,n\,\hat{\omega}_e\sin\theta\sin i)\\ v_{0,z}v_{1,z} &\approx an(\dot{z}\,\hat{\omega}_e\cos\theta\sin i)\end{aligned} \tag{4.71}$$

Dividing each of these terms by the magnitude of the zeroeth order vector, where:

$$\|\mathbf{v}_0\|^{-1} \approx \frac{1}{an}\,(1-e\cos f+\hat{\omega}_e\cos i) \tag{4.72}$$

yields the final multiplicative scalar:

$$\left(\frac{\mathbf{v}_0 \cdot \mathbf{v}_1}{\|\mathbf{v}_0\|}\right) \approx e \sin f(\dot{x} - y\,n) + \left[\dot{y} + x\,n(1 + e\cos f - \hat{\omega}_e \cos i) + z\,n\,\hat{\omega}_e \sin\theta \sin i\right] + \dot{z}\,\hat{\omega}_e \cos\theta \sin i \tag{4.73}$$

Multiplying the zeroeth order vector by this scalar results in the final desired quantity:

$$\left(\frac{\mathbf{v}_0 \cdot \mathbf{v}_1}{\|\mathbf{v}_0\|}\right)\mathbf{v}_0 \approx \begin{bmatrix} e\sin f\,(\dot{y} + x\,n) \\ \left\{ \begin{array}{r} e\sin f(\dot{x} - y\,n) + \dot{y}(1 + e\cos f - \hat{\omega}_e \cos i) \\ + x\,n(1 + 2e\cos f - 2\hat{\omega}_e \cos i) + z\,n\,\hat{\omega}_e \sin\theta \sin i + \dot{z}\,\hat{\omega}_e \cos\theta \sin i \end{array} \right\} \\ \hat{\omega}_e \cos\theta \sin i\,(\dot{y} + x\,n) \end{bmatrix} \tag{4.74}$$

Orbit-averaging of this term yields:

$$\frac{1}{2\pi}\int_0^{2\pi}\left(\frac{\mathbf{v}_0 \cdot \mathbf{v}_1}{\|\mathbf{v}_0\|}\right)\mathbf{v}_0 df \approx an\begin{bmatrix} 0 \\ \dot{y}(1 - \hat{\omega}_e \cos i) + x\,n(1 - 2\hat{\omega}_e \cos i) \\ 0 \end{bmatrix} \tag{4.75}$$

Combining these time averaged effects allows us to write the simplified drag acceleration acting on a Deputy spacecraft as follows:

$$\mathbf{a}_{Drag,Deputy} \approx \mathbf{d}_0 + \mathbf{D}_1\mathbf{x} + \mathbf{D}_2\dot{\mathbf{x}} \tag{4.76}$$

where $\mathbf{x}$ and $\dot{\mathbf{x}}$ represent the relative position and velocity vectors respectively of the Deputy with respect to the Chief expressed in the Hill frame and $\mathbf{d}_0$, $\mathbf{D}_1$, and $\mathbf{D}_2$ are given by:

$$\mathbf{d}_0 = -\frac{1}{2}\frac{1}{\beta_D}an^2\begin{bmatrix} 0 \\ 1 - 2\hat{\omega}_e \cos i \\ 0 \end{bmatrix} \tag{4.77}$$

$$\mathbf{D}_1 = -\frac{1}{2}\frac{1}{\beta_D}n^2\begin{bmatrix} 0 & -(1 - 2\hat{\omega}_e \cos i) & 0 \\ 2(1 - 2\hat{\omega}_e \cos i) & 0 & 0 \\ 0 & 0 & 0 \end{bmatrix} \tag{4.78}$$

$$\mathbf{D}_2 = -\frac{1}{2}\frac{1}{\beta_D} n \begin{bmatrix} (1-\hat{\omega}_e \cos i) & 0 & 0 \\ 0 & 2(1-\hat{\omega}_e \cos i) & 0 \\ 0 & 0 & (1-\hat{\omega}_e \cos i) \end{bmatrix} \tag{4.79}$$

In order to further simplify these expressions, two new dimensionless parameters will be defined analogous to the one defined in Chapter 2:

$$\widetilde{\sigma}_1 \equiv 1-\hat{\omega}_e \cos i \tag{4.80}$$

$$\widetilde{\sigma}_2 \equiv 1-2\hat{\omega}_e \cos i \tag{4.81}$$

In order to describe the relative atmospheric drag perturbations of a Deputy spacecraft with respect to the Chief, the drag effects of the Chief must be subtracted. The position of the Chief can be thought of as the position of the reference orbit. The reference orbit is already propagated assuming secular drift due to drag, thus the relative drag effects are found by simply subtracting the simplified orbit-averaged drag effect of the Chief expressed in the Hill frame from the above expression. The final simplified orbit-averaged relative aerodynamic drag perturbations are now given by:

$$\begin{aligned} \mathbf{a}_{Drag,rel} = & -\frac{1}{2}\left(\frac{1}{\beta_D}-\frac{1}{\beta_C}\right) a n^2 \widetilde{\sigma}_2 \begin{bmatrix} 0 \\ 1 \\ 0 \end{bmatrix} \\ & -\frac{1}{2}\frac{1}{\beta_D} n^2 \widetilde{\sigma}_2 \begin{bmatrix} 0 & -1 & 0 \\ 2 & 0 & 0 \\ 0 & 0 & 0 \end{bmatrix} \begin{bmatrix} x \\ y \\ z \end{bmatrix} - \frac{1}{2}\frac{1}{\beta_D} n\, \widetilde{\sigma}_1 \begin{bmatrix} 1 & 0 & 0 \\ 0 & 2 & 0 \\ 0 & 0 & 1 \end{bmatrix} \begin{bmatrix} \dot{x} \\ \dot{y} \\ \dot{z} \end{bmatrix} \end{aligned} \tag{4.82}$$

Where β_D and β_C represent the dimensionless ballistic coefficient of the Deputy and Chief spacecrafts respectively.

4.3 Final Equations of Motion

In this section, the final equations of relative motion will be presented. These relative motion equations express the motion of a particular Deputy or Follower spacecraft with respect to a given Chief or Leader spacecraft. These relative motion equations include the effects of orbit-averaged J_2 and aerodynamic drag perturbations as well as orbital element propagation based on mean secular drift for reference orbit propagation.

First, the relative motion equations themselves will be simplified using the small eccentricity assumption. Recall that the relative motion equations which are valid for general elliptical orbits are given by:

$$\begin{aligned}
&\ddot{x} - 2\dot{\theta}\,\dot{y} - \ddot{\theta}\,y - \left(\dot{\theta}^2 + \frac{2\mu}{r_{ref}^3}\right)x = \Delta a_{J_2,x} + \Delta a_{Drag,x} \\
&\ddot{y} + 2\dot{\theta}\,\dot{x} - \ddot{\theta}\,x - \left(\dot{\theta}^2 - \frac{\mu}{r_{ref}^3}\right)y = \Delta a_{J_2,y} + \Delta a_{Drag,y} \\
&\ddot{z} + \frac{\mu}{r_{ref}^3}z = \Delta a_{J_2,z} + \Delta a_{Drag,z}
\end{aligned} \tag{4.83}$$

where the instantaneous rotation rate of the Hill frame $\dot{\theta}$ has three components in this case due to the fact that the orbital elements are changing with time. This angular rate is given by the following:

$$\dot{\theta} = \dot{f} + \dot{\omega} + \dot{\Omega}\cos i \tag{4.84}$$

where f is the true anomaly, ω is the argument of perigee, and Ω is the right ascension of the ascending node. In the case of the Clohessy-Wiltshire equations, this angular rate is simply the mean orbital rate n of the circular reference orbit. In this case, however, f is a function of time due to the eccentric nature of the

reference orbit and the ω as well the Ω terms are changing with time primarily due to J_2 effects. In order to combine these rates, they must each be projected along the unit normal of the reference orbital plane, i.e. the z-direction of the Hill frame. The $\dot{\mathbf{f}}$ and $\dot{\boldsymbol{\omega}}$ angular velocity vectors are already aligned in this direction by definition (refer to Figure 4-2). The $\dot{\boldsymbol{\Omega}}$ angular velocity vector, however, acts along the vector normal to the orbital place. Thus, the component projected onto the orbit normal vector is $\dot{\Omega}\cos i$.

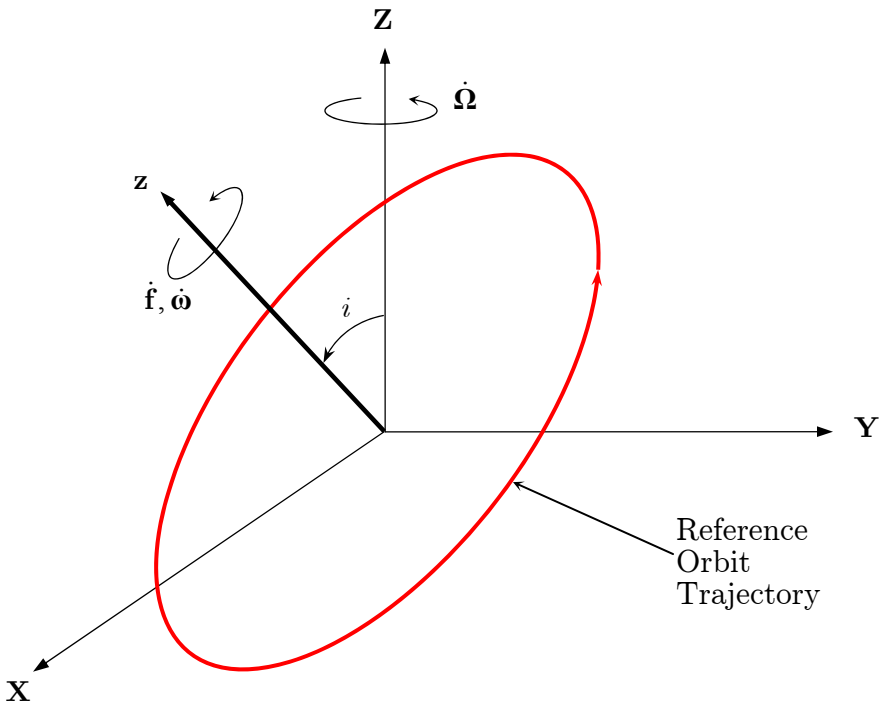

Figure 4-2: Instantaneous Rotation Rate of the Hill Frame

Based on the mean secular drift of the orbital elements described earlier, the component of the rotation rate of the Hill frame due to the argument of perigee and right ascension of the ascending node will be approximated as:

$$\dot{\omega} + \dot{\Omega}\cos i \approx \frac{d\overline{\omega}}{dt} + \frac{d\overline{\Omega}}{dt}\cos i \tag{4.85}$$

which simplifies to:

$$\begin{aligned} \frac{d\overline{\omega}}{dt} + \frac{d\overline{\Omega}}{dt}\cos i &= \frac{3}{4} J_2 n \left(\frac{R_e}{a}\right)^2 \left[3\cos^2 i - 1\right] \\ &= \frac{3}{8} J_2 n \left(\frac{R_e}{a}\right)^2 \left[1 + 3\cos 2i\right] \equiv n\, s \end{aligned} \tag{4.86}$$

From this, we can conclude that the previously defined s represents the correction in the mean rotation rate of the Hill frame due to J_2 effects. It should be noted that the orbit-averaged rate of change of the mean anomaly is also related to s by:

$$\frac{d\overline{M}}{dt} = n\,(1+s) \tag{4.87}$$

The rate of true anomaly $\dot{f}$, is given by the following for Keplerian orbits:

$$\dot{f} = \frac{h}{r^2} \approx n(1 + 2e\cos f) \tag{4.88}$$

Combining these three terms results in the following rotation rate:

$$\dot{\theta} \approx n\left[1 + 2e\cos f + s\right] \tag{4.89}$$

However, comparing this to the Schweighart-Sedwick formulation, there is an inconsistency. In their formulation, this rotation rate is given by:

$$\dot{\theta} = n\,c \equiv n(1+s)^{\frac{1}{2}} \tag{4.90}$$

which can be approximated as:

$$\dot{\theta} \approx n(1 + \tfrac{1}{2}s) \tag{4.91}$$

Thus, by setting eccentricity to zero we would expect to obtain the same result. However, this currently results in:

$$\dot{\theta} \approx n(1+s) \tag{4.92}$$

There appears to be a missing term of $-\frac{1}{2}s$ in the brackets. This term will be assumed to come from the perturbative part of the derivative of the true anomaly. With this assumption, we obtain the final rotation rate of the Hill frame which is consistent with the high fidelity Schweighart-Sedwick model:

$$\dot{\theta} \approx n\left[1 + 2e\cos f + \tfrac{1}{2}s\right] \tag{4.93}$$

Based on this rotation rate, the addition terms needed such as $\dot{\theta}^2$ and $\ddot{\theta}$ can now be determined. For $\dot{\theta}^2$:

$$\dot{\theta}^2 \approx n^2\left[1 + 2e\cos f + \tfrac{1}{2}s\right]^2 \tag{4.94}$$

Since s and e are small compared to 1, this expression may be approximated by a binomial series expansion as:

$$\dot{\theta}^2 \approx n^2\left[1 + 4e\cos f + s\right] \tag{4.95}$$

The remaining term necessary to determine the coefficients related to $\dot{\theta}^2$ of the relative motion equations is given by the following approximate relationship:

$$\frac{\mu}{r_{ref}^3} \approx n^2\left[1 + 3e\cos f\right] \tag{4.96}$$

In order to find $\ddot{\theta}$, we must differentiate the approximate expression for $\dot{\theta}$:

$$\ddot{\theta} \equiv \frac{d}{dt}\dot{\theta} \approx \frac{d}{dt}\left\{n\left[1 + 2e\cos f + \tfrac{1}{2}s\right]\right\} \tag{4.97}$$

Noting that all of the orbital elements are functions of time, applying the chain rule results in:

$$\begin{aligned}\ddot{\theta} \approx -\frac{3}{2}\frac{n}{a}\frac{da}{dt}\left[1 + 2e\cos f + \tfrac{1}{2}s\right] \\ + n\left[-2e\sin f\,\frac{df}{dt} + 2\cos f\,\frac{de}{dt} + \frac{1}{2}\frac{ds}{dt}\right]\end{aligned} \tag{4.98}$$

Substituting the approximate orbit-averaged derivatives of the orbital elements and simplifying results in the following:

$$\begin{aligned}\ddot{\theta} \approx & \frac{3}{2} n^2 \frac{1}{\beta_C}\left[1+\tfrac{4}{3} e\cos f - 2\hat{\omega}_e \cos i + \tfrac{1}{2} s\right] \\ & -2n^2 e \sin f \left[1+2e\cos f - \tfrac{1}{2} s\right] \\ & +\frac{3}{16} n^2 J_2 \left(\frac{R_e}{a}\right)^2 \frac{1}{\beta_C}\left[-4+11\hat{\omega}_e \cos i + 12\cos^2 i - 27\hat{\omega}_e \cos^2 i\right]\end{aligned} \tag{4.99}$$

The magnitude of the $\beta_C{}^{-1}$ term will vary depending on the altitude of the orbit (refer to Figure 4-3). Thus it cannot simply be neglected compared to small values of eccentricity; it depends on the situation and thus should be included in the coefficient. The J_2 term is approximately equal to $-\frac{3}{4} s$ which exactly cancels the $+\frac{3}{4} s$ in the first bracket.

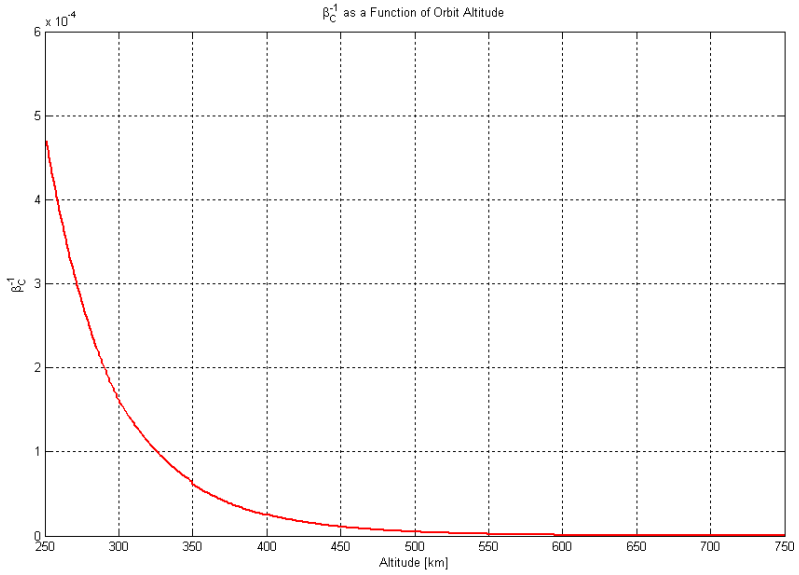

Figure 4-3: Dimensionless Ballistic Coefficient as a Function of Altitude

Thus, the rate of change of the rate of rotation of the Hill frame may be approximated as:

$$\ddot{\theta} \approx n^2 \left\{\frac{3}{2}\frac{1}{\beta_C}\left[1+\tfrac{4}{3} e\cos f - 2\hat{\omega}_e \cos i\right] - 2e\sin f\left[1+2e\cos f - \tfrac{1}{2} s\right]\right\} \tag{4.100}$$

We recognize that the term multiplying the β_C^{-1} resembles the averaged $\widetilde{\sigma}_2$ parameter defined earlier. In light of this, it seems appropriate to correct the $\widetilde{\sigma}_i$ terms for consistency and to gain back some of what was lost in the averaging process, thus these will be redefined as:

$$\widetilde{\sigma}_1 \equiv 1 + \tfrac{2}{3} e \cos f - \hat{\omega}_e \cos i \tag{4.101}$$

$$\widetilde{\sigma}_2 \equiv 1 + \tfrac{4}{3} e \cos f - 2\hat{\omega}_e \cos i \tag{4.102}$$

Including the now simplified orbit-averaged J_2 and aerodynamic drag effects allows us to write the relative motion equations in their final simplified form. In matrix-vector form, these equations can be written as:

$$\mathbf{M}_e \ddot{\mathbf{x}} + \mathbf{C}_e \dot{\mathbf{x}} + \mathbf{K}_e \mathbf{x} = \mathbf{f}_e \tag{4.103}$$

where the subscript e is used to differentiate between the matrices given in Chapter 2 and is meant to denote elliptical. The generalized matrix of inertia $\mathbf{M}_e$ is given by:

$$\mathbf{M}_e = \begin{bmatrix} 1 & 0 & 0 \\ 0 & 1 & 0 \\ 0 & 0 & 1 \end{bmatrix} \tag{4.104}$$

the damping matrix $\mathbf{C}_e$ is given by:

$$\mathbf{C}_e = n \begin{bmatrix} \frac{1}{2}\frac{1}{\beta_D}\widetilde{\sigma}_1 & -2\,(1 + 2e\cos f + \tfrac{1}{2}s) & 0 \\ 2\,(1 + 2e\cos f + \tfrac{1}{2}s) & \frac{1}{\beta_D}\widetilde{\sigma}_1 & 0 \\ 0 & 0 & \frac{1}{2}\frac{1}{\beta_D}\widetilde{\sigma}_1 \end{bmatrix} \tag{4.105}$$

and the stiffness matrix $\mathbf{K}_e$ is given by:

$$\mathbf{K}_e = n^2 \begin{bmatrix} -(3+10e\cos f+5s) & -\frac{\ddot{\theta}}{n^2}-\frac{1}{2}\frac{1}{\beta_D}\widetilde{\sigma}_2 & -4e\widetilde{s}\sin\omega \\ -\frac{\ddot{\theta}}{n^2}+\frac{1}{\beta_D}\widetilde{\sigma}_2 & -e\cos f & e\widetilde{s}\cos\omega \\ -4e\widetilde{s}\sin\omega & e\widetilde{s}\cos\omega & 1+3e\cos f+3s \end{bmatrix} \tag{4.106}$$

For consistency with the Schweighart-Sedwick formulation, these can be written in terms of c:

$$\mathbf{C}_e = n \begin{bmatrix} \frac{1}{2}\frac{1}{\beta_D}\widetilde{\sigma}_1 & -2(c+2e\cos f) & 0 \\ 2(c+2e\cos f) & \frac{1}{\beta_D}\widetilde{\sigma}_1 & 0 \\ 0 & 0 & \frac{1}{2}\frac{1}{\beta_D}\widetilde{\sigma}_1 \end{bmatrix} \tag{4.107}$$

$$\mathbf{K}_e = n^2 \begin{bmatrix} -(5c^2-2+10e\cos f) & -\frac{\ddot{\theta}}{n^2}-\frac{1}{2}\frac{1}{\beta_D}\widetilde{\sigma}_2 & -4e\widetilde{s}\sin\omega \\ -\frac{\ddot{\theta}}{n^2}+\frac{1}{\beta_D}\widetilde{\sigma}_2 & -e\cos f & e\widetilde{s}\cos\omega \\ -4e\widetilde{s}\sin\omega & e\widetilde{s}\cos\omega & (3c^2-2+3e\cos f) \end{bmatrix} \tag{4.108}$$

Notice that setting eccentricity and drag equal to zero, we obtain a version of the Schweighart-Sedwick equations. Furthermore, setting J_2 (s) equal to zero, we obtain the Clohessy-Wiltshire equations.

The forcing function $\mathbf{f}_e$ is given by:

$$\mathbf{f}_e = -\frac{1}{2}\left(\frac{1}{\beta_D}-\frac{1}{\beta_C}\right)an^2\widetilde{\sigma}_2\begin{bmatrix}0\\1\\0\end{bmatrix} = -\frac{1}{2}\frac{1}{\beta_D}\left(1-\frac{\beta_D}{\beta_C}\right)an^2\widetilde{\sigma}_2\begin{bmatrix}0\\1\\0\end{bmatrix} \tag{4.109}$$

It should be noted that this forcing function is equal to zero if the two spacecraft have identical values of dimensionless ballistic coefficient. However, changing the ratio of their ballistic coefficients results in either a positive or negative forcing in the in-track direction and can thus be used as the means of formation control. The

meaning of these dimensionless drag coefficients should be kept in mind. These terms are defined as follows for the Chief and Deputy

$$\beta_C \equiv \left[\rho_C \left(\frac{C_D A}{m} \right)_C a_{ref} \right]^{-1} \tag{4.110}$$

$$\beta_D \equiv \left[\rho_D \left(\frac{C_D A}{m} \right)_D a_{ref} \right]^{-1} \tag{4.111}$$

where ρ_C and ρ_D are the local atmospheric density for the Chief and Deputy spacecraft respectively. Generally speaking, local atmospheric density ρ is not the same for both spacecraft and should be calculated individually when doing numerical simulations. Theoretically speaking, in the case of elliptical orbits density will not be the same. When spacecraft are both in circular orbits, their altitude above a spherical Earth is constant and thus density would be constant (following a simple exponential model). In the case of elliptical orbits, the two spacecraft will be varying in altitude at different rates in time, thus local density would not be the same in theory. In reality, there are even more factors that can also affect local density, such as level of solar or geomagnetic activity and even simply passing between night and day during one orbit. Thus, this assumption is not generally valid and should be considered with care.

These equations can also be written in state-space form as follows:

$$\dot{\mathbf{X}} = \mathbf{A}_e \mathbf{X} + \mathbf{W}_e \tag{4.112}$$

where

$$\mathbf{X} = \begin{bmatrix} \mathbf{x} \\ \dot{\mathbf{x}} \end{bmatrix} \tag{4.113}$$

$$\mathbf{A}_e = \begin{bmatrix} \mathbf{0}_{3\times 3} & \mathbf{M}_e \\ -\mathbf{K}_e & -\mathbf{C}_e \end{bmatrix} \tag{4.114}$$

$$\mathbf{W}_e = \begin{bmatrix} \mathbf{0}_{3\times 1} \\ \mathbf{f}_e \end{bmatrix} \tag{4.115}$$

In all these matrices, the terms which are multiplied by $\tilde{\sigma}_i$'s or β refer to drag effects, those which are multiplied by an s or $\tilde{s}$ refer to J_2 effects, and the remaining eccentricity terms characterize the changing rotation rate of the elliptical reference orbit. More specifically, the $\tilde{\sigma}_i$ terms are those which account for the rotation rate of the Earth, the dimensionless ballistic coefficient β characterizes the magnitude of the drag effects by accounting for the spacecraft physical characteristics as well as altitude (semi-major axis) and atmospheric density, the s and $\tilde{s}$ terms characterize the magnitude of the J_2 effect for the given situation by including the J_2 (second spherical harmonic of the Earth's gravitational potential) constant as well as the orbit size (semi-major axis) and inclination. Thus, it is relatively straightforward to see at a glance what each of the terms in these matrices physically represents and how large their magnitudes will be for a given set of circumstances.

Chapter 5 - Numerical Simulations for Elliptical Reference Orbits

In this section, numerical simulation results based the linearized equations developed in Chapter 4 will be presented. The first set of results will examine the case of a circular reference orbit and will be used primarily to validate the simplified linear dynamic model by comparison with the assumed accurate non-linear simulation results presented in Chapter 3. Following this will be some preliminary results for elliptical reference orbits.

5.1 Projected Circular Formation

The details related to the geometry and initial conditions for the projected y-z circular formation were given in Chapter 3. The same formation geometry and circular reference orbit parameters will be used for a comparison of results with those obtained in Chapter 3. These reference orbit parameters were given in Table 3-4. Following this, preliminary results for elliptical reference orbits will be presented.

5.1.1 Comparison of Results for Circular Orbits

For this comparison study, the TECSAS physical parameters were selected. The first case considered was that of a 500 km altitude circular reference orbit (results shown in Figure 5-1). The results obtained here are very similar to those of

Chapter 3. The in-plane motion is identical in this case but there is a slight deviation in the prediction of the cross-track motion, namely an over estimation the cross-track drift.

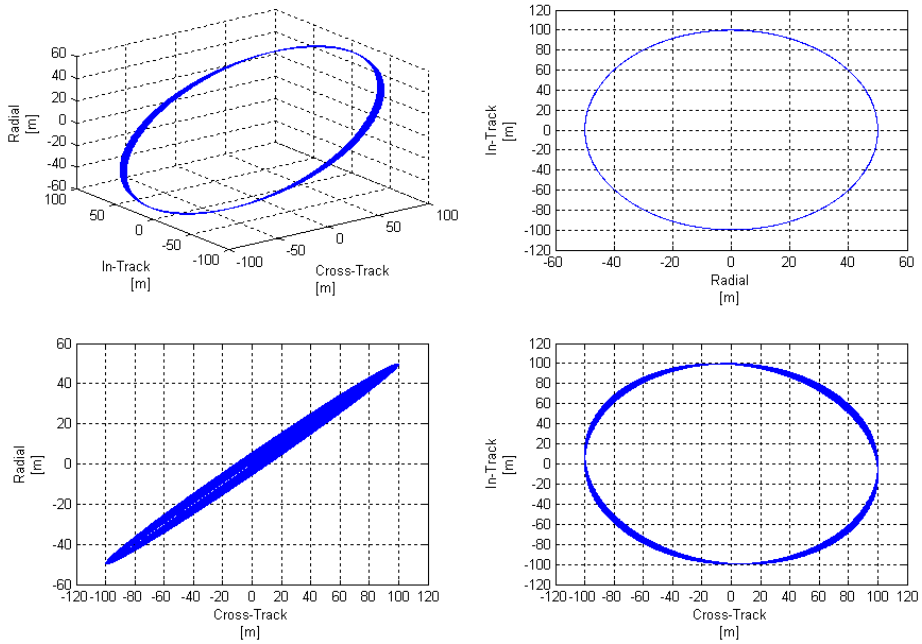

Figure 5-1: Projected y-z circular formation - J_2 and drag perturbations – 500 km altitude – 78° inclination –TECSAS Physical Parameters – 24 hour simulation

The next case considered was that of a 300 km altitude circular reference orbit. Figure 5-2 shows the resulting relative motion and Figure 5-3 shows how the average orbital elements drift with time. Here, we see a very similar in-plane response to that which was found in Chapter 3. The main discrepancy is again in the prediction of the cross-track motion. Similarly for the 250 km altitude case, (shown in Figure 5-4) the in-plane response is quite similar to what was obtained in Chapter 3, but the cross-track motion is slightly larger than previously predicted. The in-plane drift in this last case is also slightly less than that predicted in Chapter 3, however the in-plane damping appears to be approximately the same.

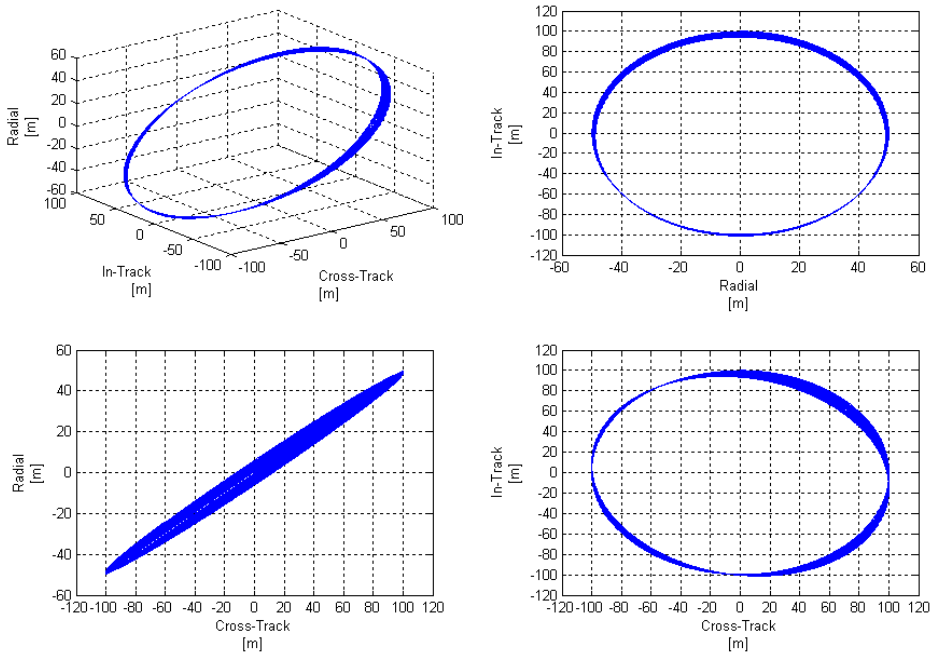

Figure 5-2: Projected y-z circular formation - J_2 and drag perturbations – 300 km altitude – 78° inclination – TECSAS Physical Parameters – 24 hour simulation

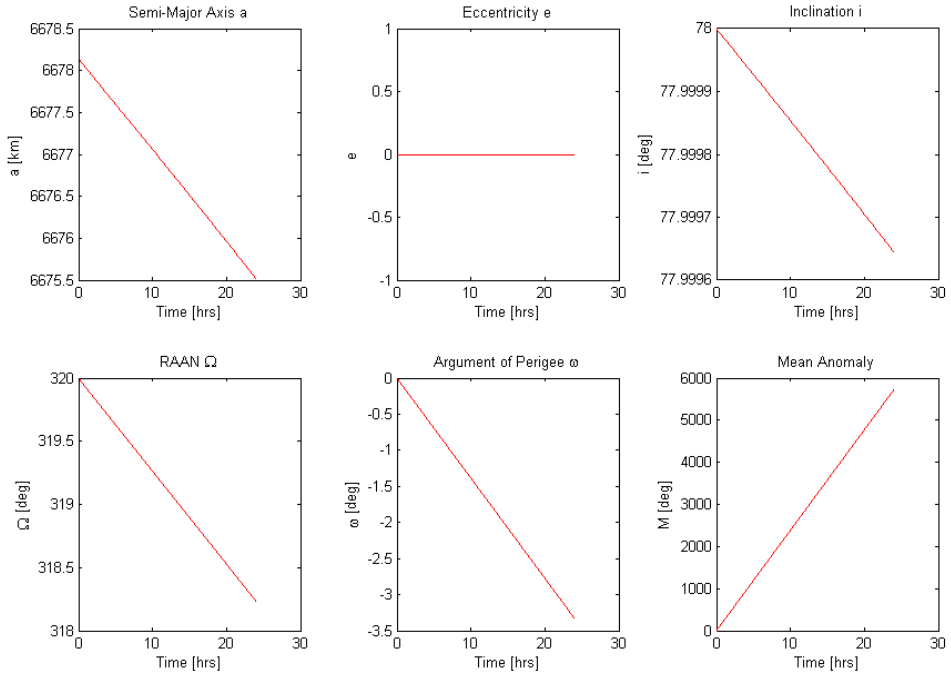

Figure 5-3: Projected y-z circular formation - J_2 and drag perturbations – 300 km altitude – 78° inclination – TECSAS Physical Parameters – 24 hour simulation – drift of the orbital elements

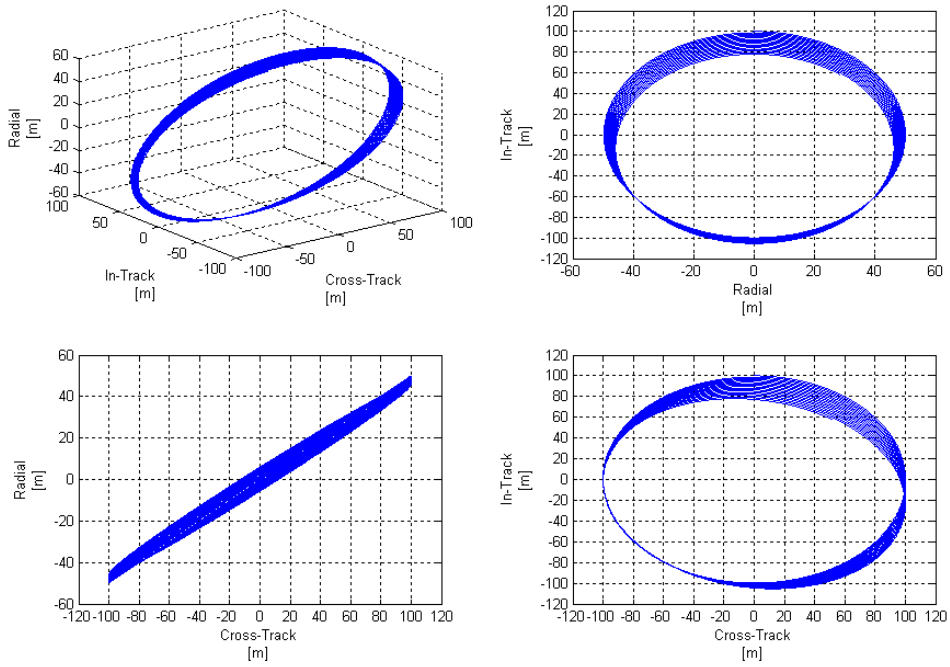

Figure 5-4: Projected y-z circular formation - J_2 and drag perturbations – 250 km altitude – 78° inclination – TECSAS Physical Parameters – 24 hour simulation

5.1.2 Results for Elliptical Orbits

The scenario considered for analysis here was a reference orbit of small eccentricity ranging from 10^{-6} to 10^{-4} with an altitude of perigee of 300 km. The initial conditions used were the same as those used in the previous section. Using these initial conditions, we would expect a secular drift to develop due simply to the fact that these initial conditions assume a circular reference orbit and do not account for its true eccentric nature. The case of zero eccentricity will be used as the baseline for comparison and is given in Figure 5-2.

The first case considered was that of an eccentricity of 10^{-6}. The result for this scenario is given in Figure 5-5. Comparing this to the circular reference orbit case, there is no noticeable difference over the 24 hour period under consideration.

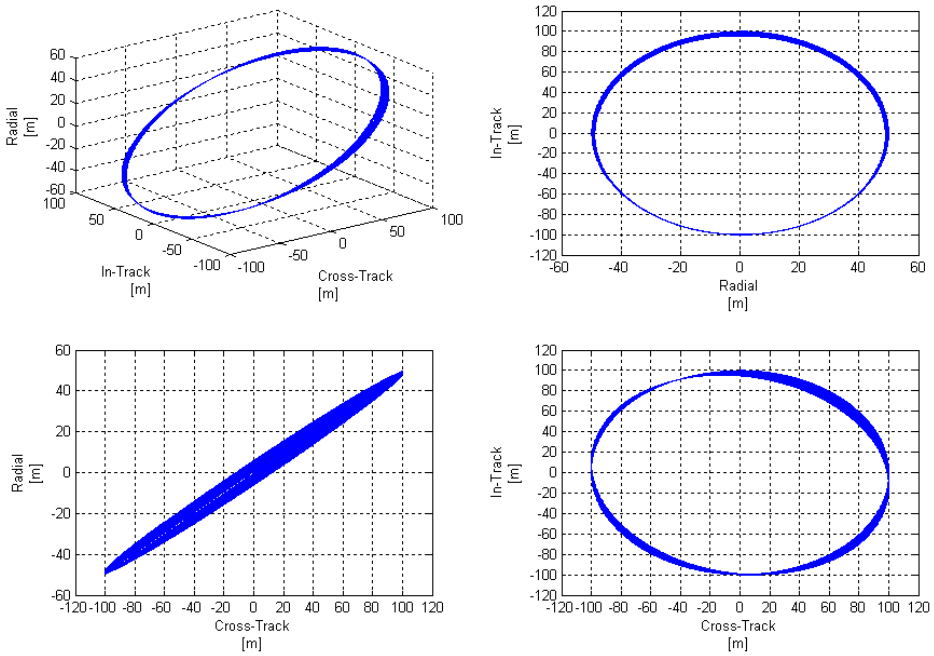

Figure 5-5: Projected y-z circular formation - J_2 and drag perturbations – 300 km altitude – 78° inclination – TECSAS Physical Parameters – 24 hour simulation – Eccentricity = 10^{-6}

The next case considered was a reference orbit of eccentricity equal to of 10^{-5}. Here, there is a visible positive in-track drift that develops (the results are shown in Figure 5-6). The results for an eccentricity of 2.5×10^{-5} and 1×10^{-4} are given in Figures 5-7 and 5-8 respectively. As eccentricity is increased this secular in-track drift also appears to increase. This secular drift is likely due primarily to the fact that eccentricity was not taken into consideration when this relative motion was initialized. Thus, further study as to how relative orbits should be setup in order to account for eccentricity and eliminate this secular drift is required.

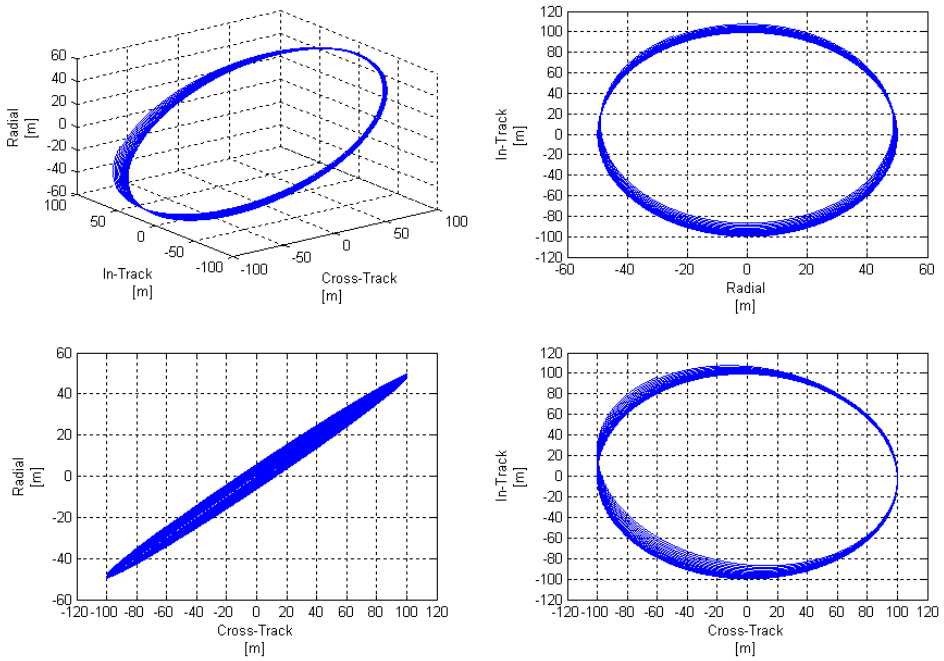

Figure 5-6: Projected y-z circular formation - J_2 and drag perturbations – 300 km altitude – 78° inclination – TECSAS Physical Parameters – 24 hour simulation – Eccentricity = 10^{-5}

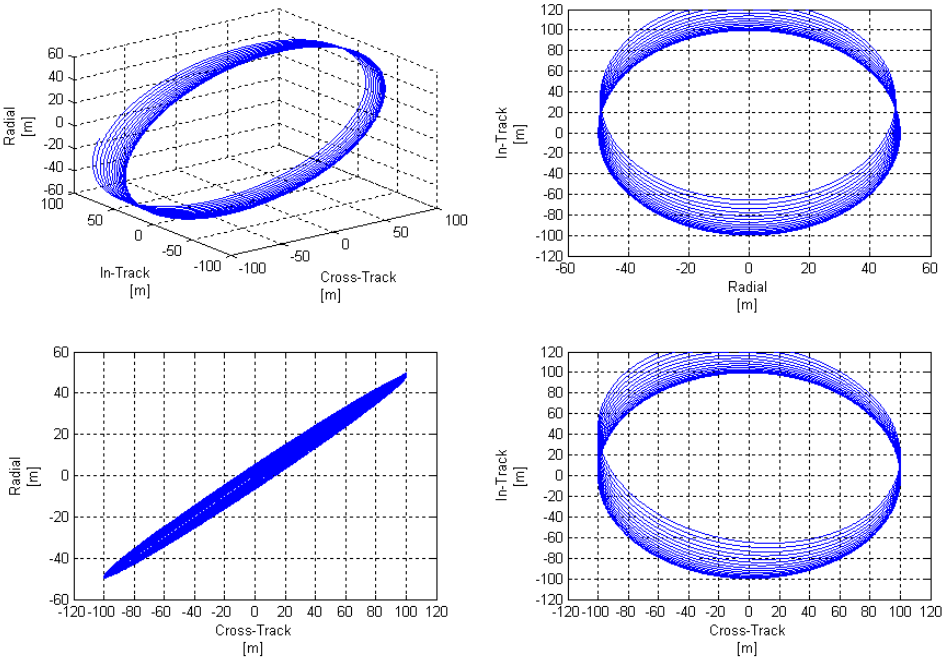

Figure 5-7: Projected y-z circular formation - J_2 and drag perturbations – 300 km altitude – 78° inclination –TECSAS Physical Parameters – 24 hour simulation – Eccentricity = 2.5×10^{-5}

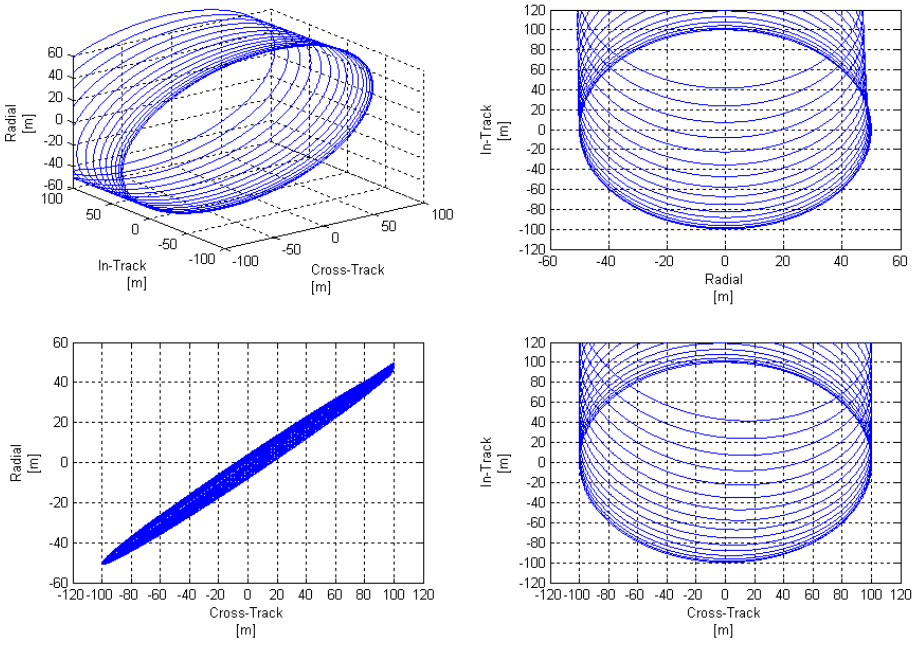

Figure 5-8: Projected y-z circular formation - J_2 and drag perturbations – 300 km altitude – 78° inclination – TECSAS Physical Parameters – 24 hour simulation – Eccentricity = 10^{-4}

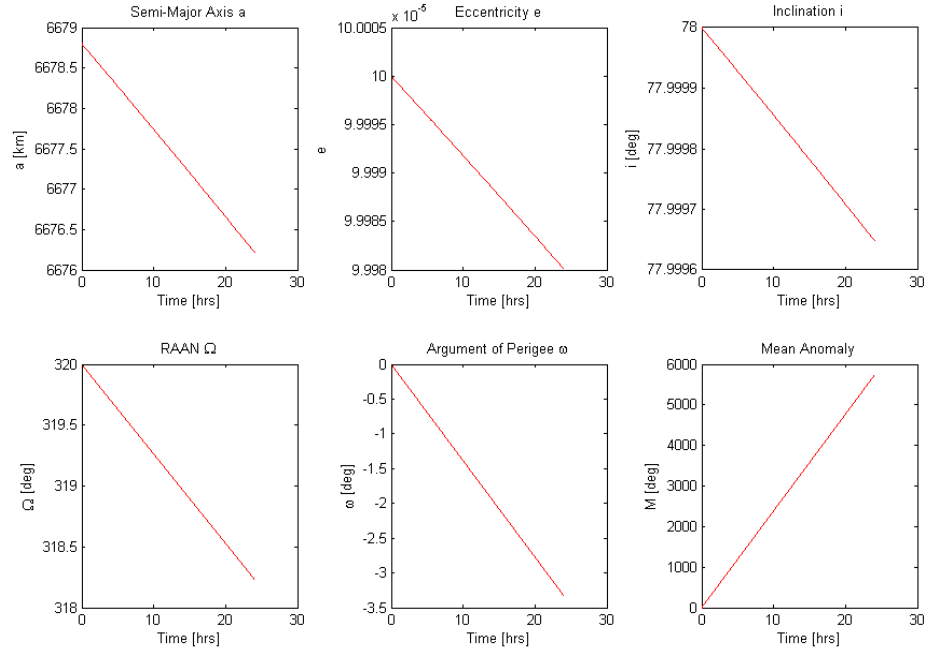

Figure 5-9: Projected y-z circular formation - J_2 and drag perturbations – 300 km altitude – 78° inclination – TECSAS Physical Parameters – 24 hour simulation – Eccentricity = 10^{-4} – drift of the orbital elements

For completeness, the feasibility of eliminating this large in-track drift via differential drag was examined. In this case, it was determined that an increase of area of the Chief with respect to the Deputy was required. For an altitude of 300 km and an eccentricity of 1×10^{-4}, less than a 1% differential drag was required to compensate for the drift (please refer to Figure 5-10 for results).

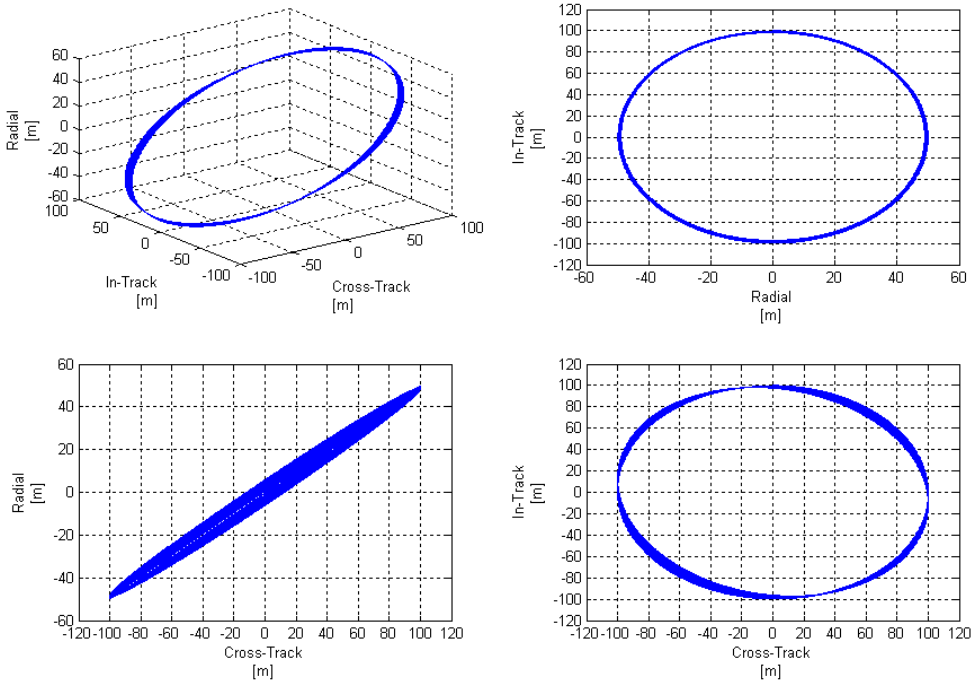

Figure 5-10: Projected y-z circular formation - J_2 and drag perturbations – 300 km altitude – 78° inclination – TECSAS Physical Parameters – 24 hour simulation – Eccentricity = 10^{-4} - Differential drag drift compensation

Although this 1% increase in area may seem like only a small amount required, consider a much higher altitude of say 700 km where the drag force is much smaller. The uncompensated motion in this case is shown in Figure 5-11. To compensate for the in-track drift in this case an increase in drag area of 43% of the Chief was required (results shown in Figure 5-12). Thus, the ease with which such drift can be compensated via differential drag diminishes quickly as altitude increases.

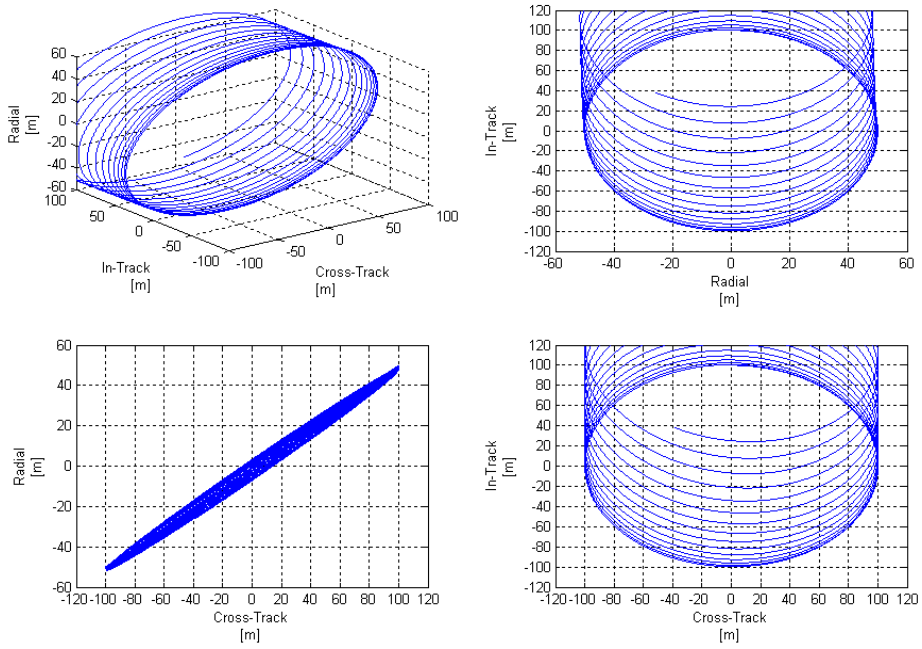

Figure 5-11: Projected y-z circular formation - J_2 and drag perturbations – 700 km altitude – 78° inclination – TECSAS Physical Parameters – 24 hour simulation – Eccentricity = 10^{-4}

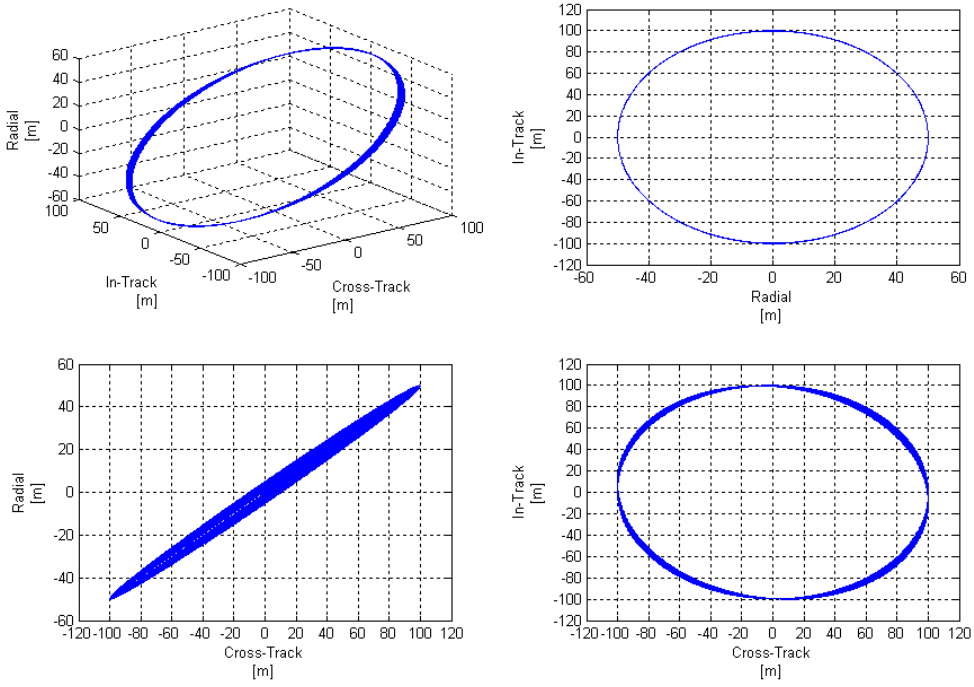

Figure 5-12: Projected y-z circular formation - J_2 and drag perturbations – 700 km altitude – 78° inclination – TECSAS Physical Parameters – 24 hour simulation – Eccentricity = 10^{-4} - Differential drag drift compensation

5.2 In-Track Formation

The geometry and initial conditions for an in-track formation are given in detail in Chapter 3. First, a comparison of results with those obtained in a study using STK's High Precision Orbit Propagator will be presented. Following this, will be a comparison of results with those obtained in Chapter 3. Preliminary results for elliptical reference orbits will then be given.

5.2.1 Comparison of Results for Circular Orbits

For a preliminary analysis the results obtained by solving these linear differential equations for an in-track formation was compared to the results obtained by Shankar Kumar and Ng (2007) in a study using Analytical Graphics Inc's (AGI) Satellite Tool Kit (STK) High Precision Orbit Propagator (HPOP). This study by Shankar Kumar and Ng (2007) was to assess the magnitude of the drift caused by differential drag at different altitudes and was done as part of a preliminary feasibility study for the upcoming JC2Sat mission. A 600 km altitude, sun synchronous orbit is the situation considered here for comparison. The spacecraft physical parameters used in the simulation were given previously in Table 3-5. When the Chief spacecraft is assumed to have an increase in drag area of 10%, the resulting in-track drift for various levels of solar activity using STK was shown previously in Figure 3-22. The results obtained using the linear model is given in Figure 5-13. The general trend in the motion is the same in both cases and the in-track and radial drift predicted by the linear model is approximately the same as that predicted by the STK simulation using an average level solar activity.

However, the results using the linear model are not quite as accurate as those obtained using the Schweighart-Sedwick equations with added non-linear drag, i.e. the numerical model used in Chapter 3. As in the case of the project circular formation results, the linear model appears to be underestimating the in-track drift due to drag.

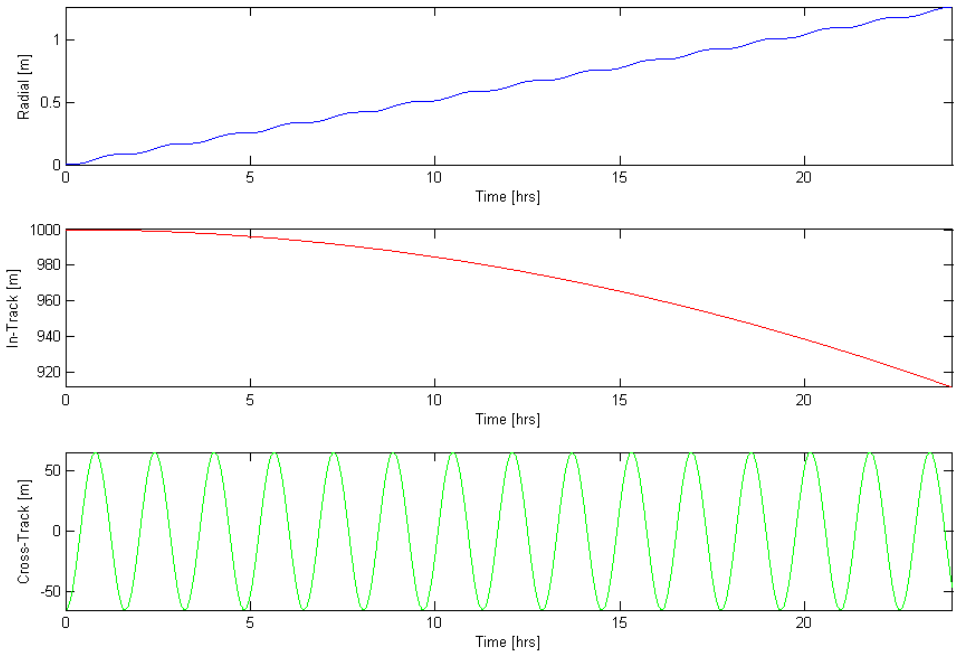

Figure 5-13: In-track drift due to a 10% differential drag area - results obtained using the linearized equations – Sun Synchronous – 600 km altitude

The next scenario considered for a comparison of results was the simulations done for the TECSAS spacecraft in Chapter 3. This represents an in-track formation with an in-track separation distance of 100 meters. The results obtained for the case of a circular reference orbit of an altitude of 500 km using the linear equations are shown in Figure 5-14. The trend in the motion, namely a predominant in-track drift is the same as what was seen in Chapter 3 and the

magnitude of the results are also similar but not exact. As before, the linear model appears to be predicting a smaller in-track drift than the equations used in Chapter 3. Discrepancies start to become very apparent in the 300 km and 250 km altitude cases (shown in Figures 5-15 and 16). In these cases, the in-track drift is much smaller in comparison to that predicted in Chapter 3.

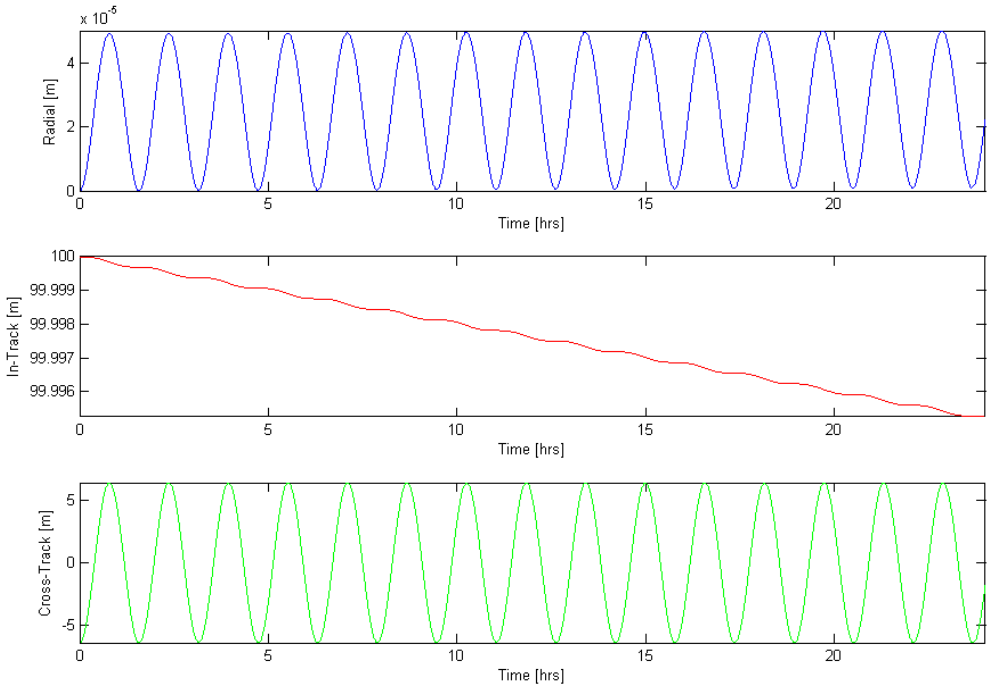

Figure 5-14: In-track formation - J_2 and drag perturbations – 500 km altitude – 78° inclination – TECSAS Physical Parameters – 24 hour simulation

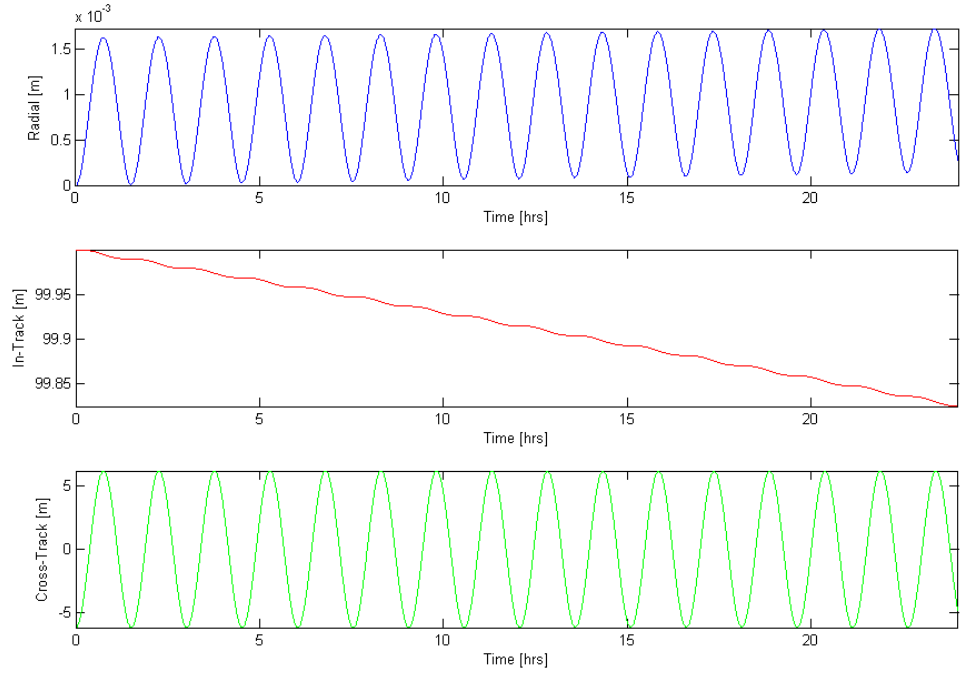

Figure 5-15: In-track formation - J_2 and drag perturbations – 300 km altitude – 78° inclination – TECSAS Physical Parameters – 24 hour simulation

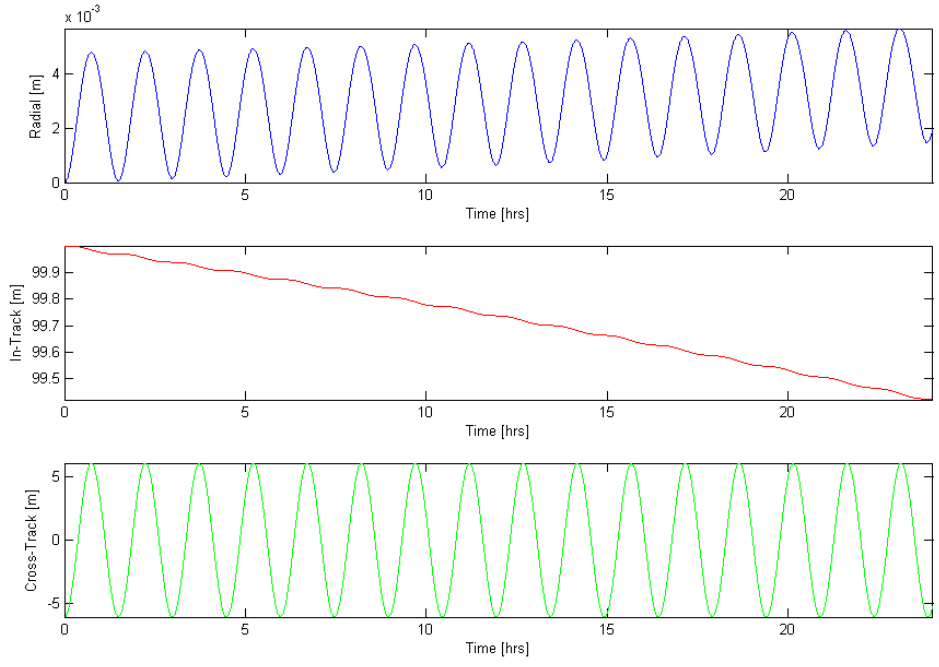

Figure 5-16: In-track formation - J_2 and drag perturbations – 250 km altitude – 78° inclination – TECSAS Physical Parameters – 24 hour simulation

5.2.2 Results for Elliptical Orbits

Although the results for the in-track formation do not agree in totality with the results obtained in Chapter 3 for the circular case, some preliminary results for an eccentric reference orbit will still be given for completeness.

The case considered here is a reference orbit with an altitude of perigee of 500 km and the remaining orbital elements are those used in the previous section. A 500 km altitude was selected as this was the altitude where the results matched closest with those obtained in Chapter 3 for the circular case. The results for an eccentricity of 10^{-4} is given in Figure 5-17. As in the case of a projected circular formation, there is a predominant in-track drift that develops in the positive direction. Similar results are given for an eccentricity of 10^{-3} (shown in Figure 5-18) and an eccentricity of 5×10^{-3} (shown in Figure 5-19). The results show the same trend as found for the projected circular formation, namely as eccentricity is increased, the resulting in-track drift also increases. Remember that these initial conditions also assume a circular reference orbit, thus a secular drift will likely be present due to this factor alone.

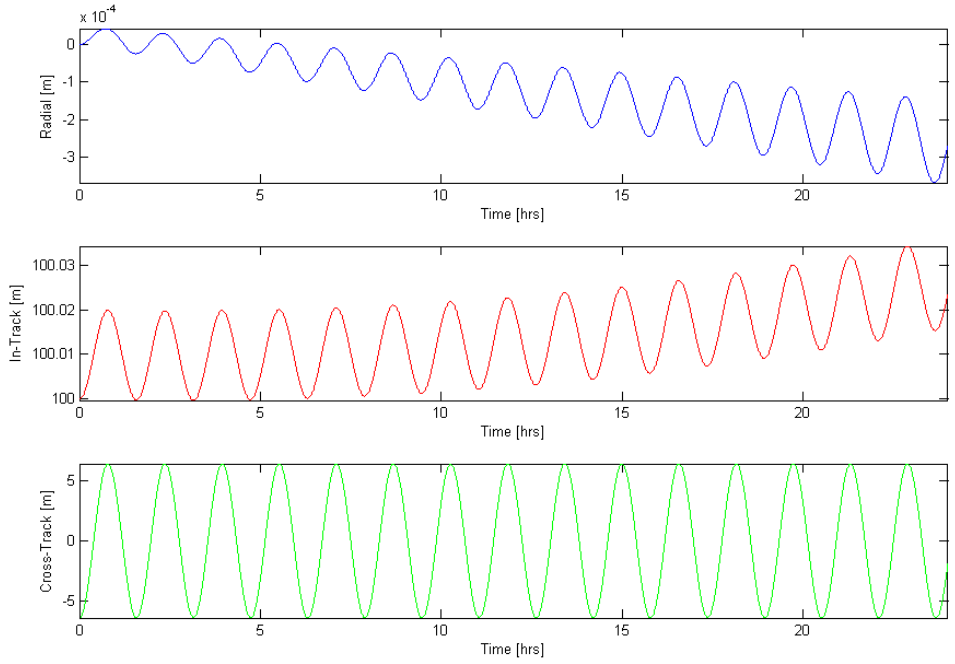

Figure 5-17: In-track formation - J_2 and drag perturbations – 500 km altitude – 78° inclination – TECSAS Physical Parameters – 24 hour simulation – Eccentricity = 10^{-4}

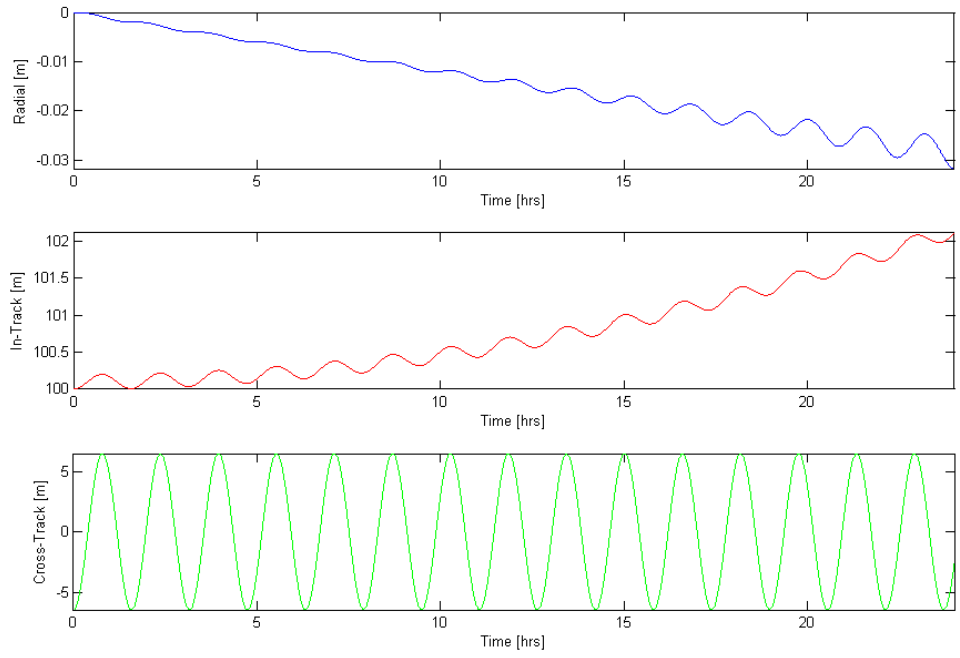

Figure 5-18: In-track formation - J_2 and drag perturbations – 500 km altitude – 78° inclination – TECSAS Physical Parameters – 24 hour simulation – Eccentricity = 10^{-3}

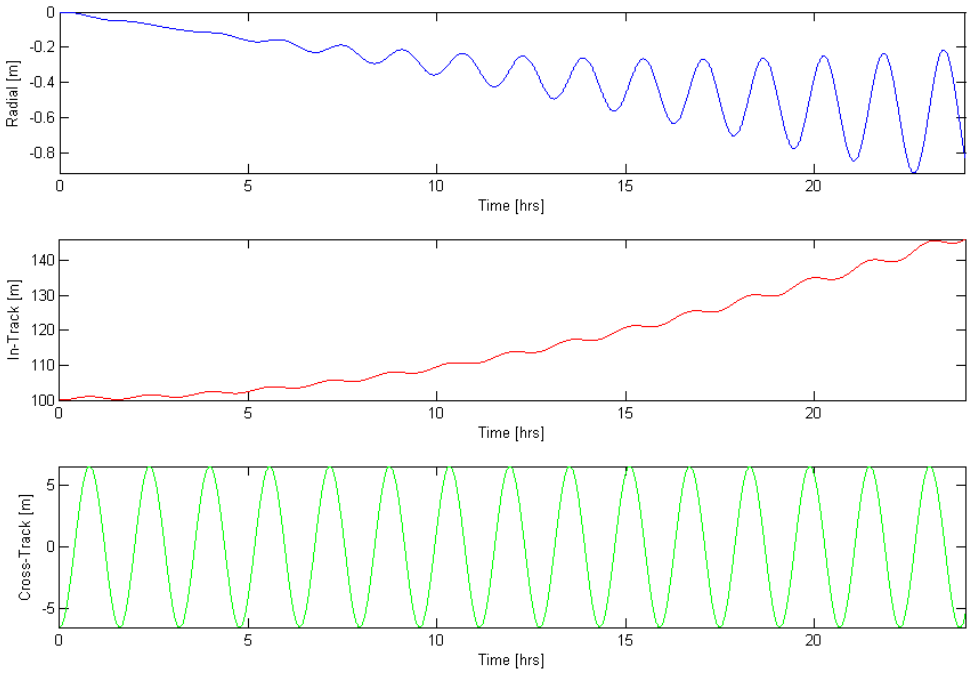

Figure 5-19: In-track formation - J_2 and drag perturbations – 500 km altitude – 78° inclination – TECSAS Physical Parameters – 24 hour simulation – Eccentricity = 5×10^{-3}

Chapter 6 - Conclusion

In this thesis, the effect of aerodynamic drag on the formation flight of satellites was examined. For this study, the linearized Schweighart-Sedwick equations, which include the effects due to J_2 perturbations, were first modified to include the effects of atmospheric drag. These drag effects were then linearized resulting in a set of linear differential equations of relative motion valid for circular orbits which include both Earth oblateness and atmospheric drag effects. These ideas were extended to include orbits of small eccentricity. The end result was a set of linear differential equations which include the aforementioned effects which are valid for certain cases of eccentric orbits. The thesis development and numerical simulation results are given in the following section

6.1 Summary of the Thesis

In the first chapter, a literature review was presented concerning satellite formation flying with an emphasis on work which involved analysis on either using drag as means of formation maintenance and control or on dynamic models which included the effects of drag.

Chapter 2 began with an introduction to the coordinate frames used in the description of spacecraft orbits as well as those used in relative motion analysis. Following this, the equations of motion used in the preliminary analysis, namely the Schweighart-Sedwick equations, were introduced. The equations that describe the drag effects were then transformed to their equivalent description in the Hill frame and added to Schweighart-Sedwick equations. This set of now non-linear

differential equations was non-dimensionalized by means of introducing dimensionless position and velocity variables as well as other dimensionless parameters. The additional drag terms were then simplified and linearized by means of a binomial series expansion. Based on this, the final simplified linear dynamic model valid for circular orbits was presented. Further simplifications were made for the special of identical spacecraft ballistic coefficients and comparable atmospheric densities. Using this simplified dynamic model, a preliminary stability analysis was completed where differential drag was specified as being the control input variable.

Chapter 3 presented numerical simulation results based on the non-dimensionlized form of Schweighart-Sedwick equations with added non-linear drag. This was done to obtain some results which can be considered as accurate in order to assess the effects due to drag on formations. Three different sets of spacecraft physical parameters were used in this analysis, specifically those of TECSAS, JC2Sat, and the invented TEST parameters. First a project y-z circular formation was considered. Results for an altitude range of 250 km to 500 km over a period of 24 hours were presented. The predominant effects due to drag occur mainly on the in-plane motion. We see two primary effects on the relative motion as a result of drag, namely a negative in-track drift as well as a damping of the in-plane motion, or a shrinking of the projected in-plane ellipse. Earth oblateness effects appear to have an effect principally on the cross-track motion. Results for an in-track type formation are also presented. Results are compared in one case with results obtained using the highly accurate commercial software STK (Satellite Tool Kit). The results for the in-track formation are consistent with those obtained for the projected circular case, that is an in-track drift appears as a result of the inclusion

drag effects. The feasibility of formation keeping using drag was also demonstrated for certain situations.

Chapter 4 presents the equations which are valid for eccentric orbits. In order to simplify this formulation, we restricted the analysis to reference orbits of small eccentricity. First, the propagation of the reference orbit was considered. The method selected to do this was to derive expressions which describe the variation of the orbital elements with time due to J_2 and drag perturbation forces. In order to obtain these equations, the Gaussian form of the Variation of Parameters of the orbital elements was employed. These equations allow for the inclusion of both dissipative forces such as drag and conservative forces such as J_2 potential to be taken into account. These perturbation forces are given for both J_2 and drag and the resulting variational equations are simplified based on the small eccentricity assumption. This set of six first order differential equations are then simplified further by using the semi-analytical method of averaging, thus capturing the mean secular drift of the orbital elements. Next, the relative perturbation forces are presented. These perturbation forces are linearized and orbit-averaged in order to simplify these expressions to a manageable size and form. The resulting linearized equations of relative motion are valid for both different values of ballistic coefficient and atmospheric density.

Chapter 5 completes the analysis by presenting numerical results based on the linearized equations of relative motion developed in Chapter 4. These simulations are consistent with those obtained using the non-linear model used in the simulations of Chapter 3. That being said, there some discrepancies in certain cases. For projected circular formations, the in-plane motion appears to be consistent with Chapter 3. However, the cross-track drift due to J_2 effects appears

to be over estimated by the linear equations. For in-track formations, the in-track drift due to drag appears to be under-estimated in some cases by the linear equations. Some preliminary results which demonstrate the effects of an eccentric reference orbit were presented for both the projected circular and in-track formations. The results in all cases indicate that a positive in-track drift arises due to eccentric effects. This is in part due to the fact that the initial conditions assume a circular reference orbit and thus do not account for its eccentricity.

6.2 Recommendations for Future Work

First, further validation of the linear model developed in Chapter 4 is required. The discrepancies which arise in numerical simulation results should be examined further. An additional examination of the cross-track motion appears to be in order. Schweighart and Sedwick (2002) employed a slightly different approach to correct the cross-track motion using spherical geometry. Perhaps these ideas can be extended to elliptical orbits and included in the formulation. Also, perhaps a more accurate numerical model should be used as a baseline for comparison for longer time periods due to the limitations on the current one which are discussed in the thesis.

Based on these linear differential equations which are valid for elliptical orbits, a stability analysis should be completed. Later, a control law using drag as the input control variable should be developed and validated via a MATLAB/SIMULINK© numerical model.

Further examination of motion in elliptical orbits should also be completed. More analysis and perhaps the development of methods of orbit initialization (i.e. initial conditions) which eliminate the secular drift inherent to those presented in this thesis which are based on circular reference orbits should be completed.

Appendix A - Coordinate Transformation

In this appendix, the velocity of a spacecraft with respect to the rotating atmosphere expressed in the Hill frame will be determined. The velocity of a spacecraft with respect to the rotating atmosphere $\mathbf{v}_{spacecraft_{rel}}$ is given by the following equation (Vallado, 2007):

$$\mathbf{v}_{spacecraft_{rel}} = \mathbf{v}_{spacecraft} - \boldsymbol{\omega}_e \times \mathbf{r}_{spacecraft} \tag{A.1}$$

where the $\mathbf{r}_{spacecraft}$ and $\mathbf{v}_{spacecraft}$ terms represent the absolute position and velocity of the spacecraft with respect to the center of the Earth respectively. The $\boldsymbol{\omega}_e$ vector represents the angular velocity vector of the Earth and it is defined in the ECI frame as follows:

$$\boldsymbol{\omega}_e = \begin{bmatrix} 0 & 0 & \omega_e \end{bmatrix}^T \tag{A.2}$$

where ω_e is the angular velocity of the Earth and is equal to 7.2921150×10^{-5} rad/s.

The objective in this section is to determine the $\mathbf{v}_{spacecraft_{rel}}$ term expressed in the Hill coordinate frame. The absolute position vector of a spacecraft $\mathbf{r}_{spacecraft}$ can be expressed in the Hill frame as follows:

$$\mathbf{r}_{spacecraft} = \mathbf{r}_{ref} + \mathbf{r}_{rel}$$

$$\mathbf{r}_{spacecraft} = \begin{bmatrix} r_{ref} \\ 0 \\ 0 \end{bmatrix} + \begin{bmatrix} x \\ y \\ z \end{bmatrix} \tag{A.3}$$

$$\mathbf{r}_{spacecraft} = \begin{bmatrix} (r_{ref} + x) & y & z \end{bmatrix}^T$$

where $\mathbf{r}_{rel}$ is the relative position of the spacecraft with respect to the reference orbit expressed in the Hill frame and r_{ref} is the magnitude of the radial vector from

the center of the Earth to the position of reference orbit Hill frame at a given time. The absolute velocity of the spacecraft $\mathbf{v}_{spacecraft}$ is given by the following:

$$\mathbf{v}_{spcecraft} = \mathbf{v}_{ref} + (\mathbf{v}_{rel})_{xyz} + \dot{\boldsymbol{\theta}} \times \mathbf{r}_{rel} \tag{A.4}$$

where $\mathbf{v}_{ref}$ is the velocity of the reference orbit Hill frame with respect to the center of the Earth expressed in the Hill frame, $(\mathbf{v}_{rel})_{xyz}$ is the velocity of the spacecraft with respect to the Hill frame as seen from an observer in the Hill frame, and $\dot{\boldsymbol{\theta}}$ is the orbital rate vector of the reference orbit expressed in the Hill frame. These quantities are defined as follows:

$$\mathbf{v}_{ref} = \begin{bmatrix} \dot{r}_{ref} & r_{ref}\dot{\theta} & 0 \end{bmatrix}^T \tag{A.5}$$

$$(\mathbf{v}_{rel})_{xyz} = \begin{bmatrix} \dot{x} & \dot{y} & \dot{z} \end{bmatrix}^T \tag{A.6}$$

$$\dot{\boldsymbol{\theta}} = \begin{bmatrix} 0 & 0 & \dot{\theta} \end{bmatrix}^T \tag{A.7}$$

where $\dot{\theta}$ is the time rate of change of the true anomaly f. It is written as the time rate of change of argument of latitude θ as this simplifies the analysis for circular orbits where the true anomaly is undefined. These rates are equivalent as the argument of perigee ω is assumed to be a constant:

$$\frac{d\theta}{dt} \equiv \frac{d}{dt}(f + \omega) = \frac{df}{dt} \tag{A.8}$$

Bringing these three velocity terms together, the $\mathbf{v}_{spacecraft}$ term can be expressed in the Hill frame as:

$$\mathbf{v}_{spacecraft} = \begin{bmatrix} \dot{x} + \dot{r}_{ref} - y\dot{\theta} \\ \dot{y} + r_{ref}\dot{\theta} + x\dot{\theta} \\ \dot{z} \end{bmatrix} \tag{A.9}$$

The next step is to determine the representation of the $\boldsymbol{\omega}_e$ expressed in the Hill frame. In order to transform this vector quantity from the ECI frame to the

Hill frame, a transformation matrix must be determined. The transformation from the ECI coordinate system to the Perifocal (PQW) coordinate system is given by the following 3-1-3 Euler sequence (Chobotov, 2002):

$$\mathbf{r}_{PQW} = \mathbf{R}_3(\omega)\mathbf{R}_1(i)\mathbf{R}_3(\Omega)\mathbf{r}_{ECI} \tag{A.10}$$

In order to transform from the PQW to the Hill frame another rotation through an angle of true anomaly about the z -axis is required. Thus, the complete sequence which defines the transformation from the ECI frame to the Hill frame is given by:

$$\begin{aligned} \mathbf{r}_{Hill} &= \mathbf{R}_3(f)\mathbf{R}_3(\omega)\mathbf{R}_1(i)\mathbf{R}_3(\Omega)\mathbf{r}_{ECI} \\ \mathbf{r}_{Hill} &= \mathbf{R}_3(f+\omega)\mathbf{R}_1(i)\mathbf{R}_3(\Omega)\mathbf{r}_{ECI} \end{aligned} \tag{A.11}$$

The resulting transformation matrix which transforms coordinates from the ECI frame to the Hill frame is as follows:

$$\mathbf{R}_{ECI\to Hill} = \mathbf{R}_3(f+\omega)\mathbf{R}_1(i)\mathbf{R}_3(\Omega) \tag{A.12}$$

where $\mathbf{R}_1$ and $\mathbf{R}_3$ are the canonical rotation matrices defined generally by:

$$\mathbf{R}_1(\psi) = \begin{bmatrix} 1 & 0 & 0 \\ 0 & \cos\psi & \sin\psi \\ 0 & -\sin\psi & \cos\psi \end{bmatrix} \tag{A.13}$$

$$\mathbf{R}_3(\delta) = \begin{bmatrix} \cos\delta & \sin\delta & 0 \\ -\sin\delta & \cos\delta & 0 \\ 0 & 0 & 1 \end{bmatrix} \tag{A.14}$$

where ψ and δ are arbitrary angles of rotation. Performing the matrix multiplication results in the desired coordinate transformation matrix:

$$\mathbf{R}_{ECI\to Hill} = \begin{bmatrix} c_{\omega+f}c_\Omega - s_{\omega+f}c_i s_\Omega & c_{\omega+f}s_\Omega + s_{\omega+f}c_i c_\Omega & s_{\omega+f}s_i \\ -s_{\omega+f}c_\Omega - c_{\omega+f}c_i s_\Omega & -s_{\omega+f}s_\Omega + c_{\omega+f}c_i c_\Omega & c_{\omega+f}s_i \\ s_i s_\Omega & -s_i c_\Omega & c_i \end{bmatrix} \tag{A.15}$$

In order to simplify this transformation matrix, the definition of the argument of latitude θ will be used:

$$\theta = f + \omega \tag{A.16}$$

The argument of latitude θ is defined as the angle measured between the ascending node and the satellite's position vector in the orbital plane. Using this, the transformation matrix can now be written more succinctly as follows:

$$\mathbf{R}_{ECI \to Hill} = \begin{bmatrix} c_\theta c_\Omega - s_\theta c_i s_\Omega & c_\theta s_\Omega + s_\theta c_i c_\Omega & s_\theta s_i \\ -s_\theta c_\Omega - c_\theta c_i s_\Omega & -s_\theta s_\Omega + c_\theta c_i c_\Omega & c_\theta s_i \\ s_i s_\Omega & -s_i c_\Omega & c_i \end{bmatrix} \tag{A.17}$$

The $\boldsymbol{\omega}_e$ vector can now be expressed in the Hill frame by applying the coordinate transformation matrix $\mathbf{R}_{ECI \to Hill}$. The result is as follows:

$$\boldsymbol{\omega}_e = \begin{bmatrix} \omega_e \sin\theta \sin i \\ \omega_e \cos\theta \sin i \\ \omega_e \cos i \end{bmatrix} \tag{A.18}$$

Now, the $\boldsymbol{\omega}_e \times \mathbf{r}_{spacecraft}$ can be determined as follows:

$$\begin{aligned} \boldsymbol{\omega}_e \times \mathbf{r}_{spacecraft} &= \begin{vmatrix} \mathbf{i} & \mathbf{j} & \mathbf{k} \\ \omega_e \sin\theta \sin i & \omega_e \cos\theta \sin i & \omega_e \cos i \\ (r_{ref} + x) & y & z \end{vmatrix} \\ \boldsymbol{\omega}_e \times \mathbf{r}_{spacecraft} &= \begin{bmatrix} z\,\omega_e \cos\theta \sin i - y\,\omega_e \cos i \\ (r_{ref} + x)\,\omega_e \cos i - z\,\omega_e \sin\theta \sin i \\ y\,\omega_e \sin\theta \sin i - (r_{ref} + x)\,\omega_e \cos\theta \sin i \end{bmatrix} \end{aligned} \tag{A.19}$$

The final expression for the velocity of a spacecraft relative to the rotating atmosphere expressed in the Hill frame is as follows:

$$\mathbf{v}_{spacecraft_{rel}} = \begin{bmatrix} \dot{x} + \dot{r}_{ref} - y(\dot{\theta} - \omega_e \cos i) - z\,\omega_e \cos\theta \sin i \\ \dot{y} + (r_{ref} + x)(\dot{\theta} - \omega_e \cos i) + z\,\omega_e \sin\theta \sin i \\ \dot{z} + (r_{ref} + x)\,\omega_e \cos\theta \sin i - y\,\omega_e \sin\theta \sin i \end{bmatrix} \tag{A.20}$$

For the case where a circular reference orbit is used and the equations of motion are those given in the formulation by Schweighart and Sedwick (2002) the velocity of a spacecraft relative to the rotating atmosphere simplifies to:

$$\mathbf{v}_{spacecraft_{rel}} = \begin{bmatrix} \dot{x} - y(nc - \omega_e \cos i) - z\,\omega_e \cos\theta \sin i \\ \dot{y} + (r_{ref} + x)(nc - \omega_e \cos i) + z\,\omega_e \sin\theta \sin i \\ \dot{z} + (r_{ref} + x)\,\omega_e \cos\theta \sin i - y\,\omega_e \sin\theta \sin i \end{bmatrix} \tag{A.21}$$

where the $\dot{r}_{ref}$ term is zero due to the fact that we are now dealing with a circular reference orbit, and the orbital rate $\dot{\theta}$ becomes nc, the constant orbital rate of the circular reference orbit used in the Schweighart-Sedwick equations.

Appendix B - Schweighart-Sedwick Equations

In this appendix, the parameters associated with the Schweighart-Sedwick Equations are summarized. The Schweighart-Sedwick Equations of motion are given by:

$$\ddot{x} - 2(nc)\dot{y} - (5c^2 - 2)n^2 x = -3n^2 J_2\left(R_e^2 / r_{ref}\right) \times \left\{\frac{1}{2} - \left[3\sin^2 i_{ref} \sin^2(kt)/2\right] - \left[\left(1 + 3\cos 2i_{ref}\right)/8\right]\right\} \tag{B.1}$$

$$\ddot{y} + 2(nc)\dot{x} = -3n^2 J_2\left(R_e^2 / r_{ref}\right)\sin^2 i_{ref} \sin(kt)\cos(kt) \tag{B.2}$$

$$\ddot{z} + q^2 z = 2lq\cos(qt + \varphi) \tag{B.3}$$

where the x-y-z terms represent the spacecraft coordinates in the Hill frame, R_e is the mean equatorial radius of the Earth, r_{ref} is the radius of the circular reference orbit, J_2 is the second spherical harmonic of the Earth's gravitational potential (a dimensionless quantity which is equal to 1.08263×10^{-3}), i_{ref} is the initial inclination of the reference orbit, t is the given time, φ is the initial phasing angle for cross-track motion, and n is the mean orbital rate defined as:

$$n = \sqrt{\frac{\mu}{r_{ref}^3}} \tag{B.4}$$

where μ is the gravitational parameter of the Earth.

The following constants are employed to correct the period of the circular reference orbit for the nodal drift due to J_2 effects:

$$s = \frac{3}{8} J_2 \left(\frac{R_e}{r_{ref}}\right)^2 \left(1 + 3\cos 2i_{ref}\right) \tag{B.5}$$

$$c = \sqrt{1 + s} \tag{B.6}$$

$$k = nc + \frac{3}{2} n J_2 \left(\frac{R_e}{r_{ref}} \right)^2 \cos^2 i_{ref} \tag{B.7}$$

In order to correctly model the secular motion present in the cross-track direction, the following set of constants are used in the formulation:

$$i_{sat1} = i_{sat2} + \frac{\Delta \dot{z}_0}{k \, r_{ref}} \tag{B.8}$$

$$\Delta\Omega_0 = \frac{\Delta z_0}{r_{ref} \sin i_{ref}} \tag{B.9}$$

$$\gamma_0 = \cot^{-1}\left[\frac{\cot i_{sat2} \sin i_{sat1} - \cos i_{sat1} \cos \Delta\Omega_0}{\sin \Delta\Omega_0} \right] \tag{B.10}$$

$$\Phi_0 = \cos^{-1}\left[\cos i_{sat1} \cos i_{sat2} + \sin i_{sat1} \sin i_{sat2} \cos \Delta\Omega_0 \right] \tag{B.11}$$

$$\dot{\Omega}_{sat1} = -\frac{3}{2} n J_2 \left(\frac{R_e}{r_{ref}} \right)^2 \cos i_{sat1} \tag{B.12}$$

$$\dot{\Omega}_{sat2} = -\frac{3}{2} n J_2 \left(\frac{R_e}{r_{ref}} \right)^2 \cos i_{sat2} \tag{B.13}$$

$$q = nc - \left(\cos\gamma_0 \sin\gamma_0 \cot\Delta\Omega_0 - \sin^2 \gamma_0 \cos i_{sat1} \right)\left(\dot{\Omega}_{sat1} - \dot{\Omega}_{sat2} \right) - \dot{\Omega}_{sat1} \cos i_{sat1} \tag{B.14}$$

$$l = -r_{ref} \frac{\sin i_{sat1} \sin i_{sat2} \sin \Delta\Omega_0}{\sin \Phi_0} \left(\dot{\Omega}_{sat1} - \dot{\Omega}_{sat2} \right) \tag{B.15}$$

The term i_{sat2} corresponds to the initial inclination of the Chief spacecraft. The initial conditions of the Chief spacecraft are chosen in such a way that it originally lies in the circular reference orbit and thus i_{sat2} is set to i_{ref}. The i_{sat1} term corresponds to the initial inclination of the Deputy spacecraft. This is determined using the initial conditions of the Deputy spacecraft with respect to the Chief expressed in the Hill frame, i.e. the $\Delta\dot{z}_0$ term in equation (B.8).

The initial conditions of the radial and in-track velocities of each spacecraft with respect to the reference orbit are also specified in order to eliminate secular motion or constant offset terms. Thus, the initial conditions of the radial and in-track must include the following in order to account for undesired secular drift:

$$\dot{x}_0 = y_0\, n\left(\frac{1-s}{2\sqrt{1+s}}\right) \tag{B.16}$$

$$\dot{y}_0 = -2\,x_0\, n\sqrt{1+s} + \frac{3}{4}n^2 J_2 \frac{R_e^2}{r_{ref}}\sin^2 i_{ref} \tag{B.17}$$

The circular reference orbit is also changing with time due to J_2 effects. In order to propagate this constant radius reference orbit, the orbital elements as a function of time were given by Schweighart and Sedwick (2002) as:

$$i(t) = i_{ref} - \left(3\sqrt{\mu}J_2 R_e^2 \Big/ 2\,k\, r_{ref}^{\frac{7}{2}}\right)\cos i_{ref}\sin i_{ref}\sin^2(kt) \tag{B.18}$$

$$\Omega(t) = \Omega_{ref} - \left(3\sqrt{\mu}J_2 R_e^2 \Big/ 2kr_{ref}^{\frac{7}{2}}\right)\cos(i_{ref})\, t \tag{B.19}$$

$$\theta(t) = k\,t \tag{B.20}$$

which can also be written as:

$$i(t) = i_{ref} - \frac{3}{2}\left(\frac{n}{k}\right)J_2\left(\frac{R_e}{r_{ref}}\right)^2 \cos i_{ref}\sin i_{ref}\sin^2(kt) \tag{B.21}$$

$$\Omega(t) = \Omega_{ref} - \left(\frac{3}{2}n\,J_2\left(\frac{R_e}{r_{ref}}\right)^2 \cos i_{ref}\right)t \tag{B.22}$$

$$\theta(t) = k\,t \tag{B.23}$$

The position vector of the reference orbit in the ECI coordinate frame can now be determined explicitly as a function of time using the above relations as:

$$\mathbf{r}_{ref} = r_{ref} \begin{bmatrix} \cos\Omega(t)\cos\theta(t) - \sin\Omega(t)\sin\theta(t)\cos i(t) \\ \sin\Omega(t)\cos\theta(t) + \cos\Omega(t)\sin\theta(t)\cos i(t) \\ \sin\theta(t)\sin i(t) \end{bmatrix} \tag{B.24}$$

This quantity is needed for the computation of the atmospheric density above the ellipsoidal model of the Earth (discussed in Appendix C). For further details please refer to the original paper by Schweighart and Sedwick (2002).

Appendix C - Atmospheric Density Model

In this appendix, a description of the atmospheric density model used in all simulations is given. This simple static model assumes that the density of the atmosphere decays exponentially with increasing altitude. This exponential relation is given by (Vallado, 2007):

$$\rho = \rho_0 \exp\left[-\frac{h_{ellp} - h_0}{H}\right] \tag{C.1}$$

where ρ_0 is a reference density for the given altitude range, h_0 is the corresponding reference altitude from which the reference density ρ_0 was measured, H is known as the scaled height and it is the fractional change in the density with height, and h_{ellp} is the height of the spacecraft above an ellipsoidal model of the Earth. The ρ_0, h_0, and H parameters are tabulated values which are given for reference in Table C-1. This model is known as the CIRA-72 semi-theoretical technique. Although it is very simple, this method is known to give moderate results for general studies.

The remaining parameter needed for the determination of atmospheric density is the height above the ellipsoidal Earth h_{ellp}. Figure C-1 shows a schematic representation of the height above an ellipsoidal. The algorithm used to determine this parameter is given by Algorithm 12 of Vallado (2007). This algorithm is outlined here for reference:

First, the ECI coordinates of the spacecraft are required, where the position vector in the ECI frame is assumed to take the following form:

$$\mathbf{r} = \begin{bmatrix} r_I & r_J & r_K \end{bmatrix}^T \tag{C.2}$$

Altitude h_{ellp} [km]	Base Altitude h_0 [km]	Nominal Density ρ_0 [kg/m^3]	Scale Height H [km]	Altitude h_{ellp} [km]	Base Altitude h_0 [km]	Nominal Density ρ_0 [kg/m^3]	Scale Height H [km]
0-25	0	1.225	7.249	150-180	150	2.070×10^{-9}	22.523
25-30	25	3.899×10^{-2}	6.349	180-200	180	5.464×10^{-10}	29.740
30-40	30	1.774×10^{-2}	6.682	200-250	200	2.789×10^{-10}	37.105
40-50	40	3.972×10^{-3}	7.554	250-300	250	7.248×10^{-11}	45.546
50-60	20	1.057×10^{-3}	8.382	300-350	300	2.418×10^{-11}	53.628
60-70	60	3.206×10^{-4}	7.714	350-400	350	9.518×10^{-12}	53.298
70-80	70	8.770×10^{-5}	6.549	400-450	400	3.725×10^{-12}	58.515
80-90	80	1.905×10^{-5}	5.799	450-500	450	1.585×10^{-12}	60.828
90-100	90	3.396×10^{-6}	5.382	500-600	500	6.967×10^{-13}	63.822
100-110	100	5.297×10^{-7}	5.877	600-700	600	1.454×10^{-13}	71.835
110-120	110	9.661×10^{-8}	7.263	700-800	700	3.614×10^{-14}	88.667
120-130	120	2.438×10^{-8}	9.473	800-900	800	1.170×10^{-14}	124.64
130-140	130	8.484×10^{-9}	12.636	900-1000	900	5.245×10^{-15}	181.05
140-150	140	3.845×10^{-9}	16.149	1000+	1000	3.019×10^{-15}	268.00

Table C-1: Exponential Atmospheric Model (Vallado, 2007)

where r_I, r_J, and r_K represent the X,Y, and Z components of the spacecraft in the ECI frame respectively. Using this input, the equatorial projection of the spacecraft's position vector $r_{\delta sat}$ is calculated as:

$$r_{\delta sat} = \sqrt{r_I^2 + r_J^2} \tag{C.3}$$

Using this value, the angle δ can be computed using the following relation:

$$\tan\delta = \frac{r_K}{r_{\delta sat}} \tag{C.4}$$

This value of δ is then used as the initial guess for the geodetic latitude φ_{gd} in the following iterative scheme:

$$C_e = \frac{R_e}{\sqrt{1 + e_e^2 \sin^2 \varphi_{gd}}} \tag{C.5}$$

$$\tan \varphi_{gd} = \frac{r_K + C_e e_e^2 \sin \varphi_{gd}}{r_{\delta sat}} \tag{C.6}$$

where R_e is the mean equatorial radius of the Earth, C_e is known as the radius of curvature in the meridian, and e_e is the eccentricity of the ellipsoidal shape of the Earth and has an approximate value of 0.081819. The new value of φ_{gd} is determined from equation (C.6) and the iteration continues until a specified tolerance is met, i.e.:

$$\left| \varphi_{gd_{new}} - \varphi_{gd_{old}} \right| < \text{Tolerance} \tag{C.7}$$

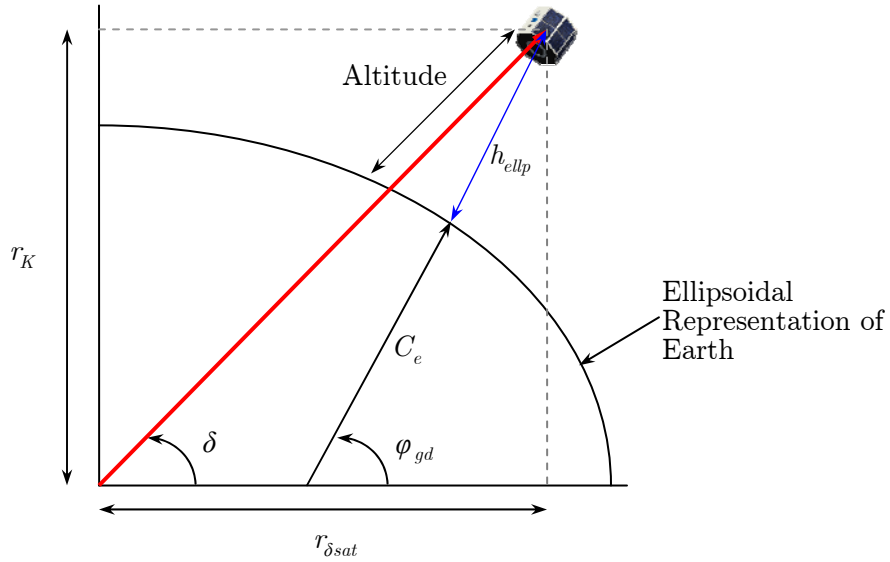

Figure C-1: Determining a Spacecraft's Height above the Ellipsoidal Earth

Once the values of C_e and φ_{gd} have been determined, the height above the ellipsoidal Earth can be calculated as follows:

$$h_{ellp} = \frac{r_{\delta sat}}{\cos \varphi_{gd}} - C_e \tag{C.8}$$

In order to use the algorithm described above, the position vector of the spacecraft in question must be transformed from its description in the Hill frame to its equivalent position in the ECI frame. This is done as follows:

The spacecraft's position in the ECI frame is given by the following relation:

$$\mathbf{r}_{spacecraft} = \mathbf{r}_{ref} + \mathbf{R}_{Hill \to ECI}\, \mathbf{r}_{rel} \tag{C.9}$$

where $\mathbf{r}_{ref}$ is the position vector of the reference orbit expressed in the ECI frame, $\mathbf{r}_{rel}$ is the relative position vector of the spacecraft with respect to the reference orbit expressed in the Hill frame, and $\mathbf{R}_{Hill \to ECI}$ is the transformation matrix which transforms Hill coordinates into the ECI frame orientation. The transformation matrix which transforms coordinates from the ECI to the Hill frame, i.e. $\mathbf{R}_{ECI \to Hill}$, was given in Appendix A. Since this transformation is described by a rotation matrix, which is an orthonormal or proper orthogonal matrix, the inverse transformation is nothing but the transpose of the original transformation. Consequently, the desired transformation is given as follows:

$$\mathbf{R}_{Hill \to ECI} = \mathbf{R}^T{}_{ECI \to Hill} \tag{C.10}$$

$$\mathbf{R}_{Hill \to ECI} = \begin{bmatrix} c_\theta c_\Omega - s_\theta c_i s_\Omega & -s_\theta c_\Omega - c_\theta c_i s_\Omega & s_i s_\Omega \\ c_\theta s_\Omega + s_\theta c_i c_\Omega & -s_\theta s_\Omega + c_\theta c_i c_\Omega & -s_i c_\Omega \\ s_\theta s_i & c_\theta s_i & c_i \end{bmatrix} \tag{C.11}$$

where c and s denote the sine and cosine functions of the angle given in the subscript, Ω is the right ascension of the ascending node, i is the inclination, and θ is the argument of latitude of the reference orbit at the time under consideration.

A more accurate algorithm for coordinate transformation from the Hill to the ECI frame is given by Algorithm 48 of Vallado (2007). This algorithm takes into

account the true curvilinear nature of the rotating Hill coordinates and yields a more accurate solution. The linear transformation method described above is consistence with the assumption that distances in the Hill frame are small in comparison to the distance of the reference orbit from the center of the Earth and thus is valid for circumstances where the equations of motion are valid.

References

Abramowitz, M., & Stegun, I. A. (1965). *Handbook of Mathematical Functions*. New York, NY: Dover Publication, Inc.

Battin, R. H. (1987). *An Introduction to the Mathematics and Methods of Astrodynamics*. New York, NY: American Institute of Aeronautics and Astronautics.

Bevilacqua, R., & Romano, M. (2008). Rendezvous Maneuvers of Multiple Spacecraft Using Differential Drag Under J_2 Perturbations. *Journal of Guidance, Control and Dynamics*,Vol. 31, No.6, pp. 1595-1607.

Carter, T., & Humi, M. (2002). Clohessy-Wiltshire Equations Modified to Include Quadratic Drag. *Journal of Guidance, Control and Dynamics*,Vol. 25, No.6, pp. 1058-1063.

Chobotov, V. A. (2002). *Orbital Mechanics* (Third ed.). Reston, Virginia: AIAA Education Series.

Clohessy, W. H., & Wiltshire, R. S. (1960). Terminal Guidance System for Satellite Rendezvous. *Journal of the Aerospace Sciences*,Vol. 27, No.9, pp. 653-658.

Fourcade, J. (2004, 11-12 October). *Mission Analysis and Orbit Control of Interferometric Wheel Formation Flying.* Paper presented at the Proceedings of the 18th International Symposium on Space Flight Dynamics (ESA SP-548), Munich.

Franconeri, J. (2003). Use of Differential Drag as a Satellite Constellation Stationkeeping Strategy. from http://ccar.colorado.edu/asen5050/projects/projects_2003/franconeri/

Hajovsky, B. B. (2007). *Satellite Formation Control Using Atmospheric Drag.* Air Force Institute of Technology.

Hamel, J.-F., & de Lafontaine, J. (2007). Linearized Dynamics of Formation Flying Spacecraft on a J_2-Perturbed Elliptic Orbit. *Journal of Guidance, Control and Dynamics*,Vol. 30, No.6, pp. 1649-1658.

Hibbler, R. C. (2007). *Engineering Mechanics: Statics and Dynamics* (Eleventh ed.). Upper Saddle River, New Jersey: Pearson - Prentice Hall.

Hill, G. W. (1878). Researches in Lunar Theory. *American Journal of Mathematics*,Vol. 1, No.1, pp. 5-26.

Humi, M., & Carter, T. (2002). Rendezvous Equations in a Central-Force Field with Linear Drag. *Journal of Guidance, Control and Dynamics*,Vol. 25, No.1, pp. 74-79.

Inalhan, G., Tillerson, M., & How, J. P. (2002). Relative Dynamics and Control of Spacecraft Formations in Eccentric Orbits. *Journal of Guidance, Control and Dynamics*,Vol. 25, No.1, pp. 48-59.

Jigang, H., & Yulin, Z. (2006). *Application of Phase-Plane Method in the Co-Plane Formation Maintenance of Formation Flying Satellites.* Paper presented at the Proceedings of the 25th Chinese Control Conference, Harbin, Heilongjiang.

Kechichian, J. A. (1998). Motion in General Elliptic Orbit with Respect to a Dragging and Precessing Coordinate Frame. *The Journal of the Astronautical Sciences*,Vol. 46, No.1, pp. 25-45.

Kelley, S. G. (1996). *Mechanical Vibrations*. Montreal: McGraw-Hill.

Kumar, B. S., & Ng, A. (2008). *A Bang-Bang Control Approach to Maneuver Spacecraft in a Formation with Differential Drag*. Paper presented at the AIAA Guidance, Navigation, and Control Conference.

Kumar, B. S., Ng, A., Yoshihara, K., & Ruiter, A. D. (2007). *Differential Drag as a Means of Spacecraft Formation Control*. Paper presented at the IEEE Aerospace Conference.

Kumar, K. D., Bang, H. C., & Tahk, M. J. (2007). Satellite formation flying using along-track thrust. *Acta Astronautica*,Vol. 61, pp. 553-564.

Landry, M. A. (2005). *Rendezvous and Formation Flying*. McGill, Montreal, Quebec.

Leonard, C. L. (1986). *Formationkeeping of Spacecraft via Differential Drag*. Unpublished MSc., Massachusetts Institute of Technology, Boston, Massachusetts.

Leonard, C. L., Hollister, W. M., & Bergman, E. V. (1989). Orbital Formationkeeping with Differential Drag. *Journal of Guidance, Control and Dynamics*,Vol. 12, No.1, pp. 108-113.

Melton, R. G. (2000). Time-Explicit Representation of Relative Motion Between Elliptical Orbits. *Journal of Guidance, Control and Dynamics*,Vol. 23, No.4, pp. 604-610.

Mishne, D. (2004). Formation Control of Satellites Subject to Drag Variations and J_2 Perturbations. *Journal of Guidance, Control and Dynamics*,Vol. 27, No.4, pp. 685-692.

Misra, A. K. (2009). Spacecraft Dynamics Lecture Notes (MECH 542). McGill University.

Païdoussis, M. P. (1994). Notes for Advanced Mechanics of Systems (MECH 419 Course Pack). McGill University.

Palmerini, G. B., Sgubini, S., & Taini, G. (2005). *Spacecraft Orbit Control Using Air Drag*. Paper presented at the 56th International Astronautical Congress of the International Astronautical Federation.

Prussing, J. E., & Conway, B. A. (1993). *Orbital Mechanics*. Toronto: Oxford University Press.

Sabatini, M., & Palmerini, G. B. (2006). *Control Effort Evaluation for Low-Altitude Formation Flying*. Paper presented at the IEEE Aerospace Conference.

Sabol, C., Burns, R., & McLaughlin, C. A. (2001). Satellite Formation Flyign Design and Evolution. *Journal of Spacecraft and Rockets*,Vol. 38, No.2, pp. 270-278.

Scharf, D. P., Hadaegh, F. Y., & Ploen, S. R. (2003). *A Survey of Spacecraft Formation Flying Guidance and Control (Part I): Guidance.* Paper presented at the Proceedings of the 2003 American Control Conference.

Scharf, D. P., Hadaegh, F. Y., & Ploen, S. R. (2004). *A Survey of Spacecraft Formation Flying Guidance and Control (Part II): Control.* Paper presented at the Proceedings of the 2004 American Control Conference.

Schaub, H., & Junkins, J. L. (2003). *Analytical Mechanics of Space Systems*. Reston, VA: American Institute of Aeronautics and Astronautics.

Schweighart, S. A., & Sedwick, R. J. (2002). High-Fidelity Linearized J_2 Model for Satellite Formation Flight. *Journal of Guidance, Control and Dynamics*,Vol. 25, No.6, pp. 1073-1080.

Shankar-Kumar, B. (2009). *JC2SAT–FF Flight Dynamics and Control* (No. JCF-000019): Canadian Space Agency.

Silva, E. D. (2008). *A Formulation of the Clohessy-Wiltshire Equations to Include Dynamic Atmospheric Drag*. Paper presented at the AIAA/AAS Astrodynamics Specialist Conference.

Slater, J. C., & Frank, N. H. (1947). *Mechanics* (1st ed.). New York: McGraw-Hill.

Théron, A., Farges, C., Peaucelle, D., & Arzelier, D. (2007, 9-13 July). *Periodic H_2 synthesis in elliptical orbits with atmospheric drag and J_2 perturbations.* Paper presented at the Proceedings of the 2007 American Control Conference, New York City.

Tschauner, J., & Hempel, P. (1965). Rendezvous zu einem Min Elliptischer Bahn Umlaufenden Ziel (Rendezvous with a Target in Elliptic Orbit). *Astronautica Acta*,Vol. 11, No.2, pp. 104-109.

Vallado, D. A. (2007). *Fundamentals of Astrodynamics and Applications* (Third ed.). Hawthorne, CA: Microcosm Press.

Wells, D. A. (1967). *Lagrangian Dynamics*. Montreal: McGraw-Hill.

Wertz, J. R., & Larson, W. J. (2007). *Space Mission Analysis and Design* (Third ed.). Hawthorne, California: Microcosm Press.